Cell-specific analysis of specialized metabolism in Catharanthus roseus

山本，浩太郎

(Degree)
博士（理学）

(Date of Degree)
2017-03-25

(Date of Publication)
2019-03-25

(Resource Type)
doctoral thesis

(Report Number)
甲第6858号

(URL)
https://hdl.handle.net/20.500.14094/D1006858

博士論文

Cell-specific analysis of specialized metabolism in *Catharanthus roseus*

細胞別網羅的解析に基づく ニチニチソウ二次代謝機構の解明

平成 29 年 1 月

神戸大学大学院理学研究科

山本　浩太郎

Table of contents

Abstract

Cell-specific analysis of specialized metabolism in *Catharanthus roseus*

細胞別網羅的解析に基づくニチニチソウ二次代謝機構の解明

理学研究科　山本浩太郎

植物は、昆虫や草食動物などの捕食者に対する防御物質として、カフェインやモルヒネのような二次代謝産物を生産している。これらの二次代謝産物の中には、人に有用な物質が数多くあり、植物の二次代謝機構を研究することは、有用二次代謝産物の効率的生産法の開発にも繋がる。

ニチニチソウ（*Catharanthus roseus*）は、Vinblastine や Vincristine などの抗がん剤となる Terpenoid indole alkaloid（TIA）をはじめとして、様々な二次代謝産物を生合成することで著名な薬用植物である。ニチニチソウの TIA 合成は、一連の生合成過程が茎や葉組織において葉肉細胞、表皮細胞など様々な細胞を経由して進むことが、遺伝子発現解析などに基づいて報告されている。特に Idioblast cell（異形細胞）や Laticifer cell（乳管細胞）が TIA 代謝の重要な過程に関与すると考えられてきたが、これらの細胞内や細胞間における二次代謝過程の分子機構は十分には理解されていない。

私は、ニチニチソウ茎組織や葉組織における細胞レベルでのアルカロイドの分布から TIA 代謝メカニズムを解明しようと考え、一細胞質量分析技術や質量顕微鏡を用いた細胞別メタボローム解析を試みた。その結果、Vindoline や Serpentine などの Idioblast cell や Laticifer cell で合成されると推測される TIA はもとより、これまで表皮細胞で合成されると考えられてきた Strictosidine などの TIA も Idioblast cell や Laticifer cell に多く蓄積されていることが明らかになった。既知の代謝経路と代謝物の分布との間に矛盾が見られることから、植物内での TIA 物質の合成、移動、分布・蓄積を制御する未知のメカニズムが存在する可能性が示唆される。さらに、茎組織と葉組織の細胞レベルでの比較メタボローム解析より、組織特異的な Idioblast cell や Laticifer cell の TIA 代謝分化が起きている可能性が示唆された。これらの違いを解明するために、Idioblast cell や Laticifer cell を単離することや、細胞特異的なトランスクリプトーム解析を試み、Idioblast cell で特異的に発現する複数の二次代謝合成酵素やトランスポーターの候補を得ることに成功した。

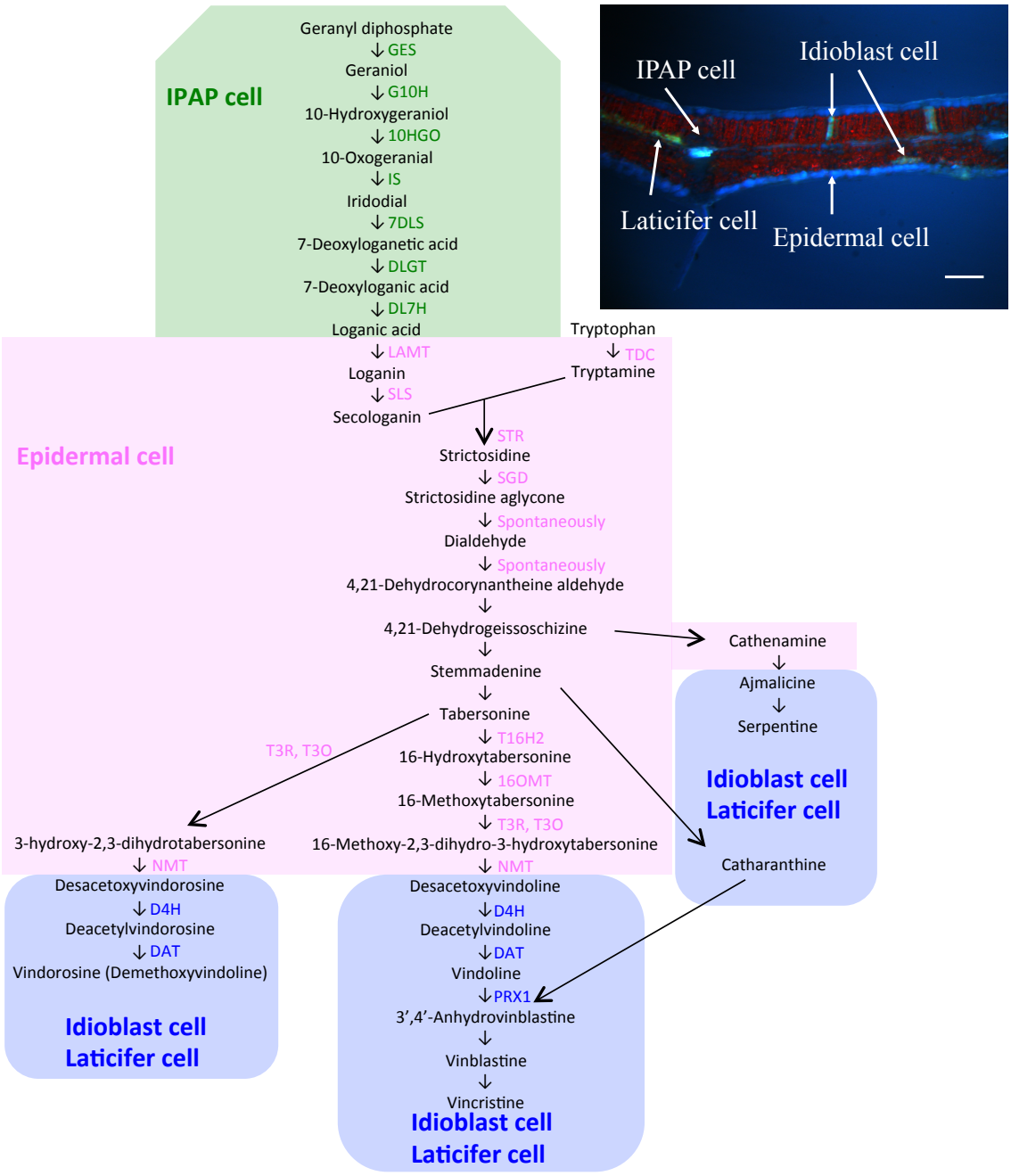

Fig. 1. TIA biosynthesis in *Catharanthus roseus* stem and leaf tissues. Green font represents the TIA enzyme localized in internal phloem associated parenchyma (IPAP) cells. Purple represents TIA enzyme localized in epidermal cells. Blue represents TIA enzyme localized in idioblast cells and laticifer cells. Inset is a fluorescent photograph of leaf cross section. Scale bar = 100 µm.

Abbreviation

BIA : Benzylisoquinoline alkaloid

C. roseus : *Catharanthus roseus*

FPKM : Fragments per kilobase of transcript per million mapped reads

FSC : Forward scatter

FW : Fresh weight

IPP : Isopentenyl diphosphate

LC-MS : Liquid chromatography mass spectrometry

MS : Mass spectrometry

PCA : Principal component analysis

SSC : Side scatter

TIA : Terpenoid indole alkaloid

UV : Ultraviolet

Abbreviation (Enzyme)

10HGO : 10-Hydroxygeraniol oxidoreductase

16OMT : 16-Hydroxytabersonine O-methyltransferase

7DLH : 7-Deoxyloganic acid 7-hydroxylase

D4H : Desacetoxyvindoline 4-hydroxylase

DAT : Deacetylvindoline 4-Oacetyltransferas

DLGT : 7-Deoxyloganetic acid glucosyltransferase

G10H : Geraniol 10-hydroxylase

GES : Geraniol synthase

IS : Iridoid synthase

LAMT : Loganic acid O-methyltransferase

NMT : 16-Methoxy-2,3-dihydro-3-hydroxy-tabersonine N-methyltransferase

SGD : Strictosidine β-glucosidase

SLS : Secologanin synthase

STR : Strictosidine synthase

T16H : Tabersonine 16-hydroxylase

T3O : Tabersonine 3-oxygenase

T3R : Tabersonine 3-reductase

TDC : Tryptophan decarboxylase

Abbreviation in figures and tables (Cell)

EC : Epidermal cell

IC : Idioblast cell

IPAP : Internal phloem associated parenchyma

LC : Laticifer cell

LEC : Leaf epidermal cell

LLC : Leaf laticifer cell

LPLC : Leaf primordium laticifer cell

PC : Parenchyma cell

PTIC : Palisade tissue idioblast cell

PTPC : Palisade tissue parenchyma cell

STIC : Spongy tissue idioblast cell

STPC : Spongy tissue parenchyma cell

General introduction

Alkaloids biosynthesis in plants

General introduction :

Alkaloids biosynthesis in plants

Many alkaloids are produced in plants.

Plants produce various kinds of specialized metabolites which have been formerly called as secondary metabolites. Those specialized metabolites have biological activities to support the life of plants. They are functioning to defend against predators like insects and herbivores, to guard against UV radiation or to attract pollinators.

Plant specialized metabolites are indispensable not only for plants themselves but also for human welfare. The significant values of specialized metabolites as medicines or luxury items in human life have been attracting widespread interests from researchers in a broad range of scientific fields. These researchers have extensively studied how specialized metabolites are produced at biochemical, cell and tissue levels in each plant (Kutchan, 2005).

Plant specialized metabolites are classified into three major categories, such as terpenoids, flavonoids and alkaloids, on the basis of their chemical structures. Alkaloids contain nitrogen in their molecular forms. About 20% of plant species are known to contain alkaloids (De Luca, 2011). It has been reported that certain biosynthetic pathways of plant specialized metabolites, including alkaloids synthesis, often involve multiple cell types that are biochemically and morphologically distinct (Hagel et al., 2008; Pan et al., 2016). Thus far, there is no answer about a question “why and how their specialized metabolisms are progressed across various different kinds of

cells ? “.

Alkaloids producing pathways have been studied well for their pharmaceutical and biological properties. Opium poppy is one of the famous medicinal plants producing morphine and codeine. This plant has been used as a model system to investigate benzylisoquinoline alkaloids (BIA) biosynthesis in plants (Beaudoin et al., 2014). At least 3 distinct cell types, such as companion cells, sieve elements and laticifer cells, are involved in the biosynthesis and storage of BIA in opium poppy. It has been suggested that the end product, such as morphine, is synthesized and accumulated in laticifer cells (Beaudoin et al., 2014). Since these BIAs have biological activities, the laticifer cells in opium poppy might be afforded to sequester toxic alkaloids and pathway intermediates from other BIA-sensitive cells (Facchini et al., 2005). However, the relations between each type of cell and specialized metabolism have been mostly unknown, yet. This is the same in other plants even certain famous plants producing specialized metabolites. In the present study, in order to reveal the relationship between cell-specific specialized metabolism and unique differentiating cells (such as idioblast cells or laticifer cells), I have focused on investigating indole alkaloid metabolism at cell levels in *Catharanthus roseus* (L.) G. Don.

Alkaloids biosynthesis in *Catharanthus roseus* (L.) G. Don.

Terpenoid indole alkaloids (TIA) classified as a kind of alkaloids are synthesized in Apocynaceae, Rubiaceae and Loganiaceae (Balsevich et al., 1988). TIA biosynthesis involves the assembly of tryptamine, which is produced from L-tryptophan, with a

secologanin. *Catharanthus roseus* (L.) G. Don (Apocynaceae) is one of the best-characterized TIA producing plants. This plant can produce many commercially valuable TIAs, including antitumor drugs such as vinblastine and vincristine. That is one of reasons why specialized metabolisms in this plant have been studied well. These researches revealed that this plant has many sub TIA metabolic pathways (Fig. 1). Since the finding and development of TIAs as antitumor drugs in the 1970s, leaf extracts of *C. roseus* have been the sole source of vindoline and catharanthine, both of which are monomeric precursors for the commercial production of TIA (O'Keefe et al., 1997). Extensive studies have revealed that more than 130 TIAs are produced from the central precursor (i.e. strictosidine) in *C. roseus* (Fig. 1) (Verma et al., 2012).

The TIA biosynthetic pathway in *C. roseus* consists of many sub-pathways, including iridoid pathway, serpentine pathway, catharanthine pathway and vindoline pathway. It is believed that most TIAs are also produced thorough various cell types and organelles in *C. roseus* from the results based on the localization of TIA and iridoid biosynthesis enzymes by *in situ* hybridization, immunoblot or transcriptomic analysis (Van Der Heijden et al., 2004; Gigant et al., 2005; Kavallaris, 2010). Recently, the entire iridoid pathway, from geranyl diphosphate to secologanin, in *C. roseus* has been biochemically and genetically elucidated (Fig. 1). It is suggested that most of this pathway are proceeding in internal phloem associated parenchyma cell (IPAP cell). Loganic acid produced in the IPAP cell is transported to epidermal cell where this iridoid is converted to secologanin. Subsequent strictosidine biosynthesis is conducted by strictosidine synthase (STR) in vacuoles of epidermal cells. Then, strictosidine

β-glucosidase (SGD) acts in the cleavage of strictosidine in nucleus to produce aglycone precursors required for various chemical skeletons, such as corynanthe type (serpentine pathway), aspidosperma type (vindoline pathway, vindorosine (demethoxyvindoline) pathway) and iboga type (catharanthine pathway) (Figs. 1 and 2) (Qu et al., 2015).

Although serpentine and catharanthine pathway have still been most unknown, the vindoline pathway have been studied well and characterized from tabersonine to vindoline or to vindorosine (Qu et al., 2015). It is believed that most TIA intermediates of these pathways are converted within the epidermal cells. TIA products of last 2-steps in vindoline pathway (deacetylvindoline and vindoline) are produced in both idioblast cells and laticifer cells (Fig. 1). It has been considered that these TIA end products are finally accumulated in the vacuoles of idioblast cells or laticifer cells.

These days, immunoblot and GFP-fusion analyses also revealed which organelle is localizing TIA enzymes in *C. roseus* cells. MEP pathway started from plastid in IPAP cells and produces geraniol there (Verma et al., 2012; Pan et al., 2016). It is believed that loganic acid is produced from geraniol in ER or the cytosol in IPAP cells. Secologanin is produced in the cytosol or ER in epidermal cells and transported into the vacuole to produce strictosidine. Then β-glucosidase produces strictosidine aglycone from strictosidine in the nucleus in epidermal cells. It is believed that subsequent TIA metabolisms are conducted among various organelles in epidermal cells. Desacetoxyvindoline is transported from epidermal cells to idioblast cells and laticifer cells and this TIA is converted to vindoline in the cytosol in idioblast cells and laticifer cells finally. Then vindoline is accumulated into the vacuoles in idioblast cells and

laticifer cells.

At present, it has still been mostly unknown how metabolites are transported between cells or organelles and how the expression of TIA-relating genes in idioblast cells and laticifer cells are regulated.

In the present study, I aimed to clarify TIA biosynthetic mechanism at cellular levels in stem and leaf tissues in *C. roseus*. At Chapter 1, I tried to reveal the cell-specific localization of TIA intermediates in *C. roseus* stem tissue. At Chapter 2, I also attempted to measure the cell-specific localization of TIA intermediates in *C. roseus* leaf tissue. In both cases, I used cutting-edge metabolome techniques, that is, Imaging MS and Single-cell MS. From these analyses, I found that the idioblast cells and laticifer cells are playing key roles in the specialized metabolism in this plant. At Chapter 3, I focused on the molecular mechanisms of the specialized metabolism of these cells by conducting cell-specific transcriptome analysis.

Chapter 1

Cell-specific TIA localization in *Catharanthus roseus* stem tissue

Chapter 1 :

TIA localization in *C. roseus* stem tissue

Summary

Catharanthus roseus (L.) G. Don is a medicinal plant well known for producing antitumor drugs such as vinblastine and vincristine, which are classified as terpenoid indole alkaloids (TIAs). The TIA metabolic pathway in *C. roseus* has been extensively studied. However, the localization of TIA intermediates at the cellular level has not been demonstrated directly. In this chapter, the metabolic pathway of TIA in *C. roseus* was studied with two forefront metabolomic techniques (i.e. Imaging MS and live Single-cell MS) to elucidate cell-specific TIA localization in the stem tissue. Imaging MS indicated that most TIAs localize in the idioblast cells and laticifer cells, which emit blue fluorescence under UV excitation. Single-cell MS was applied to four different kinds of cells [idioblast (specialized parenchyma cell), laticifer, parenchyma and epidermal cells] in the stem longitudinal section. Principal component analysis of Imaging MS and Single-cell MS spectra of these cells showed that similar alkaloids accumulate in both idioblast cells and laticifer cells. From MS/MS analysis of Single-cell MS spectra, catharanthine, ajmalicine and strictosidine were found in both cell types in *C. roseus* stem tissue. Serpentine was also accumulated in the same cells. Based on these data, I discuss the significance of TIA synthesis and accumulation in the idioblast cells and laticifer cells of *C. roseus* stem tissue.

Introduction

Alkaloids constitute one of the largest groups of specialized metabolites, many of which have biological functions that are indispensable, not only for plants themselves but also for human health. Approximately 20% of plant species are known to contain alkaloids (De Luca, 2011). *Catharanthus roseus* (L.) G. Don (Apocynaceae) is one of the best-characterized terpenoid indole alkaloid (TIA) producing plants. This plant produces many commercially valuable TIAs, including antitumor drugs such as vinblastine and vincristine (Van Der Heijden et al., 2004; Gigant et al., 2005; Kavallaris, 2010).

TIA metabolism in *C. roseus* involves more than 20 enzymatic steps and occurs in various cell types, starting from internal phloem associated parenchyma cells (IPAP cells) through epidermal cells (ECs) to both idioblast cells (ICs) and laticifer cells (LCs) where vindoline and other TIAs are believed to be accumulated (Yoder et al., 1976; Mahroug et al., 2006; Dugé de Bernonville et al., 2015). Cell type-specific localization of TIA metabolic pathways has been primarily inferred indirectly from the results of *in situ* RNA hybridization and immunocytochemical localization of the pathway enzymes (St-Pierre et al., 1999). The current understanding, mainly deduced from studies on leaf tissue, is that iridoid metabolism begins in IPAP cells and that loganic acid produced in IPAP cells is transferred to epidermal cells. Further synthesis involving secologanin and tryptamine occurs in the epidermal cells. Finally, a TIA intermediate, desacetoxyvindoline, moves to the idioblast cells and laticifer cells, and TIAs are accumulated in the vacuole of those cells (Yoder et al., 1976; Burlat et al.,

2004; Dugé de Bernonville et al., 2015). In the stem, a similar localization of enzymes in TIA metabolism (TDC, tryptophan decarboxylase; STR, strictosidine synthase; D4H, desacetoxyvindoline 4-hydroxylase; and DAT, deacetylvindoline 4-O-acetyltransferase in Fig. 1) has been proposed (St-Pierre et al., 1999). Thus far, however, the actual localization of TIA intermediates at the cellular level has not been directly measured in either leaf or stem tissues.

Recently, similar specialized metabolite biosynthetic pathways have been reported in other plants at the cellular level. For example, polyterpenes are highly accumulated in so-called laticifer cells in rubber trees (Hevea brasiliensis), and enzymes that are responsible for polyterpene biosynthesis have been identified (Hagel et al., 2008). Likewise, a benzylisoquinoline alkaloid morphine is accumulated in laticifer cells in opium poppy (*Papaver somniferum*). In both cases, cutting the laticifer cells located in the stem of rubber trees or seed capsule in opium poppy permits the collection of these valuable plant metabolites. Moreover, proteome analysis of opium poppy shows that enzymes for morphine biosynthesis are localized either in sieve elements or laticifer cells (Bird et al., 2003; Lee et al., 2013; Onoyovwe et al., 2013). These results suggest that the metabolic intermediates in morphine biosynthesis are likely to be shuttled between the two cell types of sieve elements and laticifer cells, and that laticifer cells are metabolically active (Onoyovwe et al., 2013). To understand in detail the metabolic pathways, however, identification of not only the localization of the enzymes but also the localization of these specialized metabolites themselves at the cellular level is necessary.

Novel methods for detecting metabolites *in situ* at the cellular level have been developed. Examples include matrix-assisted laser desorption/ionization imaging mass spectrometry (Imaging MS), which was applied to animal brain sections (Stoeckli et al., 2001), and desorption electrospray ionization mass spectrometry, which has been applied to many plant species, including *C. roseus* (Hemalatha et al., 2013) and *Hypericum perforatum* (Thunig et al., 2011). These studies succeeded in detecting target metabolites, but the resolution of the mass image was very low. Recent imaging MS revealed localization of many secondary metabolites in the rhizome of *Glycyrrhiza glabra*, with high resolution of about 20 μm (Li et al., 2014). The localization of metabolites at the cellular level of *Arabidopsis* tissues is also reported (Takahashi et al., 2015).

Another option for analyzing metabolite localization at the cellular level is Single-cell MS, which identifies cell contents from a single cell collected by using microcapillaries (Mizuno et al., 2008). In the Geraniaceae, *Pelargonium zonale* (L.) L'Herit, the metabolites from a single cell were measured by video-assisted MS and revealed differences between metabolite contents among cells in different tissues (Lorenzo Tejedor et al., 2012).

Stem tissue consists of various cell types that are similar to those in leaf tissue, and *in situ* RNA hybridization of genes for enzymes involved in TIA metabolism in stems has also been reported (St-Pierre et al., 1999). In the present study, I combined the above two forefront metabolomic techniques, Imaging MS and Single-cell MS, to elucidate cell-specific TIA localization in *Catharanthus* stem tissue.

Result

Localization of idioblast cells and laticifer cells in *C. roseus* stem tissue.

C. roseus stem tissue is composed of various types of cells : idioblast cell, laticifer cell, parenchyma cell (PC) and epidermal cell. Idioblast cell and laticifer cell were easily distinguishable from parenchyma cell and epidermal cell by blue or yellow autofluorescence emitted from the chemical compounds accumulated in these cells, when the specimen was excited by UV (Mersey et al., 1986). The blue autofluorescence occurs most likely from serpentine (Hisiger et al., 2005). In longitudinal sections, idioblast cells were found throughout the stem tissue, whereas short and elongated laticifer cells localized near the vascular bundles (Figs. 3L and 4).

TIAs in stem tissue.

Liquid chromatography mass spectrometry (LC-MS) analysis of the extracts from whole stem tissue identified mass spectral peaks of various TIAs, including catharanthine, ajmalicine, serpentine and vindoline (Table 1). Loganic acid, loganin, and secologanin were also detected (Table 2). Some of the peaks were subjected to MS/MS or LC-MS/MS analyses for further confirmation (Figs. 5-9 and Table 3), and quantitative data were obtained for the main alkaloids in the extracts from both stem tissue and the first leaf tissue (Table 1). In stem tissue, the concentrations were [$\mu g\ mg^{-1}$ fresh weight (FW)] catharanthine, 0.506 ± 0.044; ajmalicine, 0.071 ± 0.022; serpentine, 0.397 ± 0.031; tabersonine, 0.017 ± 0.003; and vindoline, 0.0026 ± 0.0002.

Imaging MS analysis.

To study the localization of TIA in the whole stem tissue, I conducted Imaging MS analysis using a longitudinal section of *C. roseus* stem tissue (Fig. 3). The results showed that monoterpenes, such as loganin (Fig. 3B) and secologanin (Fig. 3C), were localized in epidermal cell as reported previously (Guirimand et al., 2011).

Although it has been proposed from *in situ* RNA hybridization experiments that most TIAs are synthesized in epidermal cell (St-Pierre et al., 1999), MS images revealed that various TIAs, including ajmalicine and serpentine, were accumulated not in epidermal cell but rather in idioblast cell and laticifer cell (Fig. 3D-J). An MS image of *m/z* 337.19 (a possible candidate is catharanthine; see Fig. 3I) showed that this compound was localized in idioblast cell, laticifer cell and epidermal cell.

The mass spectrum data of four cell types (idioblast cell, laticifer cell, parenchyma cell and epidermal cell) were selected from Imaging MS figures and analyzed by principal component analysis (PCA). The various cell types could be distinguished as different groups. The PCA result showed that idioblast cell and laticifer cell accumulated similar compounds, which differed from those in parenchyma cell and epidermal cell (Fig. 10A). Loading data for PCA are shown in Fig. 10B.

Single-cell MS analysis.

To obtain quantitative data of various TIAs that complement the results of Imaging MS, I conducted Single-cell MS on idioblast cell, laticifer cell, parenchyma cell and epidermal cell (Fig. 4). The data obtained from the four cell types could also separate

the cells into different groups by PCA. The PCA result showed that idioblast cell and laticifer cell accumulated similar compounds, which differed from those in parenchyma cell and epidermal cell, in agreement with the data from Imaging MS (Fig. 10). I also obtained PC loading data that suggested some alkaloid peaks, such as *m/z* 337.19 (catharanthine) and *m/z* 349.15 (serpentine), mainly occur in specific cell types (Fig. 10C and D).

I conducted target mass analysis of *C. roseus* TIA using Single-cell MS data (Tables 4 and 5). The mass spectra of idioblast cell and laticifer cell showed that catharanthine (*m/z* 337.19) and serpentine (*m/z* 349.15) were detected in the top 100 peaks in those spectra. Catharanthine (*m/z* 337.19) was also detected in the mass spectra of parenchyma cell and epidermal cell.

I examined MS/MS analyses of a peak having *m/z* 337.19 to clarify whether this was mainly catharanthine or tabersonine (Figs. 5 and 11). As a result of MS/MS, I detected a catharanthine-specific fragment peak (*m/z* 93.07) from all types of cells (Table 4 and Figs. 5 and 11), although the peak intensity in parenchyma cell and epidermal cell was low. Other catharanthine-specific peak was not detected in parenchyma cell (*m/z* 133.07).

The MS/MS analysis strongly suggested that the peak having the *m/z* 337.19 that localized in idioblast cell and laticifer cell and the whole stem tissue is catharanthine. MS/MS fragments corresponding to serpentine (*m/z* 349.15) and ajmalicine (*m/z* 353.18) were also detected in Single-cell MS and LC-MS/MS analyses (Table 3 and Figs. 6 and 7). I also speculated on the possible TIA identities of several

other peaks (Table 1). To determine whether these peaks were really TIA, I examined their MS/MS fragments. In *m/z* 427.22 peak, which is supposed to be demethoxyvindoline, the major MS/MS fragments had *m/z* of 158.10, 367.20, and 409.21 (Fig. 8). These peaks are similar to the vindoline MS/MS fragment pattern (*m/z* 188.10, 397.20, and 439.21), although demethoxyvindoline MS/MS fragments may alter by *m/z* 30 owing to the deletion of the methoxy group and addition of a proton. At *m/z* 531.23 ion peak, detected fragment ion peaks (*m/z* 144.08, 165.05, 282.11, 320.13, 334.14, 352.16, and 514.21) were similar to the major MS/MS fragments of strictosidine that was produced by transformed yeast (Table 3) (Brown et al., 2015).

Semiquantitative analysis of Single-cell MS.

The metabolome of *C. roseus* stem tissues was analyzed using LC-MS. Single peaks at *m/z* 349.15, 427.22, and 531.23 correspond to serpentine, demethoxyvindoline and strictosidine, respectively (Table 1). According to the LC-MS result, I can consider that these *m/z* values show a single molecular species in each cell type of *C. roseus* stem tissue. Semiquantitative calculations were made in regard to *m/z* 349.15, 389.14, 427.22, and 531.23 ion peaks from the Single-cell MS data measured with mass range *m/z* = 100-1,000 (Fig. 12A and B) and mass range *m/z* = 385-550 (Fig. 12C and D). Serpentine (*m/z* 349.15) was detected in both idioblast cell and laticifer cell (Fig. 12A), whereas secologanin (*m/z* 389.14) was only accumulated in epidermal cell (Fig. 12B). Demethoxyvindoline (*m/z* 427.22) was detected in every type of cell, but with large variations; it was mainly accumulated in idioblast cell and laticifer cell (Fig. 12C).

Strictosidine (*m/z* 531.23) was also accumulated in idioblast cell and laticifer cell (Fig. 12D).

Discussion

TIA synthesis in the stem tissue *C. roseus* var. Equator White Eye.

LC-MS data of *C. roseus* stem extracts showed major peaks from TIAs, including catharanthine and vindoline (Table 1). These data suggest that the variety Equator White Eye also produces major TIAs in stem tissue; previous reports on other *C. roseus* varieties have focused on TIA in leaf tissue (Murata et al., 2005). I could not detect all of the vindoline-related intermediates in Single-cell MS data of this variety, even though I succeeded in detecting vindoline and demethoxyvindoline (Tables 4 and 5). It is known that *C. roseus* stem tissue produces less vindoline than leaf tissue (Singh et al., 2008). The present LC-MS quantitative data showed also that the first pair of leaves accumulated more vindoline than stem tissue (Table 1).

Identification of TIA peaks.

Many peaks corresponding to TIAs were detected using these recent metabolome techniques (i.e. Imaging MS and Single-cell MS). Both of these mass spectrometry systems have quite high mass resolution and high mass accuracy. Values of *m/z* suggested elemental compositions that could be tentatively assigned to TIAs based on their molecular formulae. To verify that these peaks were TIAs, I measured chemical structures of commercially available TIAs by MS/MS analysis using the same MS apparatus (Table 3 and Figs. 5-9). I was able to confirm, using standard MS/MS fragment data, that idioblast cell and laticifer cell contain catharanthine, serpentine and ajmalicine.

Cell-specific localization of TIAs in *C. roseus* stem tissue.

Imaging MS data showed that loganin and secologanin localized in the epidermal cell (Fig. 3). Single-cell MS showed the same localization for secologanin (Fig. 12). These iridoid metabolites have previously been shown to be synthesized in epidermal cell in *C. roseus* stem tissue (Dugé de Bernonville et al., 2015), and this has been confirmed using my metabolome analyses, too.

I was not able to ionize loganic acid and loganin in Single-cell MS. Although I could not semiquantify these substances, but I assumed that loganic acid was localized in IPAP cells from Imaging MS observation (Fig. 3A).

Imaging MS and Single-cell MS data also showed that most TIAs, including catharanthine (*m/z* 337.19), were localized in idioblast cell and laticifer cell (Table 4 and Figs. 3 and 13). These data contrast with previously published reports that showed most catharanthine localized in the wax layer of the leaf tissue (Roepke et al., 2010; Yu et al., 2013). The reasons for these differences are unclear but may reflect differences between cultivars or differences between stem and leaf tissue. The stem tissue has no clear wax layer. I do not detect substances in the wax layer.

When I measured extracts of both tissues with LC-MS, leaf tissue was found to contain more TIA metabolites than stem tissue (Table 1), which Góngora-Castillo et al. (2012) attributed to differences in expression levels of genes involved in TIA biosynthesis between stem and leaf tissues.

TIA synthesis and accumulation in *C. roseus* idioblast cells and laticifer cells.

It has been proposed that TIA synthesis initially occurs in IPAP cell, and then the products shift from IPAP cell to epidermal cell, parenchyma cell, idioblast cell and laticifer cell. It is proposed that loganic acid is transferred from IPAP cell to epidermal cell and 16-methoxytabersonine is transferred from epidermal cell to other cells at that time. This hypothesis is mainly based on *in situ* hybridization data of mRNAs of genes encoding enzymes involved in TIA synthesis (Dugé de Bernonville et al., 2015) rather than on the actual localization of TIA molecules themselves at the cellular level (Mersey et al., 1986).

The chemical compounds contained in idioblast cell and laticifer cell have not previously been accurately measured. To identify TIA compounds accumulated in idioblast cells, I used the recent technologies of Imaging MS and Single-cell MS. My measurements showed that most alkaloids are localized in idioblast cell and laticifer cell (Tables 4 and 5). These data are consistent with a previous report, which showed that serpentine, ajmalicine and vindoline accumulated in the idioblast fraction (Mersey et al., 1986), although the purity of their idioblast fraction was quite low. To our surprise, the present metabolome results showed that strictosidine also localized in idioblast cell and laticifer cell (Tables 4 and 5). Strictosidine might move from epidermal cell to idioblast cell and laticifer cell as soon as it is produced.

Movement of TIA intermediates between cells.

Imaging MS and Single-cell MS results revealed that many TIAs are localized in idioblast cell and laticifer cell. Catharanthine, whose presence was inferred from *m/z* 337.19, was detected in all types of cells. TIA intermediates, such as strictosidine, catharanthine and tabersonine, are proposed to be synthesized in epidermal cell, and further metabolism of these compounds occurs in the same cell (St-Pierre et al., 1999; Dugé de Bernonville et al., 2015). The present results lead to my presumption that catharanthine metabolism might not only occur in epidermal cell but may also be progressed in idioblast cell and laticifer cell.

Imaging MS and Single-cell MS data showed that loganin and secologanin localized in the epidermal cell (Figs. 3 and 12). These iridoid metabolites have previously been shown to be synthesized in epidermal cell in *C. roseus* stem tissue (Dugé de Bernonville et al., 2015), and this has been also confirmed by using my metabolome analyses.

Single-cell MS measurements suggested that TIA intermediates were accumulated in idioblast cell and laticifer cell (Fig. 12). If they are not synthesized in these cells, TIA intermediates must move from synthetic cells to other cells and accumulate in idioblast cell and laticifer cell. Because I could not detect an *m/z* value for strictosidine, which is produced by condensation of secologanin and tryptamine in epidermal cell, it is possible that strictosidine migrated to idioblast cell and laticifer cell immediately after synthesis. An *m/z* value corresponding to strictosidine (*m/z* 531.23) was detected in idioblast cell and laticifer cell, and I also obtained MS/MS fragment ion

peaks (*m/z* 144.08, 165.05, 282.11, 320.13, 334.14, 352.16, and 514.21), which are consistent with the speculated strictosidine MS/MS fragment ion peaks (Tables 3-5 and Fig. 9) (Brown et al., 2015). A compound peak at *m/z* 427.22 was detected in every type of cells (Tables 4 and 5). MS/MS fragment ions of this peak were similar to demethoxyvindoline (vindorosine) (Zhou et al., 2005), although I could not obtain a commercially available standard to verify this. I have tentatively assigned the *m/z* 427.22 peak as demethoxyvindoline, which accumulated in idioblast cell and laticifer cell (Fig. 12).

The complex distribution pattern of the TIA intermediates suggests that the enzymes responsible for synthesis are located in one cell type, but that the enzyme products are then moved to other cells. A catharanthine transporter responsible for efflux from epidermal cell to the wax layer in *C. roseus* leaf tissue has been already reported (Yu et al., 2013). It is also possible that symplasmic transport via plasmodesmata may drive movements of TIA intermediates between adjacent cells (Fig. 13). Further studies are needed to clarify how these compounds become distributed between the different cell types.

Material and method

Plant material and sample preparation.

C. roseus (L.) G Don (cv. Equator White Eye) was grown at 25 °C under 14 light/10 dark h white fluorescent light photoperiod in a growth chamber (NKsystem). Seeds were purchased from Sakata Seed Corporation.

Stem tissue of *C. roseus* was harvested from about 3-month-old plants just before experiments.

Observation of idioblast cells and laticifer cells with microscope.

Bright field and epifluorescence microscopy were performed on a Leica M205FA microscope (Leica Microsystems). Ultraviolet long pass filter (ET UV LP, Leica Microsystems) was used as the epifluorescence filter for observation of idioblast cells and laticifer cells.

Chemicals.

Commercially available TIA standards, catharanthine (Enzo Life Sciences), tabersonine HCl (AvaChem Scientific), ajmalicine (AdipoGen), serpentine hydrogen tartrate (ChromaDex), vindoline (ChromaDex) and vindoline-d3 (Tronto Research Chemicals) were used. One-parts-per-million (ppm) solutions of these chemicals were used as standards in LC-MS/MS analysis and infusion analysis with LTQ Orbitrap (LTQ Orbitrap Velos Pro; Thermo Fisher Scientific) used for the Single-cell MS (MS/MS) analysis.

Extraction of TIAs from *C. roseus* tissues.

C. roseus stem and leaf tissues were frozen with liquid nitrogen immediately after harvesting and ground to fine powder by frost shattering with Multibeads shocker (Yasui Kikai). Metabolites were extracted from the powdered sample with 1 mL extraction solution (0.5% formic acid and 1 ppm vindoline-d3 in methanol). Samples were lyophilized with a freeze-dryer (Model 77400; Labconco Co.) and stored at -80 °C until measurement.

LC-MS analysis.

Crude extracts of *C. roseus* stem and leaf tissues were analyzed by LC-MS (Prominence). The mobile phases A and B were 25 mM ammonium acetate and acetonitrile, respectively. The ratio of solvent A to B was isocratic at 20 : 80. TIAs were separated by reverse-phase octadecylsilyl (ODS) column (Eclipse XDB-C18, 5 μm, 4.6×150 mm; Agilent). The flow rate was 0.25 mL min^{-1} at 40 °C. I used vindoline-d3 as an internal standard for quantification of TIA intermediates.

Mass spectrometric detection was performed on LTQ-Orbitrap (LTQ Orbitrap Velos Pro; Thermo Fisher Scientific) mounted on ESI ion source. The spray voltage for positive measurement was 3,800 V. Target mass peaks were detected in ± 5 ppm.

Imaging MS.

Longitudinal sections (100 μm thickness) of *C. roseus* stem were prepared with a microtome (Plant Microtome MTH-1; NKsystem) and visually inspected with a

fluorescent stereoscopic microscope (M250FA; Leica Microsystems). Suitable sections were then washed with MilliQ water to remove alkaloid contamination from dead cells and mounted on Indium Tin Oxide glass slides (Luminescence Technology Co.) using Cryoglue type I (SECTION-LAB Co. Ltd.). The samples on glass slides were lyophilized by freeze-drying (Model 77400; Labconco Co.) then sublimated by α-cyano-4-hydroxycinnamic acid with a conductive glass using a sublimation apparatus (ChemGlass CG-3038; ChemGlass Life Sciences). Mass spectrometric detection was performed on Fourier transform ion cyclotron resonance mass spectrometry (FT-ICRMS) (APEX-Qe 9.4T with dual source; Bruker Daltonics Inc.). The space resolution of Imaging MS was 20 μm. MS images were reconstituted using an in-house software called LabMSI (Takahashi et al., 2015). Target mass peaks were detected in a bin size = 0.02.

Infusion analysis with LTQ-Orbitrap.

Stem extracts were prepared as described in the procedure for LC-MS analysis. Stem extract (3 μL) was transferred to a nano-electrospray tip (1 μm, Humanix) from the bottom. The tip was then set on the nano-electrospray ionization (nano-ESI) ion source attachment. Mass spectrometric detection was performed on LTQ Orbitrap Velos Pro. The spray voltage for positive measurement was 1,000 V. Alkaloid detection was performed in the range of *m/z* 100-1,000 and *m/z* 385-550. The spectrometer was calibrated by polytyrosine (CS Bio) before experiments. MS/MS analyses of alkaloids with known standards were also conducted. Data analysis was conducted using Xcalibur

software (Thermo Fisher Scientific). Target mass peaks were detected in ± 5 ppm range, relative to the theoretical mass of TIA.

Single-cell MS in *C. roseus* stem tissue.

To identify cell-specific alkaloid localizations, I used live single-cell video mass spectrometry, termed "Single-cell MS" analysis (Mizuno et al., 2008). Longitudinal sections (100 μm thickness) of the stem were prepared with a microtome (Plant Microtome MTH-1; NKsystem), washed with ultrapure water to remove alkaloid contamination, and specimens were then mounted on a glass slide fixed with double-faced adhesive tape and monitored with a stereomicroscope (M205FA; Leica Microsystems). The contents of single cells from four different cell types, namely idioblast cells, laticifer cells, parenchyma cells and epidermal cells, were sucked into a gold-coated glass capillary nano-electrospray tip via tubing using a syringe under the stereoscopic microscope (Fig. 4). After the addition of 3 μL of ionization solvent (0.5% formic acid in methanol) into the nanoelectrospray tip from the bottom, the tip was set on a nano-ESI ion source attachment. Mass spectrometric detection was performed on LTQ Orbitrap Velos Pro. The spray voltage for positive measurement was 1,000 V. Alkaloid and secologanin detection was mainly performed in the range of *m/z* 100-1,000. Strictosidine was detected in the range of *m/z* 385-550 in samples. The spectrometer was calibrated with polytyrosine before experiments. Data analysis was conducted by using Xcalibur software. Target mass peaks were detected within ± 5 ppm, compared with the theoretical mass. Because no isomers of serpentine (alstonine),

demethoxyvindoline and strictosidine were found in the extract of whole stem tissue by LC-MS analysis, I quantified these alkaloids in each of the four kinds of cell types by semiquantitative calculation using Single-cell MS data on *m/z* intensity values of 349.15, 389.14, 427.22 and 531.23, which were normalized to values of the total ion intensities (y axis of Fig. 12 shows percent of intensity normalized by the value of the total ion intensities).

PCA analysis.

Principal component analysis (PCA) of both technologies was conducted with MarkerView software (version1.2.1; AB Sciex) on 12 samples (three samples per cell type) for grouping each cell type (idioblast cell, laticifer cell, parenchyma cell and epidermal cell). I used total peaks, which were selected under the condition signal-to-noise ratio $\geqq$ 3.

Figure and Table

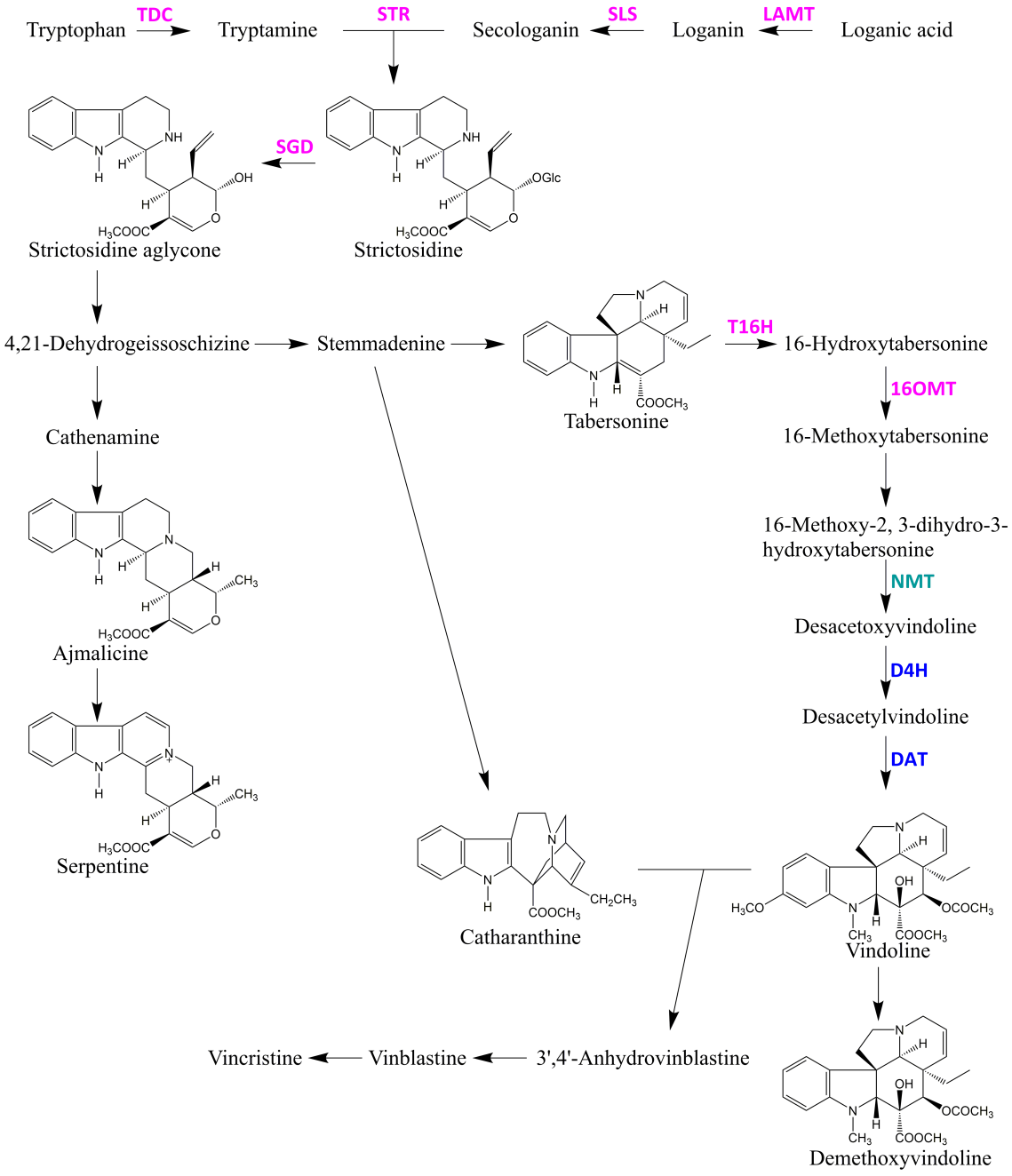

Fig. 2. TIA metabolic pathway in *Catharanthus roseus*. Purple font represents TIA enzymes localized in epidermal cells. Green represents the TIA enzyme localized in parenchyma cells. Blue represents TIA enzymes localized in idioblast cells and laticifer cells.

Abbreviation, LAMT : Loganic acid O-methyltransferase, SLS : Secologanin synthase, TDC : Tryptophan decarboxylase, STR : Strictosidine synthase, SGD : Strictosidine β-glucosidase, T16H : Tabersonine 16-hydroxylase, 16OMT : 16-Hydroxytabersonine O-methyltransferase, NMT : 16-Methoxy-2,3-dihydro-3-hydroxy-tabersonine N-methyltransferase, D4H : Desacetoxyvindoline 4-hydroxylase, DAT : Deacetylvindoline 4-O-acetyltransferase.

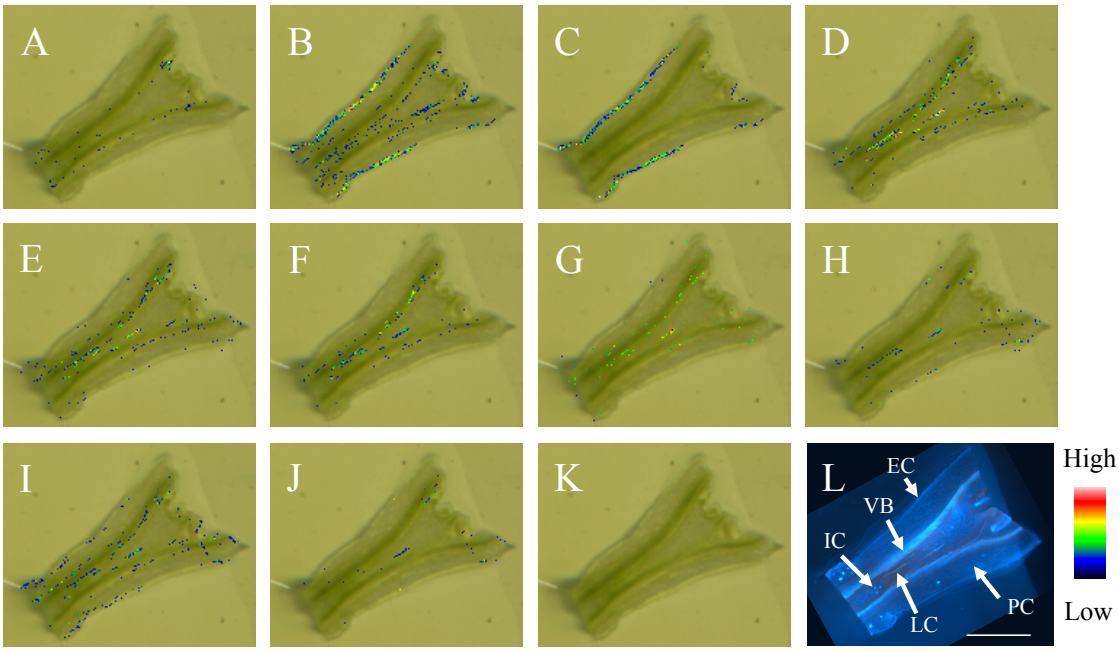

Fig. 3. MS images of *C. roseus* stem longitudinal section. Most TIA localized in idioblast cell and laticifer cell. (A) *m/z* 415.1001 (Loganic acid). (B) *m/z* 429.1157 (Loganin). (C) *m/z* 427.1001 (Secologanin). (D) *m/z* 351.1703 (Cathenamine). (E) *m/z* 353.1859 (Ajmalicine). (F) *m/z* 349.1546 (Serpentine). (G) *m/z* 355.2016 (Stemmadenine). (H) *m/z* 367.2016 (16-Methoxytabersonine). (I) *m/z* 337.1910 (Catharanthine). (J) *m/z* 427.2227 (Demethoxyvindoline). (K) MS image control. (L) Longitudinal section excited by UV. Color bar represents MS signal intensity. Scale bar = 1 mm.

Abbreviation, IC : Idioblast cell, LC : Laticifer cell, PC : Parenchyma cell, EC : Epidermal cell, VB : Vascular bundle.

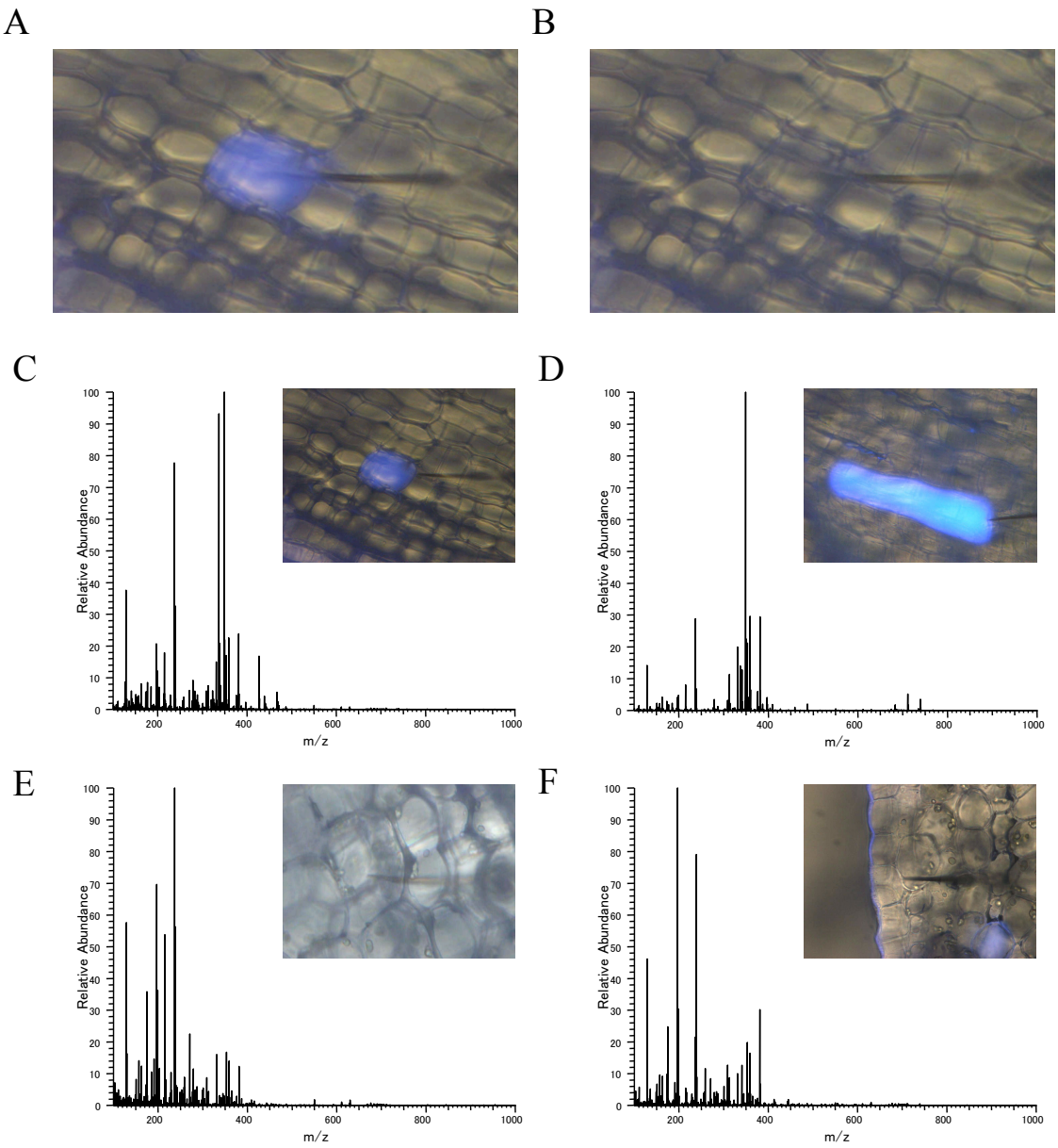

Fig. 4. Sampling of the four types of cells contents with nano-electrospray tip. (A) Idioblast cell emitting blue fluorescence under UV excitation, before sampling. (B) The same cell after contents were sucked up with nano-electrospray tip. (C) Idioblast cell. (D) Laticifer cell. (E) Parenchyma cell. (F) Epidermal cell.

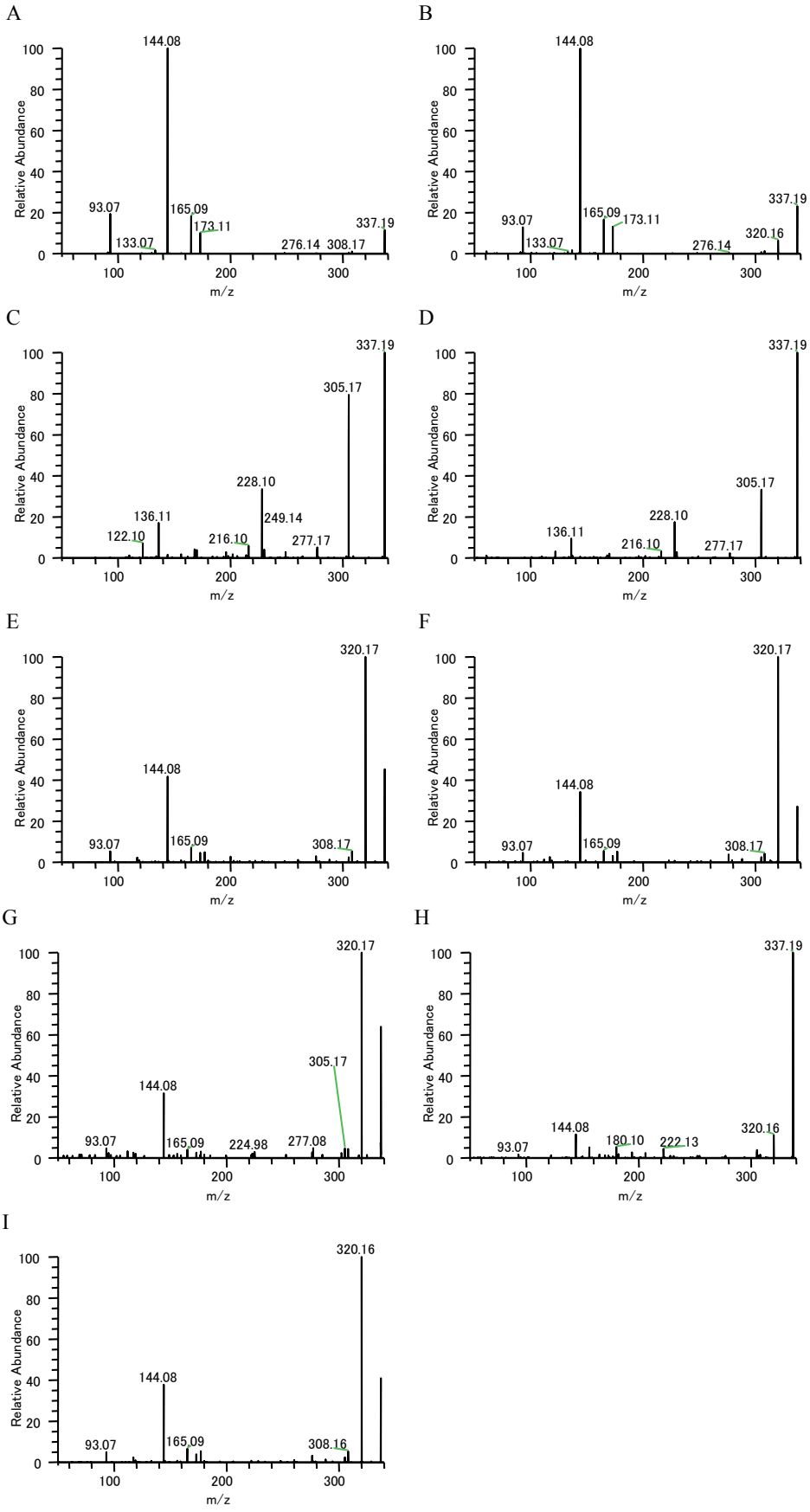
A
144.08
93.07
165.09
173.11
133.07
276.14
308.17
337.19
B
144.08
93.07
165.09
173.11
133.07
276.14
320.16
337.19
C
337.19
305.17
228.10
136.11
249.14
122.10
216.10
277.17
D
337.19
305.17
228.10
136.11
216.10
277.17
E
320.17
144.08
93.07
165.09
308.17
F
320.17
144.08
93.07
165.09
308.17
G
320.17
305.17
144.08
93.07
165.09
224.98
277.08
H
337.19
144.08
180.10
222.13
320.16
93.07
I
320.16
144.08
93.07
165.09
308.16
Relative Abundance
m/z

Fig. 5. MS/MS analysis of *m/z* 337.19. (A) Catharanthine standard (LC-MS). (B) Catharanthine standard (Infusion). (C) Tabersonine standard (LC-MS). (D) Tabersonine standard (Infusion). (E) Idioblast cell sample (Single-cell MS). (F) Laticifer cell sample (Single-cell MS). (G) Parenchyma cell (Single-cell MS). (H) Epidermal cell (Single-cell MS). (I) Stem sample *m/z* 337.19 specific MS/MS fragment (Infusion).

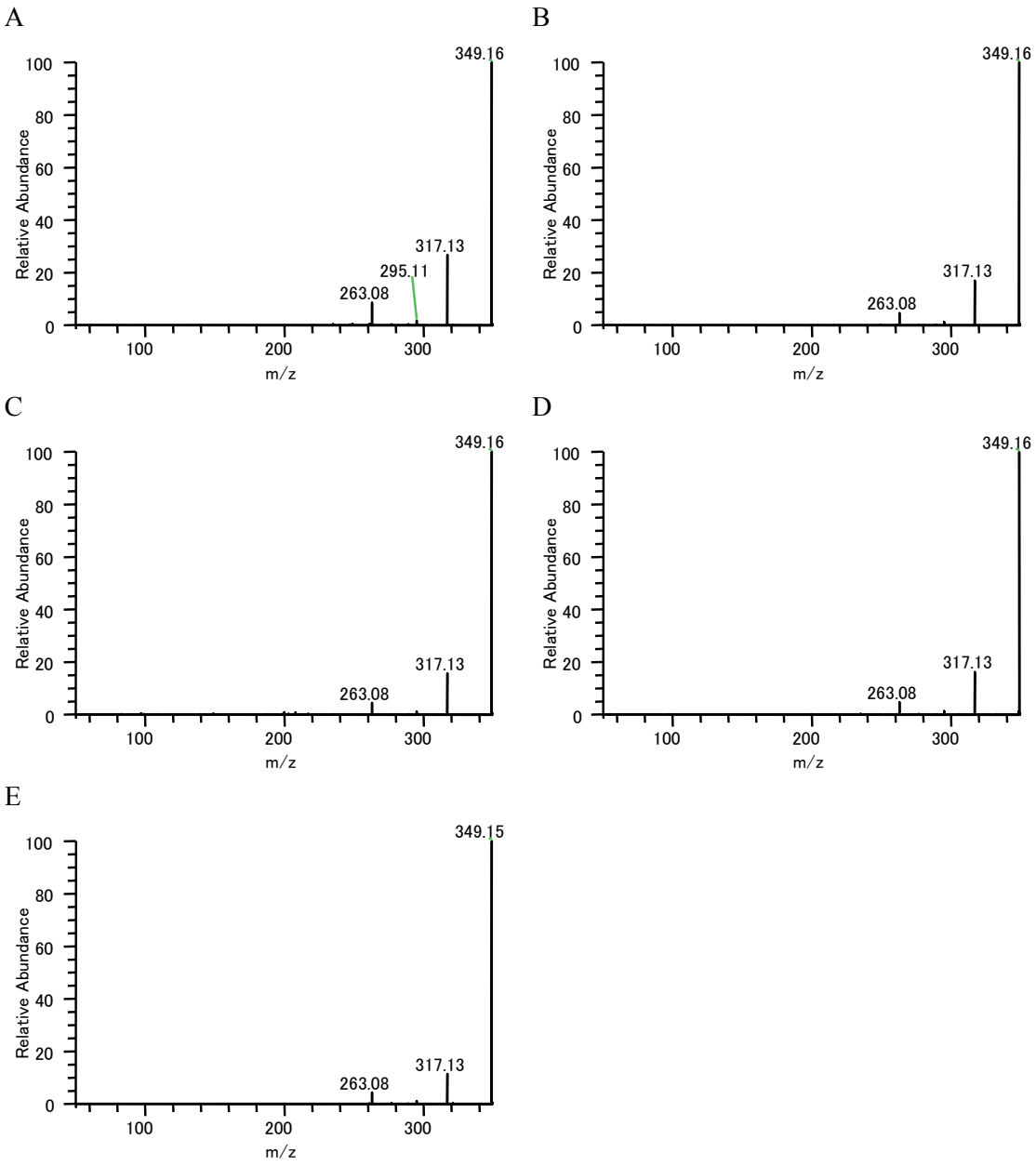

Fig. 6. MS/MS analysis of *m/z* 349.15. (A) Serpentine standard (LC-MS). (B) Serpentine standard (Infusion). (C) Idioblast cell sample (Single-cell MS). (D) Laticifer cell sample (Single-cell MS). (E) Stem sample *m/z* 349.15 specific MS/MS fragment (Infusion).

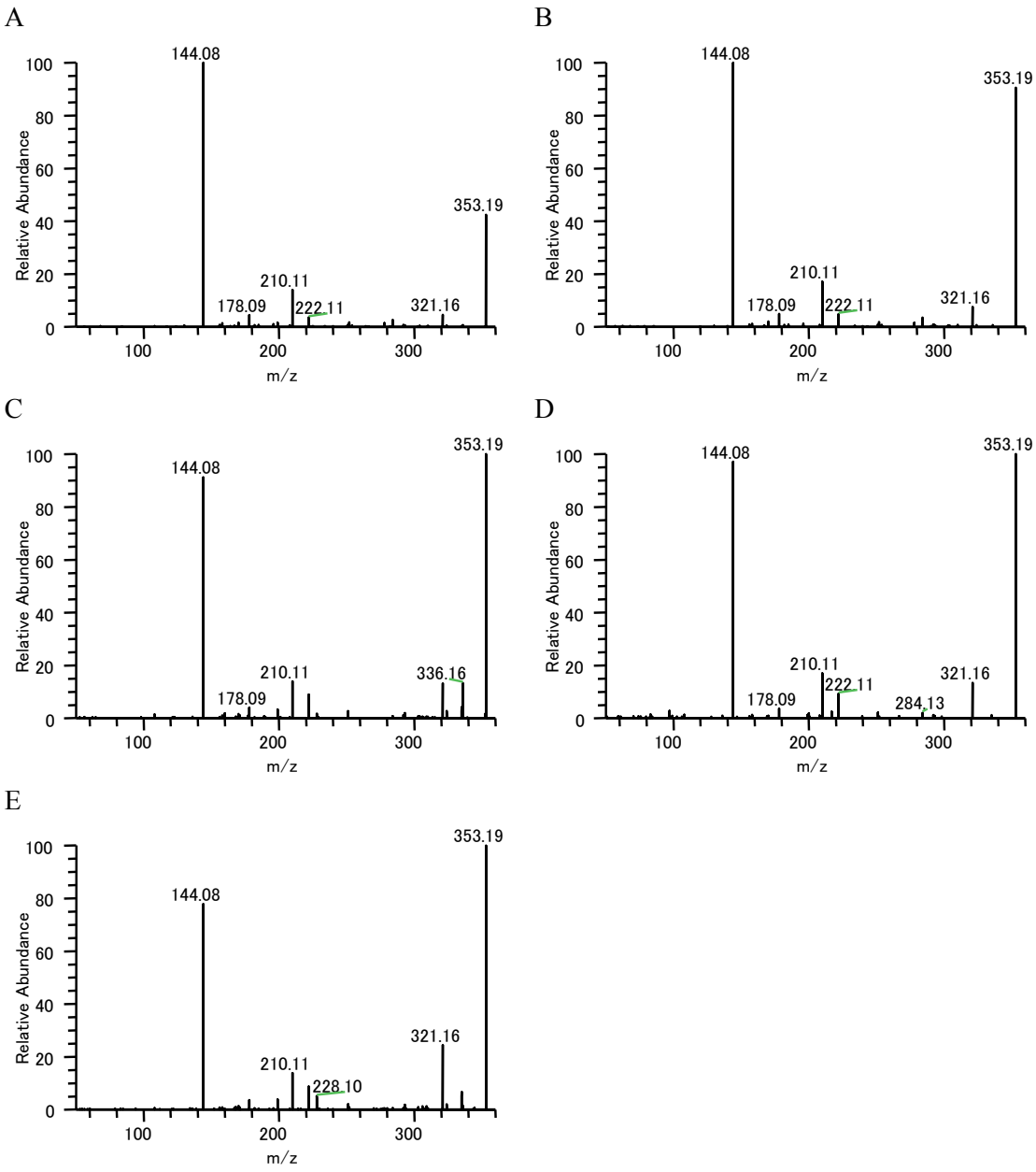

Fig. 7. MS/MS analysis of *m/z* 353.18. (A) Ajmalicine standard (LC-MS). (B) Ajmalicine standard (Infusion). (C) Idioblast cell sample (Single-cell MS). (D) Laticifer cell sample (Single-cell MS). (E) Stem sample *m/z* 353.18 specific MS/MS fragment (Infusion).

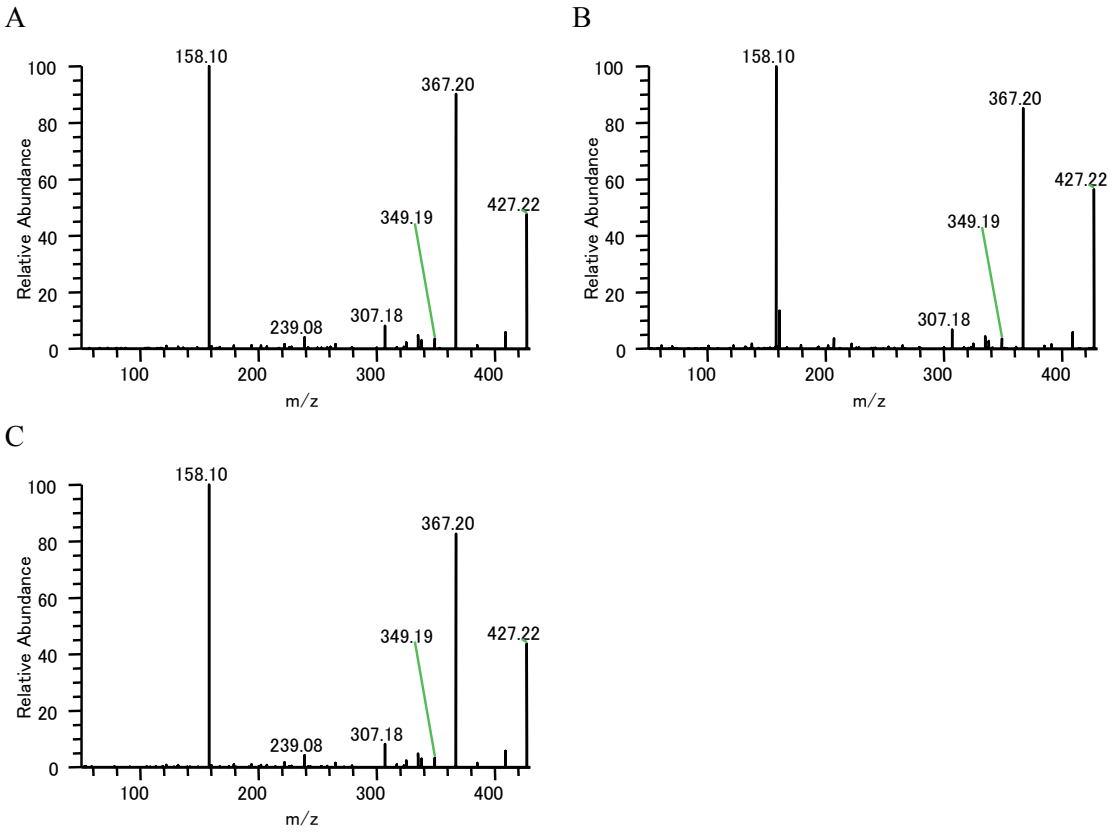

Fig. 8. MS/MS analysis of *m/z* 427.22. (A) Idioblast cell sample (Single-cell MS). (B) Laticifer cell sample (Single-cell MS). (C) Stem sample *m/z* 427.22 specific MS/MS fragment (Infusion).

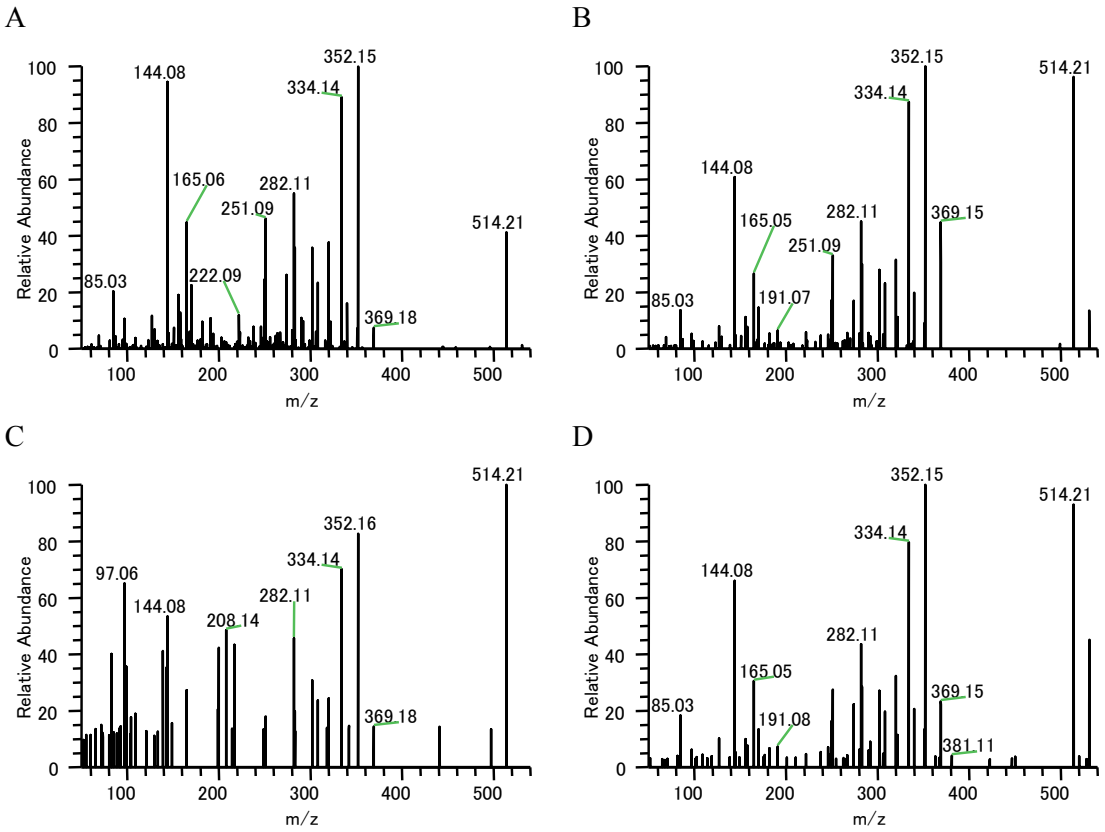

Fig. 9. MS/MS analysis of *m/z* 531.23. (A) Stem sample *m/z* 531.23 specific MS/MS fragment (LC-MS). (B) Idioblast cell sample (Single-cell MS). (C) Laticifer cell sample (Single-cell MS). (D) Stem sample *m/z* 531.23 specific MS/MS fragment (Infusion).

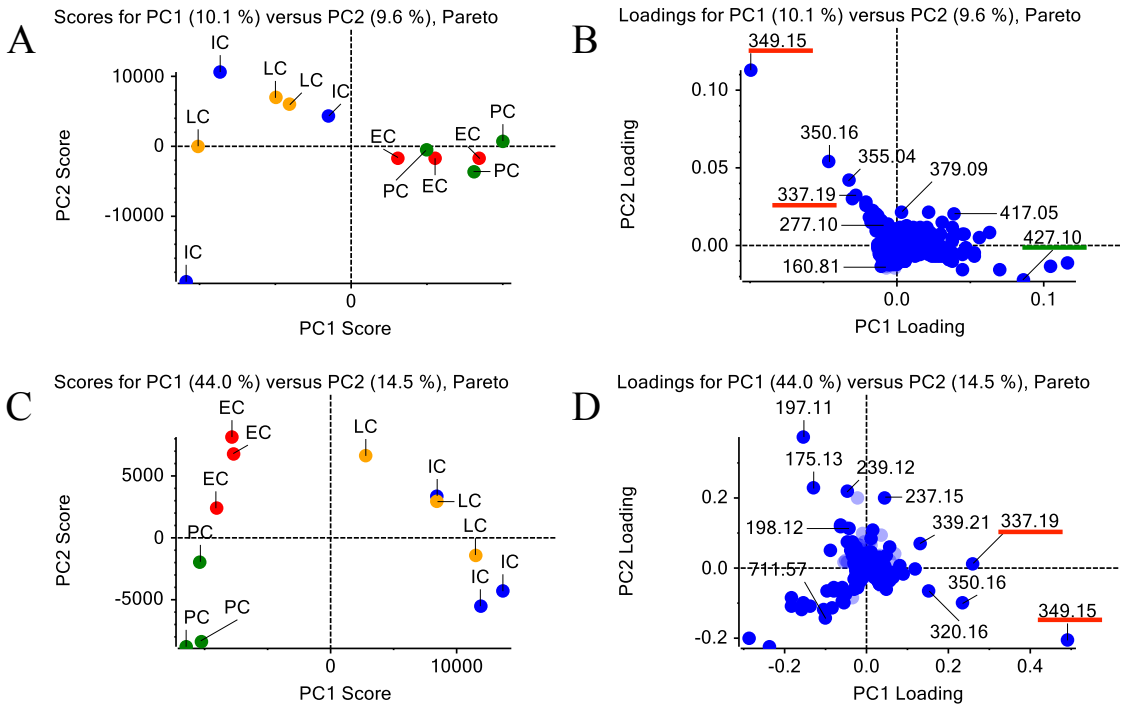

Fig. 10. PCA of metabolome data according to cell type. (A) PCA derived from intensities of idioblast cell, laticifer cell, parenchyma cell and epidermal cell samples in Imaging MS analysis. (B) PC loadings derived from all *m/z* peaks of idioblast cell, laticifer cell, parenchyma cell and epidermal cell samples in Imaging MS analysis. (C) PCA derived from intensities of idioblast cell, laticifer cell, parenchyma cell and epidermal cell samples in Single-cell MS analysis. (D) PC loadings derived from all *m/z* peaks of idioblast cell, laticifer cell, parenchyma cell and epidermal cell samples in Single-cell MS analysis. (B and D) Blue points show monoisotopic and isotope data, and pale blue points show undefined data. Many TIA compounds were detected from idioblast cell and laticifer cell spectra. Red underbar shows TIA related ion peak. Green underbar shows iridoid related ion peak.

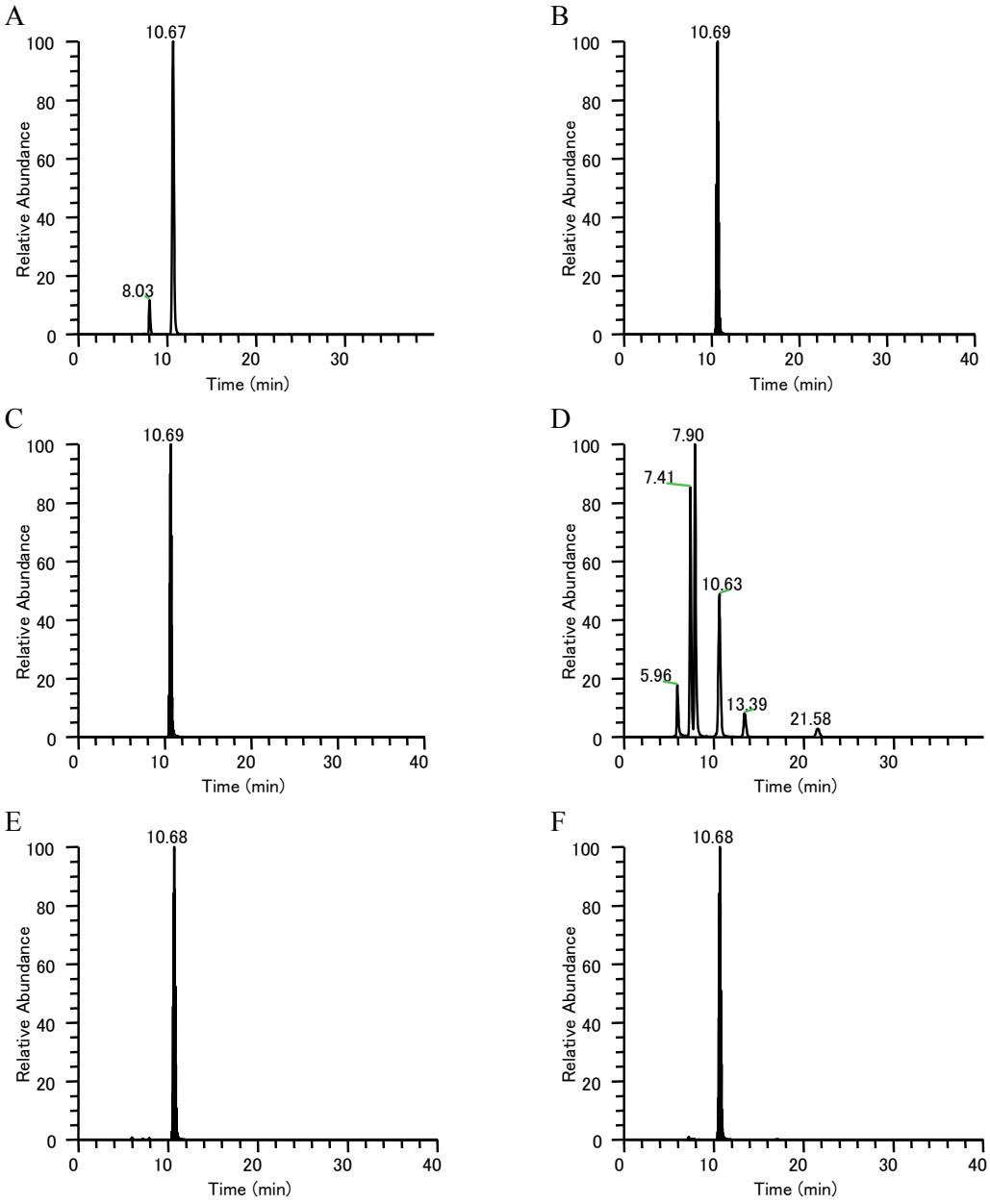

Fig. 11. LC chromatogram of catharanthine specific MS/MS fragment. (A) LC chromatogram of catharanthine standard (LC-MS). (B) Extracted chromatogram of catharanthine standard specific MS/MS fragment ion (*m/z* 93.07). (C) Extracted chromatogram of catharanthine standard specific MS/MS fragment ion (*m/z* 133.07). (D) Extracted chromatogram of stem sample (*m/z* 337.19). (E) Extracted chromatogram of stem sample of catharanthine specific MS/MS fragment ion (*m/z* 93.07). (F)

Extracted chromatogram of stem sample of catharanthine specific MS/MS fragment ion (*m/z* 133.07).

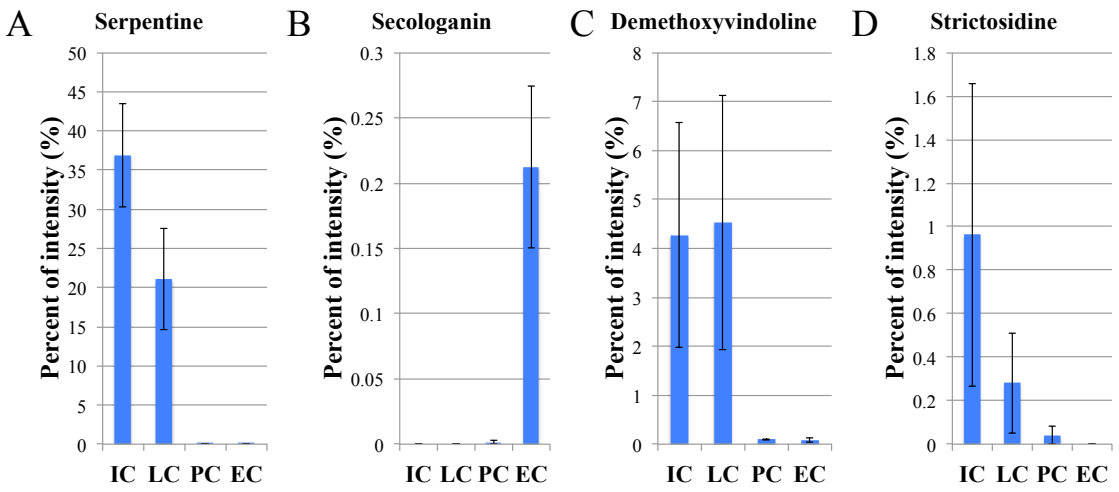

Fig. 12. Semiquantitative analysis of TIAs calculated by Single-cell MS analysis data. (A) Serpentine was detected in idioblast cell and laticifer cell (*m/z* 349.15). (B) Secologanin was detected in epidermal cell (*m/z* 389.14). (C) Demethoxyvindoline was detected in all cell types (*m/z* 427.22). (D) Strictosidine was detected in idioblast cell and laticifer cell (*m/z* 531.23). The y axis shows percent of intensity normalized by the value of the total ion intensity of each sample. Values are the mean of three measurements (± SEM).

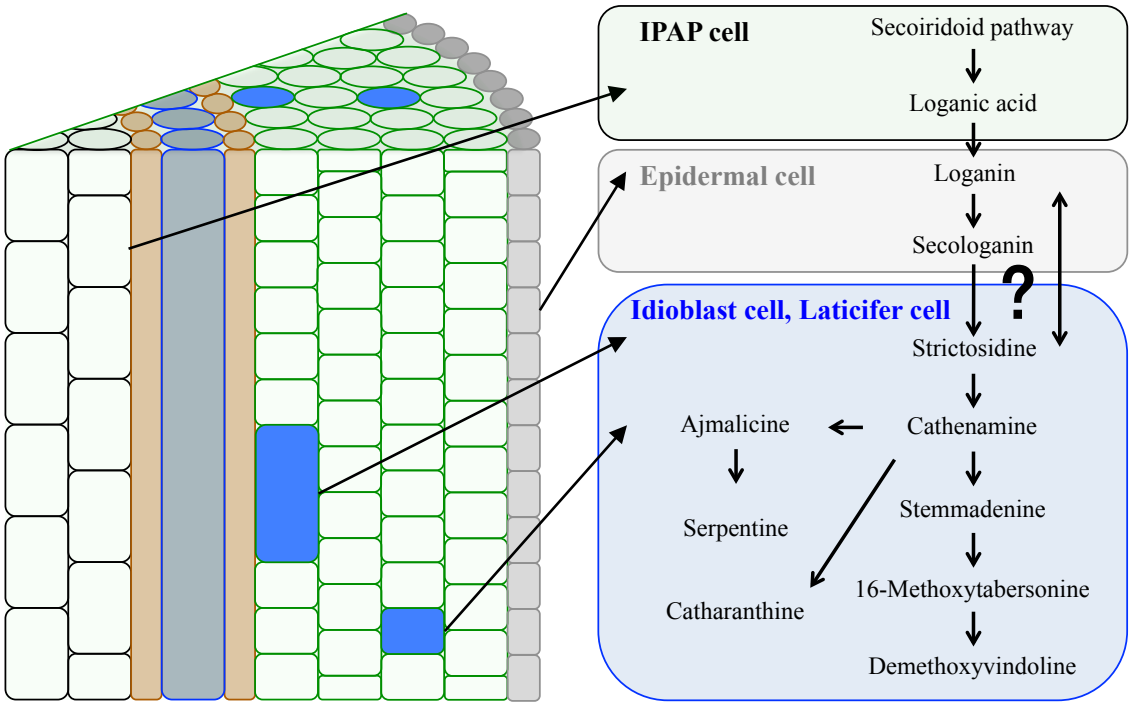

Fig. 13. Cell-specific localization of TIA in *C. roseus* stem tissue. Most TIA localized in the idioblast cells and laticifer cells.

Table 1. TIA detected by LC-MS analysis of stem tissue samples

Molecular Formula	[M+H]+	measured *m/z*	Delta ppm	Stem tissue	Retention time of sample (min)	Compound	Retention time of standard (min)	Alkaloid content in stem (μg/mg FW)	Alkaloid content in leaf (μg/mg FW)
C21H24N2O2	337.191054	337.19104	-0.04	○	5.96, 7.41, 7.90, 10.63, 13.39, 21.58	Catharanthine	10.67	0.506±0.044	5.199±0.260
C21H24N2O2	337.191054	337.19080	-0.75	○	5.96, 7.41, 7.90, 10.63, 13.39, 21.58	Tabersonine	21.47	0.017±0.003	0.286±0.024
C21H20N2O3	349.154668	349.15421	-1.31	○	6.06	Serpentine	6.04	0.397±0.031	0.037±0.006
C21H22N2O3	351.170318	351.17023	-0.25	○	5.69, 7.41, 7.85, 8.71, 11.02				
C21H24N2O3	353.185968	353.18600	0.09	○	5.77, 6.64, 7.13, 7.52, 8.31, 9.79, 12.11, 13.88	Ajmalicine	9.77	0.071±0.022	0.169±0.007
C21H26N2O3	355.201618	355.20135	-0.75	○	5.77, 6.39, 6.89, 7.41, 10.27, 11.91, 13.20				
C22H26N2O3	367.201618	367.20166	0.11	○	6.75, 8.82, 16.98, 20.13				
C21H24N2O4	369.180883	369.18054	-0.93	○	4.87, 5.58, 6.33, 6.89, 7.82				
C22H28N2O4	385.212183	385.21188	-0.79	○	6.33, 6.99, 8.23, 9.03, 9.51				
C23H30N2O4	399.227833	399.22714	-1.74	○	10.38				
C23H30N2O5	415.222748	415.22238	-0.89	○	6.30, 7.63				
C24H30N2O5	427.222748	427.22272	-0.07	○	8.82				
C25H32N2O6	457.233312	457.23367	0.78	○	8.23	Vindoline	8.24	0.0026±0.0002	1.6470±0.071
C27H34N2O9	531.233706	531.23389	0.35	○	5.25				

○ : Chemical compound exists in the stem tissues (n=3). Retention time : Mass specific peaks in the stem tissue.

Table 2. Iridoid detected by LC-MS analysis of stem tissue samples

Molecular Formula	Monoisotopic mass	[M+H]+ (measured m/z) Delta ppm	Stem tissue [H+]	[M+Na]+ (measured m/z) Delta ppm	Stem tissue [Na+]	[M+K]+ (measured m/z) Delta ppm	Stem tissue [K+]	Speculated Compound
C16H24O10	376.136946	377.144222 (377.14420) -0.06	○	399.126164 (399.12619) 0.07	○	415.100104 (415.10007) -0.08	○	Loganic acid
C17H24O10	388.136946	389.144222 (389.14426) -0.10	○	411.126164 (411.12631) 0.36	○	427.100104 (427.10022) 0.27	○	Secologanin
C17H26O10	390.152597	391.159873 (391.15988) 0.02	○	413.141815 (413.14188) 0.16	○	429.115755 (429.11603) 0.64	○	Loganin

○ : Chemical compound exist in the stem tissues (n=3). Monoisotopic mass was calculated from molecular formula of TIA.

Table 3. LC-MS/MS analysis of whole stem data

Compound	[M+H]+	MS/MS fragments of stem tissue (%)	MS/MS fragments of standard (%)
Catharanthine	337.191054	93.07(18), 133.07(2), 144.08(100), 165.09(18), 173.11(10), 337.19(12)	93.07(18), 133.07(2), 144.08(100), 165.09(17), 173.11(9), 337.19(12)
Tabersonine	337.191054	122.10(6), 136.11(18), 168.08(5), 170.10(4), 216.10(6), 228.10(33), 230.12(4), 249.14(3), 277.17(5), 305.17(76), 337.19(100)	122.10(7), 136.11(17), 168.08(4), 170.10(4), 216.10(6), 228.10(33), 230.12(4), 249.14(3), 277.17(5), 305.17(81), 337.19(100)
Serpentine	349.154668	263.08(7), 295.11(2), 317.13(18), 349.16(100)	263.08(9), 295.11(2), 317.13(28), 349.16(100)
Ajmalicine	353.185968	144.08(100), 178.09(4), 210.11(14), 222.11(21), 321.16(21), 335.18(3), 353.19(56)	144.08(100), 178.09(4), 210.11(14), 222.11(3), 321.16(5), 353.19(43)
Demethoxyvindoline	427.222748	158.10(100), 307.18(5), 325.19(2), 335.17(3), 349.19(2), 367.20(41), 409.21(2), 427.22(11)	*143, 158, 367, 409, 427
Vindoline	457.233312	162.09(3), 188.11(100), 222.11(3), 337.19(4), 397.21(23), 457.23(7)	162.09(2), 188.11(100), 222.11(3), 337.19(4), 397.21(24), 457.23(8)
Strictosidine	531.233706	144.08(93), 165.05(43), 170.10(23), 250.09(25), 251.09(46), 274.12(25), 282.11(55), 283.12(35), 302.12(36), 308.13(23), 320.13(38), 334.14(89), 352.15(100), 514.21(40)	**139.04, 144.08, 165.05, 170.09, 181.09, 222.09, 250.09, 282.12, 302.12, 320.13, 334.14, 352.15, 514.21

* : MS/MS fragments of demethoxyvindoline was cited by Zhou et al. (2005). ** : MS/MS fragments of strictosidine was cited by Brown et al. (2015).

Table 4. TIA detected by Single cell MS analysis (mass range *m/z* = 100-1000)

Molecular Formula	[M+H]+	measured m/z	Delta ppm	Stem tissue	IC	LC	PC	EC	Speculated compound
C21H24N2O2	337.191054	337.19097	-0.25	○	○	○	○	○	Catharanthine
C21H20N2O3	349.154668	349.15456	-0.31	○	○	○			Serpentine
C21H22N2O3	351.170318	351.16950	-2.33	○	○	○			Cathenamine
C21H24N2O3	353.185968	353.18578	-0.53	○	○	○			Ajmalicine
C21H26N2O3	355.201618	355.20129	-0.92	○	○	○			Stemmadenine
C22H26N2O3	367.201618	367.20096	-1.79	○	○	○			16-Methoxytabersonine
C21H24N2O4	369.180883	369.18066	-0.60	○	○	○			Horhammericine
C22H28N2O4	385.212183	385.21165	-1.38	○					16-Methoxy-2,3-dihydro-3-hydroxytabersonine
C24H30N2O5	427.222748	427.22248	-0.63	○	○	○			Demetoxyvindoline
C25H32N2O6	457.233312	457.23253	-1.71	○					Vindoline
C27H34N2O9	531.233706	531.23268	-1.93		○				Strictosidine

○ : Chemical compound exists in stem tissue each cell type (n=3).

Table 5. TIA detected by Single cell MS analysis (mass range *m/z* = 385-550)

Molecular Formula	[M+H]+	measured m/z	Delta ppm	Stem tissue	IC	LC	PC	EC	Speculated Compound
C22H28N2O4	385.212183	385.21191	-0.71	○	○	○			16-Methoxy-2,3-dihydro-3-hydroxytabersonine
C23H30N2O5	415.222748	415.22254	-0.50	○					Deacetylvindoline
C24H30N2O5	427.222748	427.22244	-0.72	○	○	○	○	○	Demetoxyvindoline
C25H32N2O6	457.233312	457.23420	1.94	○					Vindoline
C27H34N2O9	531.233706	531.23262	-2.04	○	○	○			Strictosidine

○ : Chemical compound exists in stem tissue each cell type (n=3).

Chapter 2

Cell-specific TIA localization in *Catharanthus roseus* leaf tissue

Chapter 2 :

Cell-specific TIA localization in *Catharanthus roseus* leaf tissue

Summary

Catharanthus roseus (L.) G. Don is a medicinal plant well known for producing bioactive compounds such as vinblastine and vincristine, which are classified as terpenoid indole alkaloids (TIAs). Although the gene expressions of TIA producing enzymes have been studied well in *C. roseus* suspension-cultured cell and leaf tissue, the localization of TIA intermediates at the cellular level in the leaf tissue has not been revealed directly. In this chapter, I have succeeded in showing cell-specific TIA localization in *C. roseus* leaf tissue in addition to the stem tissue shown in Chapter 1, with Imaging MS and Single-cell MS. These metabolomic studies revealed that most iridoid compounds localized in epidermal cells, but major TIAs including serpentine and vindoline localized in idioblast cell and laticifer cell. Interestingly, strictosidine and catharanthine are also accumulated in *C. roseus* among epidermal cell, idioblast cell and laticifer cell. Moreover, I measured metabolome data in laticifer cells of leaf primordium. Comparing the present metabolome data to our former analysis of the stem tissue, I found that TIA biosynthesis in idioblast cell might be differentiated dependent on the different tissues or growth stages of the same tissue.

Introduction

Catharanthus roseus (L.) G. Don (Apocynaceae) is one of the best-characterized Terpenoid indole alkaloids (TIA) producing plants (Van Der Heijden et al., 2004; Gigant et al., 2005; Kavallaris, 2010). Leaf extracts of *C. roseus* have still been the sole source of vindoline and catharanthine, both of which are monomeric precursors for the commercial production of vinblastine (O'Keefe et al., 1997).

The current understanding of TIA metabolism in *C. roseus*, which has been mainly deduced from studies on leaf tissues, was shown in the previous section, that is, iridoid metabolism begins in IPAP cells and that loganic acid produced in IPAP cells is transferred to epidermal cells. Further synthesis involving secologanin and strictosidine also occurs in the epidermal cells. Finally, a TIA intermediate, desacetoxyvindoline moves to the idioblast cell or/and laticifer cell and TIAs are accumulated in the vacuole of those cells (Fig. 14) (Yoder et al., 1976; Burlat et al., 2004; Dugé de Bernonville et al., 2015).

In Chapter 1, I have shown the cell-specific localization of intermediates of TIA metabolism in the stem tissue in *C. roseus*, using Imaging MS and Single-cell MS (Yamamoto et al., 2016). In this measurement, loganin and secologanin are localized in the epidermal cells similar to localization of iridoid biosynthetic enzymes (LAMT : Loganate O-methyltransferase, SLS : Secologanin synthase). Most of TIAs including strictosidine and serpentine, however, localized in both idioblast cells and laticifer cells of *C. roseus* stem tissue (Yamamoto et al., 2016). The new aspect of localization of TIAs in *C. roseus* stem tissue made us suppose that the TIA pathway localization in the

stem tissue might be different in the leaf tissue. Thus far, the actual localization of TIA intermediates at the cellular level has not been directly measured in *C. roseus* leaf tissues.

In this chapter, I have applied cutting-edge methods of Imaging MS and Single-cell MS for detecting metabolites *in situ* at the cellular level in leaf tissue of *C. roseus* as well as the stem tissue conducted in Yamamoto et al. (2016). Since leaf cell size is much smaller than that of stem tissue, spatial resolution caused technical difficulties to detect metabolites at the cellular level. By improving methods of laser irradiation for Imaging MS and of micro-capillary and video-assisted system for Single-cell MS, I elucidated cell-specific TIA localization in leaf tissue of *C. roseus*.

Result

Localization of idioblast cells and laticifer cells in *C. roseus* leaf tissue.

C. roseus leaf tissue is composed of various types of cells : Leaf primordium laticifer cell (LPLC), Internal phloem associated parenchyma cell (IPAP), Leaf epidermal cell (LEC), Palisade tissue parenchyma cell (PTPC), Spongy tissue parenchyma cell (STPC), Palisade tissue idioblast cell (PTIC), Spongy tissue idioblast cell (STIC), Leaf laticifer cell (LLC) (Fig. 15). In the cross sections, idioblast cells were randomly found in parenchyma tissues and elongated laticifer cells were localized near the vascular bundles (xylem) (Fig. 15). Idioblast cells and laticifer cells were easily distinguishable from parenchyma cells by blue autofluorescence emitted from the chemical compounds accumulated in these cells when the specimen was excited by UV (Mersey et al., 1986; Carqueijeiro et al., 2016). The autofluorescence of laticifer cells derived from serpentine was observed in leaf primordium (Fig. 15). Morphogenesis of both idioblast cells and laticifer cells started at the leaf primordium and the number of idioblast cells and laticifer cells increased as leaf expands (Fig. 15).

Imaging MS analysis in *C. roseus* leaf cross-section.

When I investigated the localization of TIAs in *C. roseus* stem tissue with the Imaging MS, I measured it with 20 μm spatial resolution, because the size of cells in the stem tissue is much larger than that of cells in the leaf tissue. Diameter of leaf cells, such as epidermal cell, is about 10 μm. When I measured leaf tissues with 20 μm spatial resolution, I could identify where those compounds localized in leaf sections, but it is

difficult to distinguish which kinds of cells TIAs localized (Fig. 16). In order to study the localization of TIA in the leaf tissue precisely, I need to improve spatial resolution (10 μm) of Imaging MS analysis by adjusting laser diameter and strength, compared to the data obtained when I measured longitudinal section of *C. roseus* stem tissue. By the improvement of laser radiation system by Dr. Takahashi's excellent technique, I succeeded in detecting various TIA compounds in leaf tissue precisely, although total ions created by MALDI ionization decreased (Figs. 16 and 17).

In this experiment, I have detected that loganic acid clearly localized near the vascular bundle and epidermal cells (Fig. 17A). Previous report suggested that catharanthine, strictosidine, loganin and secologanin localized in the epidermal cells. However, my results showed that most TIAs including catharanthine and strictosidine also localized in the idioblast cells (Fig. 16). Although it has been proposed that most TIAs were synthesized in the epidermal cells based on the *in situ* hybridization experiments (Fig. 14) (St-Pierre et al., 1999), MS images revealed that various TIAs, including vindoline, ajmalicine and serpentine, were accumulated not in the epidermal cell but in the idioblast cell and laticifer cell (Figs. 16 and 17*)*.

Single-cell MS analysis in *C. roseus* leaf tissue.

In order to obtain quantitative data and MS/MS spectrum data of various TIAs that complement the results of Imaging MS, I conducted Single-cell MS analyses on internal phloem associated parenchyma cell (IPAP), Leaf epidermal cell (LEC), Palisade tissue parenchyma cell (PTPC), Spongy tissue parenchyma cell (STPC), Palisade tissue

idioblast cell (PTIC), Spongy tissue idioblast cell (STIC), and Leaf laticifer cell (LLC) (Fig. 15). When I measured cell contents in *C. roseus* stem tissue, I detected unstable ionization time which means the detection time decreased the intensities of peaks because of nano-electrospray method. This nano-electrospray analysis is unstable compared to the conventional electrospray analysis. In this study, I attempted to add external standard in elution buffer (0.5% formic acid in methanol solved 1 ppm vindoline-d3) so as to correct the observational error dependent on the nano-spray analysis.

I conducted target mass analysis of *C. roseus* TIA using Single-cell MS and LC-MS data (Tables 6 and 7). The mass spectra of idioblast cells and laticifer cells showed that major TIA peaks including catharanthine (*m/z* 337.19), serpentine (*m/z* 349.15) and vindoline (*m/z* 457.23) were detected as primal peaks in those spectra. Catharanthine (*m/z* 337.19) was also detected in the mass spectra of parenchyma cells and epidermal cells.

I examined MS/MS analyses of a peak having *m/z* 337.19 in order to clarify whether this is catharanthine, tabersonine or other alkaloids (Table 8). As a result of MS/MS, a catharanthine-specific fragment peak (*m/z* 93.07) from all types of cells showing *m/z* 337.19 was detected (Tables 6 and 8) (Yamamoto et al., 2016). The result of LC-MS/MS in *C. roseus* leaves also supported that *m/z* 337.19 in *C. roseus* leaf tissue is entirely composed of catharanthine. These analyses strongly suggested that catharanthine also accumulated in the idioblast cells and laticifer cells. MS/MS fragments corresponding to serpentine (*m/z* 349.15) and vindoline (*m/z* 457.23) were

detected in Single-cell MS and LC-MS/MS analyses (Tables 6 and 8 and Fig. 18) (Yamamoto et al., 2016). Moreover, I speculated on the possible TIA identities of several other peaks (Table 7). In order to determine whether these peaks were real TIAs, their MS/MS fragments in a similar manner as a former experiment of the stem tissue was analyzed (Table 8).

Semi-quantitative analysis of Single-cell MS.

The metabolome of *C. roseus* leaf tissues was analyzed using LC-MS. I detected that a single peak at *m/z* 349.15, 389.14, 399.22, 415.22, 427.22, 457.23 and 531.23 correspond to serpentine, secologanin, desacetoxyvindoline, deacetylvindoline, demethoxyvindoline, vindoline and strictosidine respectively (Table 7). Due to the LC-MS result, I can prospect that these *m/z* values show a single molecular species in each cell type of *C. roseus* leaf tissue (Yamamoto et al., 2016). Semi-quantitative calculations were made in regard to *m/z* 337.19, 349.15, 389.14, 399.22, 415.22, 427.22, 457.23 and 531.23 ion peaks from the Single-cell MS data measured with mass range *m/z* = 100-1000 (Table 6). Most of TIAs (*m/z* 337.19, 349.15, 399.22, 415.22, 427.22, 457.23 and 531.23) are accumulated in idioblast cells and laticifer cells. Secologanin and strictosidine, which are supposed to be produced in the epidermal cells, were detected in those epidermal cells, too.

Comparison of semi-quantitative data of laticifer cells between leaf primordium and leaf tissue.

The contents of specialized metabolites are different among the tissues. In previous research, I compared TIA contents in the first pair leaf and the stem tissue with LC-MS/MS. There was a large difference of vindoline contents between the first leaf and the stem samples. The first leaf sample accumulated more vindoline and vindoline intermediates than the stem tissue. In order to confirm whether vindoline biosynthetic pathway is activated in the first leaf, I measured contents of laticifer cells with Single-cell MS, which are suspected to accumulate vindoline and deacetylvindoline, in the leaf primordium (Fig. 19). The metabolome data of laticifer cells in the leaf primordium showed low accumulation of vindoline.

Discussion

TIA production in the *C. roseus* leaf tissue.

LC-MS analysis data of *C. roseus* leaf extracts showed that the major peaks from TIAs were catharanthine, vindoline and various vindoline intermediates (Table 7) (Yamamoto et al., 2016). To verify that these peaks were real TIAs, I measured chemical structures of commercially available TIAs by MS/MS analysis using the same MS apparatus (Table 8). As for TIAs peaks having no standards, such as vindoline intermediates, I tried to obtain MS/MS fragments and detected a skeleton specific MS/MS fragment (*m/z* 188) among the aspidosperma skeleton. Interestingly, *m/z* peaks of vindoline intermediates, such as desacetoxyvindoline and deacetylvindoline, were detected as a single peak with LC-MS analysis. There was no isomer (Table 7). Based on such MS/MS information, I deduced these TIA peaks as vindoline intermediates.

I was able to confirm that idioblast cells and laticifer cells contained catharanthine, serpentine and ajmalicine, using standard MS/MS fragments data. To our surprise, not only stem tissue but also leaf tissue contained catharanthine in idioblast cells and laticifer cells. So far, it has been considered that catharanthine was transported to wax layer after biosynthesis in the epidermal cells in other *C. roseus* cultivars (cv. Little delicata) (Roepke et al., 2010; Yu et al., 2013). There might be the possibility that catharanthine is transported into idioblast cells and laticifer cells. The conversion from ajmalicine to serpentine may occur in the vacuoles of idioblast cells and laticifer cells, since these compounds also localized in idioblast cells and laticifer cells.

Improvement of Imaging MS.

I needed to improve spatial resolution from previous condition, because the epidermal cells in leaf tissue are much smaller than every cell in the stem tissue. When the diameter of laser for ionization was changed, the ion intensity induced by laser radiation decreased. However, I finally succeeded in detecting alkaloids every 10 μm spatial resolution. These MS images were possible to distinguish each cell where TIAs localized. For example, MS images of *m/z* 457.23 showed that this compound localized in palisade tissue idioblast cell and spongy tissue idioblast cell (Fig. 17).

Changes in vindoline accumulation in laticifer cells depending on leaf stages.

The contents of vindoline were different between the stem and leaf tissues (Yamamoto et al., 2016). In order to investigate whether vindoline is produced in *C. roseus* idioblast cells and laticifer cells in the leaf tissue, I also measured laticifer cells localized in leaf primordium with Single-cell MS (Fig. 19). TIA composition in laticifer cells in leaf primordium was different from that of laticifer cells localized in the first pair leaves (about 1 cm). Interestingly, I could not detect in any vindoline intermediates, such as desacetoxyvindoline and deacetylvindoline in the leaf primordium. Vindoline biosynthetic pathway might be function in expanding leaf. Tabersonine 16-hydroxylase 2 (T16H2), which is considered as a key enzyme to vindoline biosynthesis in leaf tissue (Fig. 14), seems to increase its activity as the leaf grows (from leaf primordium up to larger than 1 cm leaf) (Fig. 20).

Cell-specific localization of TIAs in *C. roseus* leaf tissue.

It has been proposed that TIA biosynthesis initially occurs in IPAP cells and then the products move from IPAP cells to epidermal cells, parenchyma cells, idioblast cells and laticifer cells. It has been proposed that loganic acid is transferred from IPAP cells to epidermal cells and desacetoxyvindoline from epidermal cells to other cells (Fig. 1). This hypothesis is mainly based on *in situ* hybridization data and localization of mRNAs of genes encoding enzymes involved in TIA synthesis (Dugé de Bernonville et al., 2015). The actual localization of TIA molecules at the cellular level has been never detected (Mersey et al., 1986).

Imaging MS data showed that loganin and secologanin localized in the epidermal cells (Fig. 17). Single-cell MS showed the same localization, as for secologanin (Fig. 18). Unfortunately, loganin was not detected by using Single-cell MS, because the ionization efficiency of this compound decreases by using electrospray ionization (ESI). These iridoid metabolites have previously been shown to be synthesized in the epidermal cells of *C. roseus* stem tissue (Dugé de Bernonville et al., 2015), and this also was confirmed by using my analysis (Yamamoto et al., 2016).

I was not able to detect loganic acid and loganin ionized as a proton adducted ion in Single-cell MS analysis. Although I could not semi-quantify these substances, I assumed that loganic acid was localized in IPAP cells, according to MS image of *m/z* 415.1001 (loganic acid) (Fig. 17A).

Imaging MS and Single-cell MS data also showed that most TIAs, including catharanthine (*m/z* 337.19), were localized in the idioblast cells and laticifer cells (Table

6 and Figs. 16 and 18). These data contrast with previously published reports that showed catharanthine localized in the wax layer of the leaf tissue (Roepkea et al., 2010; Yu et al., 2013). The reasons for these differences are unclear but might reflect differences of cultivars.

My measurements also showed that most alkaloids are localized in the idioblast cell and laticifer cell (Table 6). These data are consistent with a previous report which showed that serpentine, ajmalicine and vindoline accumulated in the fraction of idioblast cells (Mersey et al., 1986; Carqueijeiro et al., 2016; Yamamoto et al., 2016). These metabolome results showed that compound of *m/z* 531.23 (strictosidine) localized not only in the epidermal cells but also in the idioblast cells and laticifer cells (Table 6). Strictosidine might be transported from vacuole in epidermal cells as soon as it is produced, and accumulated in cells which have strictosidine transporter. It is also possible that symplasmic transport via plasmodesmata might drive movements of TIA intermediates between adjacent cells (Fig. 20). Further studies are needed to clarify how these compounds distribute between the different cell types.

Material and method

Plant material and sample preparation.

Observation of idioblast cells and laticifer cells with microscope.

Extraction of TIAs from *C. roseus* tissues.

LC-MS Analysis.

Those methods are described in Chapter 1.

Chemicals.

Commercially available TIA standards, catharanthine (Enzo Life Sciences), tabersonine HCl (AvaChem Scientific), ajmalicine (AdipoGen), serpentine hydrogen tartrate (ChromaDex), deacetylvindoline (Tronto Research Chemicals), vindoline (ChromaDex) and vindoline-d3 (Tronto Research Chemicals) were used. Strictosidine was divided from Dr. Sarah O'Connor (John innes centre). One ppm solutions of these chemicals were used as standards in LC-MS/MS analysis with LTQ Orbitrap (LTQ Orbitrap Velos Pro, Thermo Fisher Scientific, USA) used for the Single-cell MS (MS/MS) analysis.

Imaging mass spectrometry.

Cross sections (80 μm thickness) of *C. roseus* first leaf were prepared with a microtome (Plant Microtome MTH-1, NKsystem, Japan) and visually inspected with a fluorescent stereoscopic microscope (M250FA, Leica Microsystems, Germany). Suitable sections were then washed with MilliQ water to remove alkaloid contamination from dead cells and mounted on Indium Tin Oxide (ITO) glass slides (Luminescence Technology Co.,

Hsin-Chu, Taiwan) using Cryoglue type I (SECTION-LAB Co. Ltd., Japan). The samples on glass slides were lyophilized by freeze-drying (Model 77400, LABCONCO Co. MO, USA) then sublimated by α-cyano-4-hydroxycinnamic acid (CHCA) with a conductive glass using a sublimation apparatus (ChemGlass CG-3038, ChemGlass Life Sciences). Mass spectrometric detection was performed on FT-ICR MS (APEX-Qe 9.4T with dual source, Bruker Daltonics Inc., USA). The spatial resolution of Imaging MS was 10-20 μm. MS images were reconstituted using Lab-MSI (Takahashi et al., 2015). Target mass peaks were detected in a bin size = 0.02.

Single-cell MS in *C. roseus* leaf tissue.

To identify cell-specific alkaloid localizations, I used live single cell video mass spectrometry, termed "Single-cell MS" analysis. Cross sections (100 μm thickness) of the leaf were prepared with a microtome (Plant Microtome MTH-1, NKsystem, Japan), washed with ultrapure water to remove alkaloid contamination, and then specimens were mounted on a glass slide fixed with double-faced adhesive tape and monitored with a stereomicroscope (M205FA, Leica Microsystems, Germany). The contents of single cells from eight different kinds of cell types, namely Leaf primordium laticifer cell (LPLC), Internal phloem associated parenchyma cell (IPAP), Leaf epidermal cell (LEC), Palisade tissue parenchyma cell (PTPC), Spongy tissue parenchyma cell (STPC), Palisade tissue idioblast cell (PTIC), Spongy tissue idioblast cell (STIC), Leaf laticifer cell (LLC), were sucked into a gold-coated glass capillary nano-electrospray tip via tubing using a syringe under the stereoscopic microscope (Fig. 15). After the addition of

3 μL of ionization solvent (0.5% formic acid and 1 ppm vindoline-d3 in methanol) into the nano-electrospray tip from the bottom, the tip was set on a nano-ESI ion source attachment. Mass spectrometric detection was performed on LTQ Orbitrap Velos Pro. The spray voltage for positive measurement was 1,000 V. Alkaloid detection was mainly performed in the range of *m/z* 100-1,000. The spectrometer was calibrated with poly-tyrosine before experiments. Data analysis was conducted by using Xcalibur software. Target mass peaks were detected within ± 5 ppm, compared to the theoretical mass. Since no isomers of *m/z* 337.19, 349.15, 389.14, 399.22, 415.22, 427.22, 457.23 and 531.23 ion peaks were found in the extract of whole leaf tissue by LC-MS analysis (Yamamoto et al., 2016), I quantified these alkaloids in each of the seven kinds of cell type by semi-quantitative calculation using Single-cell MS data on *m/z* intensity values of above ion peaks. When I compare the contents of TIA in laticifer cells between leaf primordium and leaf, the peak intensities of TIAs were corrected with values of the vindoline-d3 ion intensities.

Figure and Table

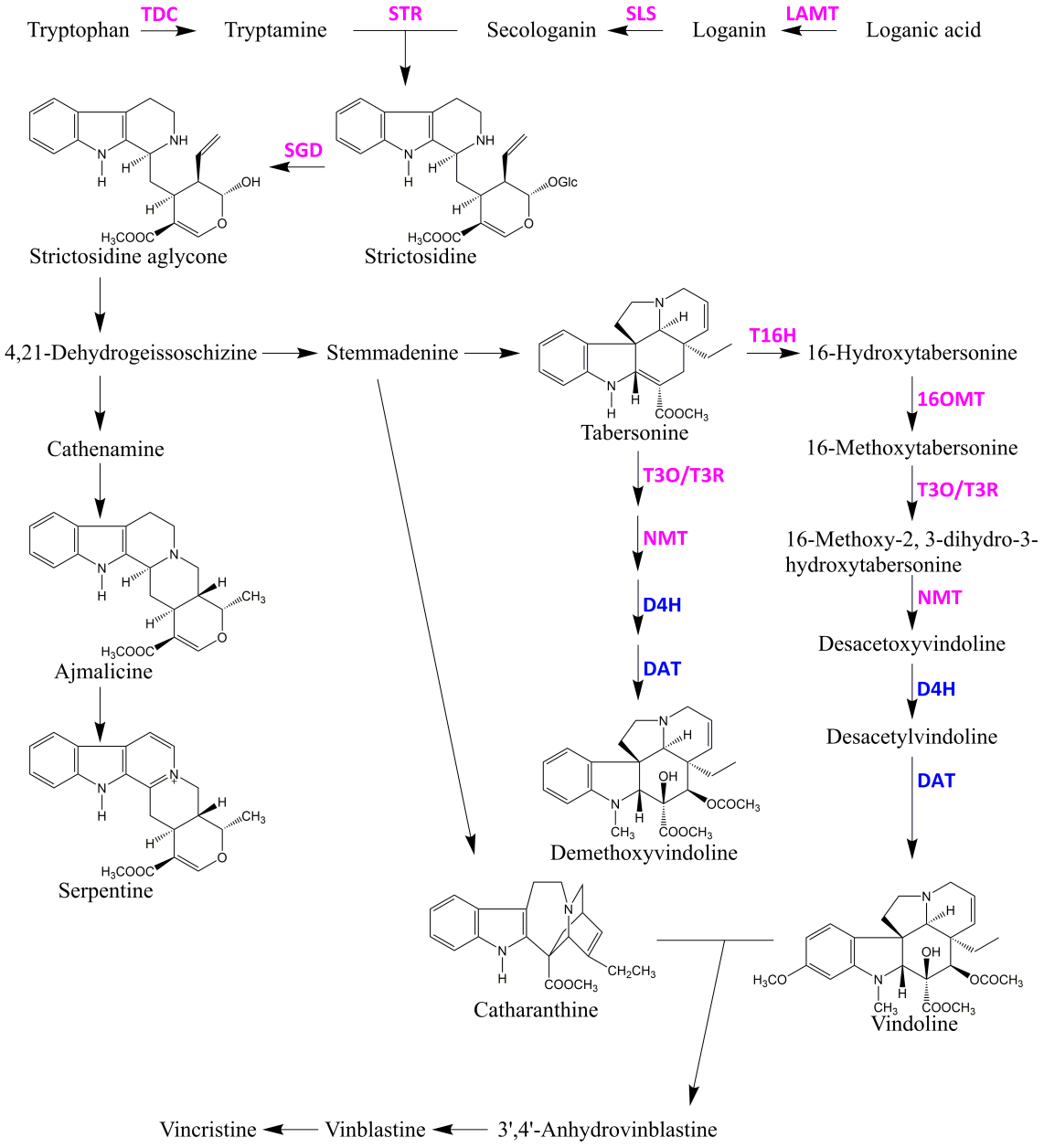

Fig. 14. Speculated TIA metabolic pathway in *Catharanthus roseus*. Purple font represents TIA enzymes localized in epidermal cells. Blue represents TIA enzymes localized in idioblast cells and laticifer cells. Abbreviation, LAMT : Loganic acid O-methyltransferase, SLS : Secologanin synthase, TDC : Tryptophan decarboxylase, STR : Strictosidine synthase, SGD : Strictosidine β-glucosidase, T16H : Tabersonine

16-hydroxylase, 16OMT : 16-Hydroxytabersonine O-methyltransferase, T3O : tabersonine 3-oxygenase, T3R : Tabersonine 3-reductase, NMT : 16-methoxy-2,3-dihydro-3-hydroxy-tabersonine N-methyltransferase, D4H : Desacetoxyvindoline 4-hydroxylase, DAT : Deacetylvindoline 4-O-acetyltransferase.

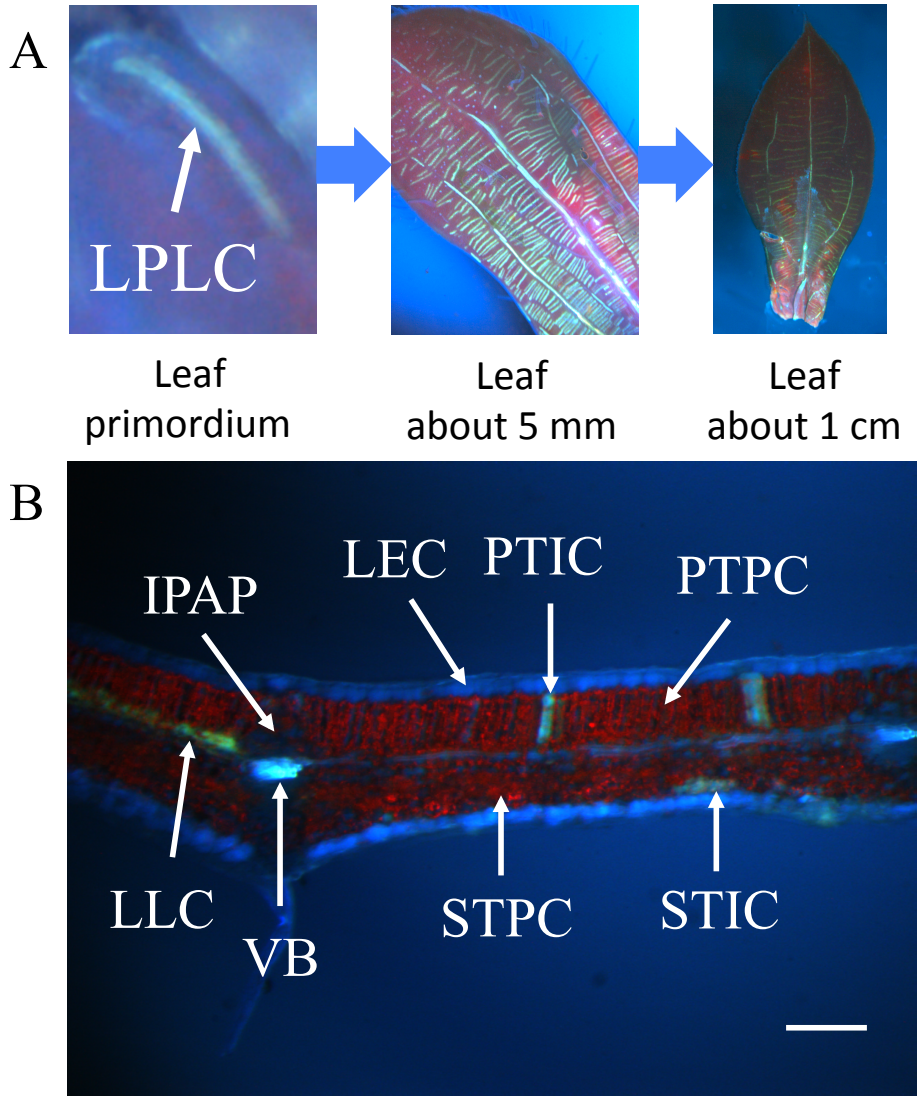

Fig. 15. Localization of idioblast cells and laticifer cells in *C. roseus* leaf tissue. (A) Leaf expansion from leaf primordium. (B) The cross section of *C. roseus* leaf (about 1 cm). Scale bar = 100 μm.

Abbreviation, LPLC : Leaf primordium laticifer cell, IPAP : Internal phloem associated parenchyma cell, LEC : Leaf epidermal cell, PTPC : Palisade tissue parenchyma cell, STPC : Spongy tissue parenchyma cell, PTIC : Palisade tissue idioblast cell, STIC : Spongy tissue idioblast cell, LLC : Leaf laticifer cell.

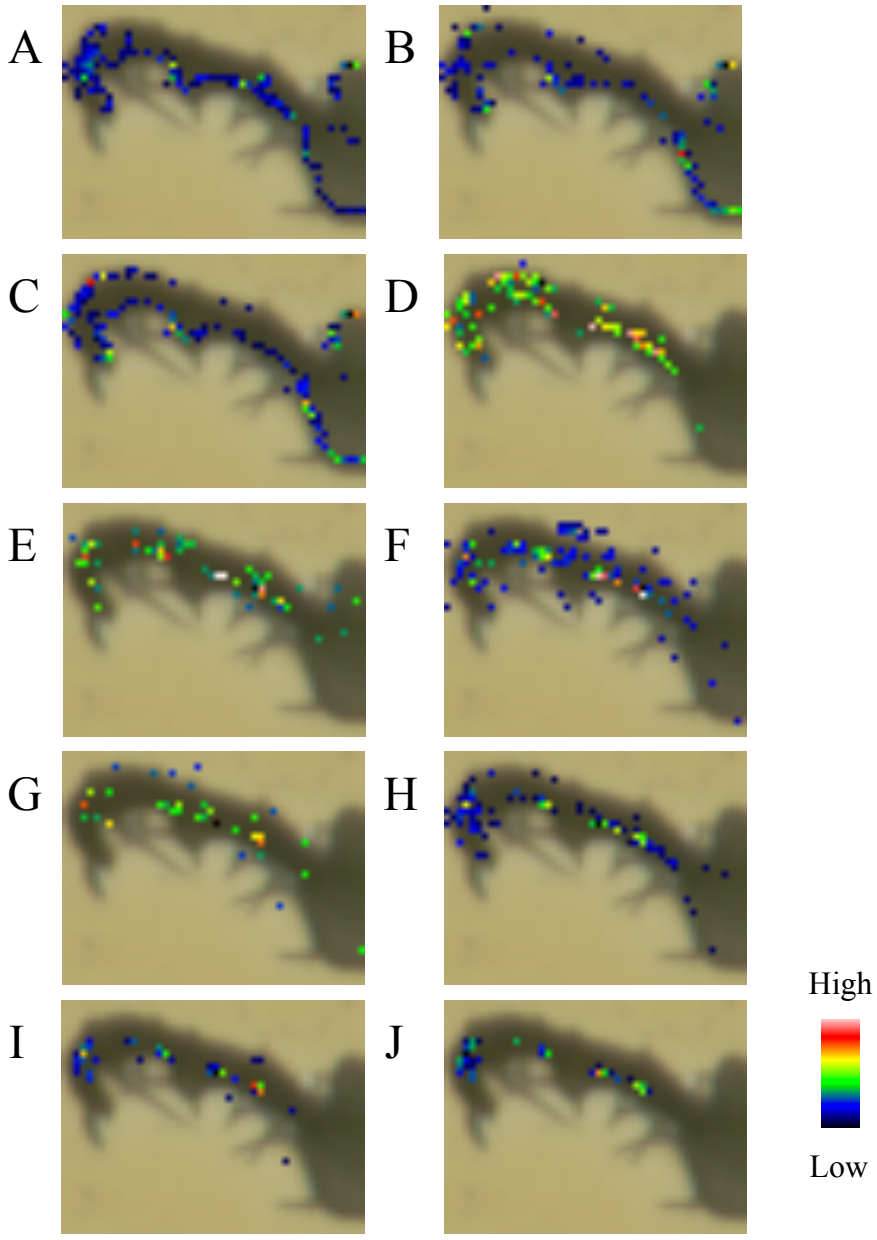

Fig. 16. MS images of *C. roseus* leaf section measured with 20 μm spatial resolution. (A) *m/z* 415.1001 (Loganic acid). (B) *m/z* 429.1157 (Loganin). (C) *m/z* 427.1001 (Secologanin). (D) *m/z* 531.2333 (Strictosidine). (E) *m/z* 351.1703 (Cathenamine). (F) *m/z* 353.1859 (Ajmalicine). (G) *m/z* 349.1546 (Serpentine). (H) *m/z* 337.1910 (Catharanthine). (I) *m/z* 427.2227 (Vindorosine (Demethoxyvindoline)). (J) *m/z* 457.2333 (Vindoline). Color bar represents MS signal intensity.

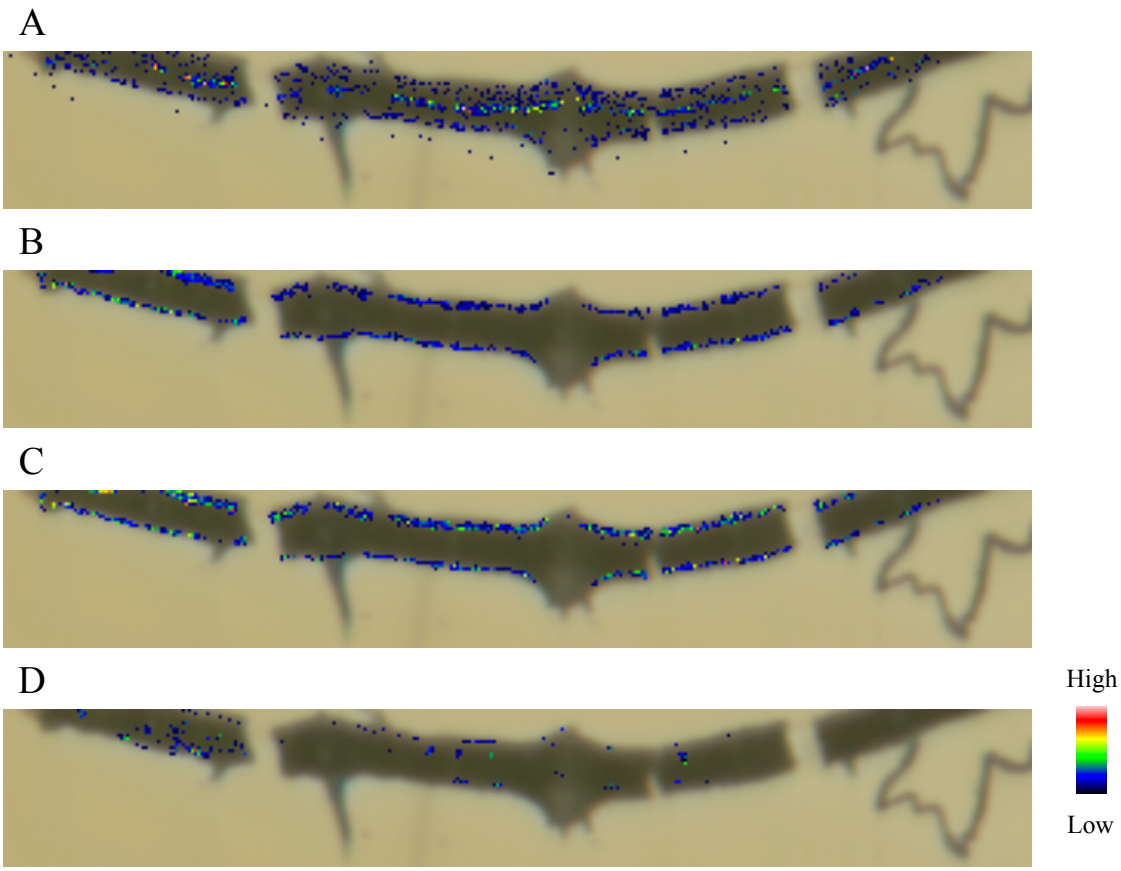

Fig. 17. MS images of *C. roseus* leaf section measured with 10 μm spatial resolution. Most TIA localized in idioblast cell and laticifer cell. (A) *m/z* 415.1001 (Loganic acid). (B) *m/z* 429.1157 (Loganin). (C) *m/z* 427.1001 (Secologanin). (D) 457.2333 (Vindoline). Color bar represents MS signal intensity.

A

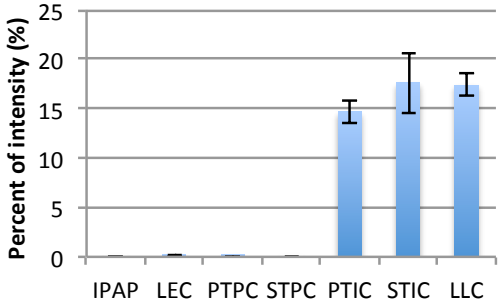
Catharanthine
Percent of intensity (%)
25
20
15
10
5
0
IPAP LEC PTPC STPC PTIC STIC LLC

B

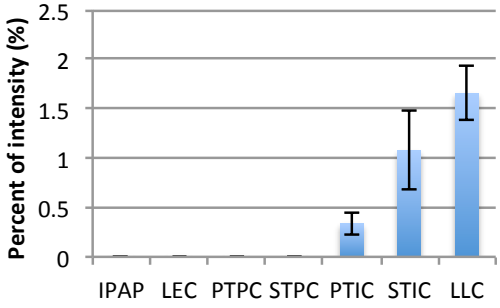
Serpentine
Percent of intensity (%)
2.5
2
1.5
1
0.5
0
IPAP LEC PTPC STPC PTIC STIC LLC

C

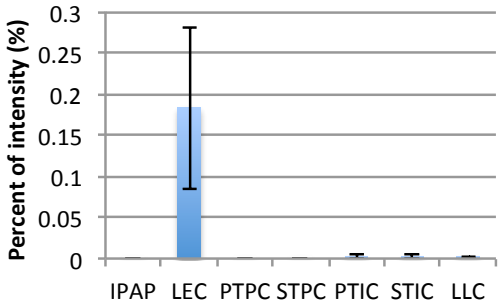
Secologanin
Percent of intensity (%)
0.3
0.25
0.2
0.15
0.1
0.05
0
IPAP LEC PTPC STPC PTIC STIC LLC

D

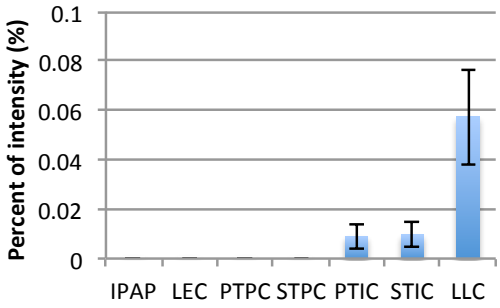
Desacetoxyvindoline
Percent of intensity (%)
0.1
0.08
0.06
0.04
0.02
0
IPAP LEC PTPC STPC PTIC STIC LLC

E

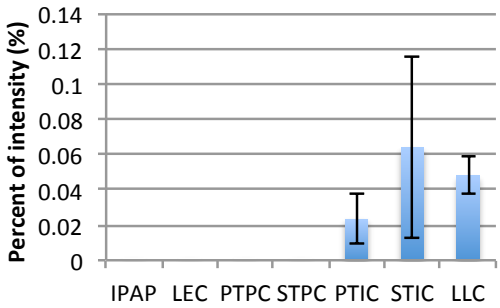
Deacethylvindoline
Percent of intensity (%)
0.14
0.12
0.1
0.08
0.06
0.04
0.02
0
IPAP LEC PTPC STPC PTIC STIC LLC

F

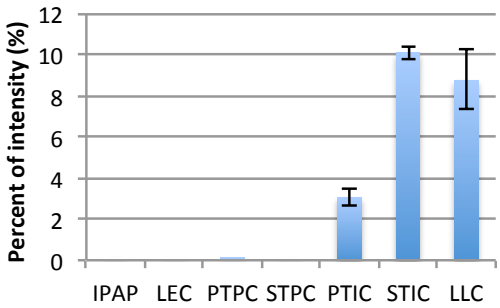
Demethoxyvindoline
Percent of intensity (%)
12
10
8
6
4
2
0
IPAP LEC PTPC STPC PTIC STIC LLC

G

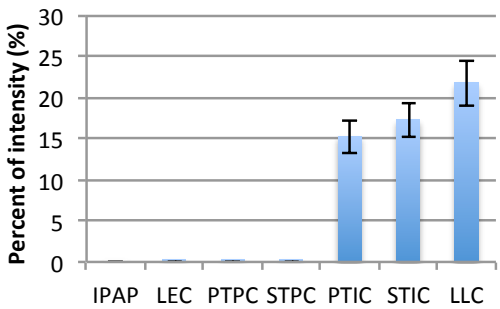
Vindoline
Percent of intensity (%)
30
25
20
15
10
5
0
IPAP LEC PTPC STPC PTIC STIC LLC

H

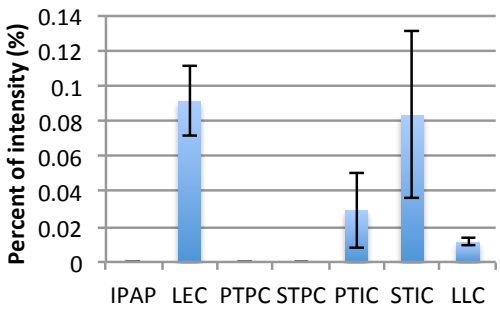
Strictosidine
Percent of intensity (%)
0.14
0.12
0.1
0.08
0.06
0.04
0.02
0
IPAP LEC PTPC STPC PTIC STIC LLC

Fig. 18. Semi-quantitative analysis of TIAs calculated by using Single-cell MS analysis data. (A) Catharanthine (*m/z* 337.19). (B) Serpentine (*m/z* 349.15). (C) Secologanin (*m/z* 389.14). (D) Desacetoxyvindoline (*m/z* 399.22). (E) Deacetylvindoline (*m/z* 415.22). (F) Demethoxyvindoline (*m/z* 427.22). (G) Vindoline (*m/z* 457.23). (H) Strictosidine (*m/z* 531.23). Y-axis shows percent of intensity normalized by the value of the total ion intensity of each sample. Values are the mean of three measurements (± SEM).

Abbreviation, IPAP : Internal phloem associated parenchyma cell, LEC : Leaf epidermal cell, PTPC : Palisade tissue parenchyma cell, STPC : Spongy tissue parenchyma cell, PTIC : Palisade tissue idioblast cell, STIC : Spongy tissue idioblast cell, LLC : Leaf laticifer cell.

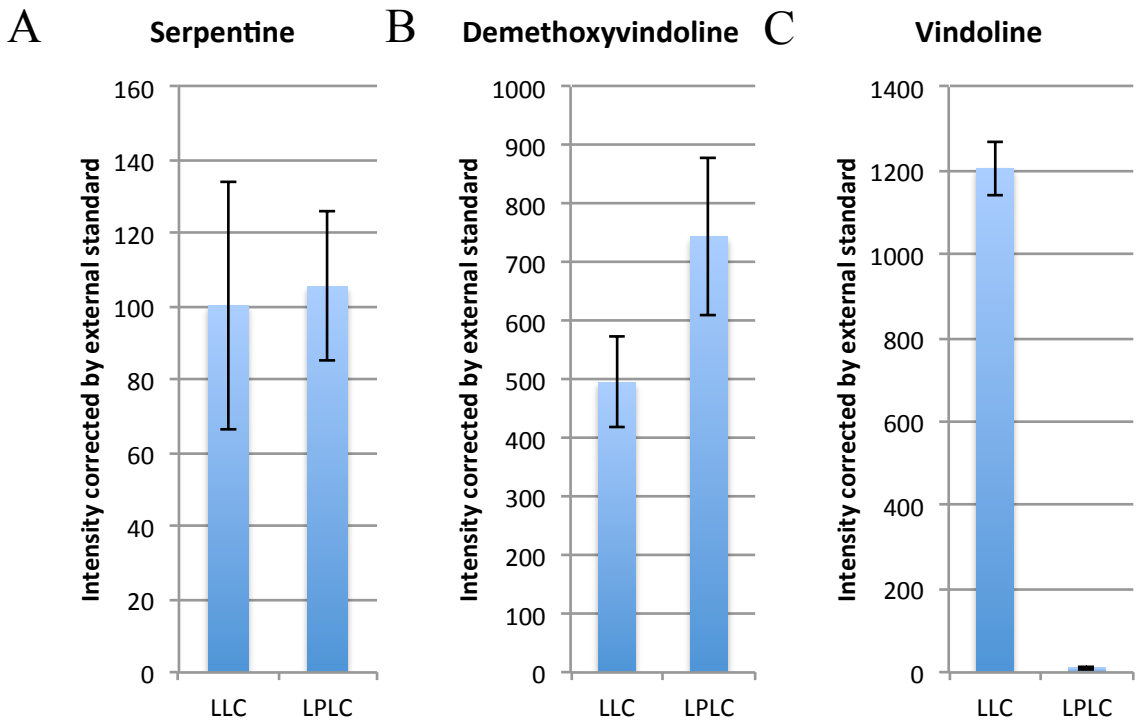

Fig. 19. TIA contents in leaf laticifer cell (LLC) and leaf primordium laticifer cell (LPLC). (A) Intensity of serpentine content. (B) Intensity of demethoxyvindoline content. (C) Intensity of vindoline content. Values are the mean of three measurements (± SEM).

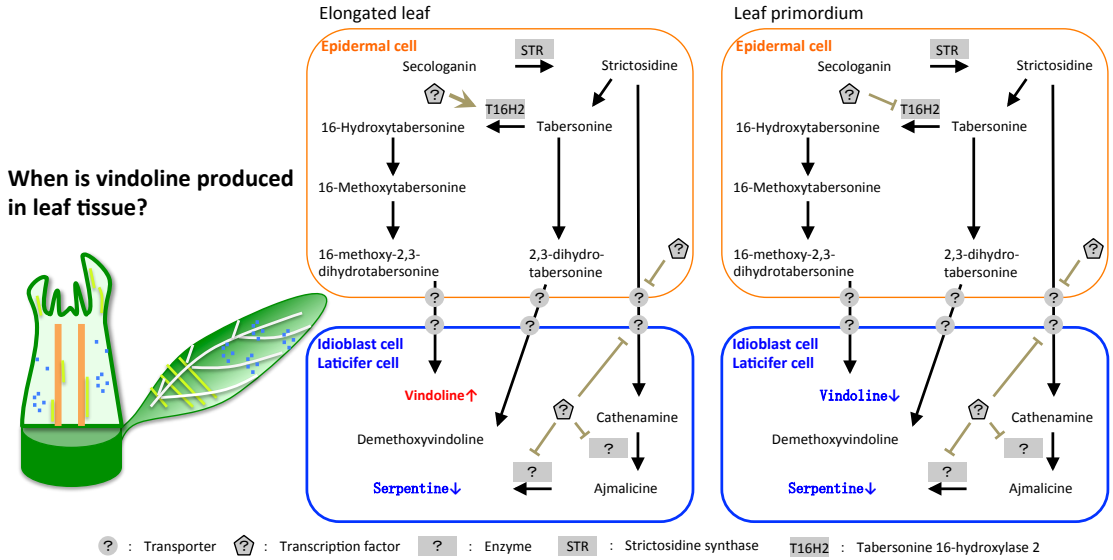

Fig. 20. Cell-specific localization of TIA in *C. roseus* leaf tissue. Vindoline is accumulated in idioblast and laticifer cells of elongated leaf.

Table 6. TIA and iridoid detected in leaf tissue by using Single-cell MS analysis (mass range *m/z* = 100-1000)

Molecular Formula	[M+H]+	IPAP	LEC	PTPC	STPC	PTIC	STIC	LLC	Speculated compound
C21H24N2O2	337.191054		○			○	○	○	Catharanthine
C21H20N2O3	349.154668					○	○	○	Serpentine
C21H22N2O3	351.170318					○	○	○	Cathenamine
C21H24N2O3	353.185968					○	○	○	Ajmalicine
C21H26N2O3	355.201618					○	○	○	Stemmadenine
C16H24O9	361.149308								7-Deoxyloganic acid
C22H26N2O3	367.201618					○	○	○	16-Methoxytabersonine
C21H24N2O4	369.180883								Horhammericine
C16H24O10	377.144222								Loganic acid
C22H28N2O4	385.212183						○	○	16-Methoxy-2,3-dihydro-3-hydroxytabersonine
C17H24O10	389.144222		○						Secologanin
C17H26O10	391.159873								Loganin
C23H30N2O4	399.227833						○	○	Desacetoxyvindoline
C23H30N2O5	415.222748					○	○	○	Deacetylvindoline
C24H30N2O5	427.222748					○	○	○	Demetoxyvindoline
C25H32N2O6	457.233312					○	○	○	Vindoline
C27H34N2O9	531.233706		○			○	○	○	Strictosidine

○ : Chemical compound exists in leaf tissue each cell type (n=3).

Table 7. TIA detected by LC-MS analysis of leaf tissue samples

Molecular Formula	[M+H]+	Leaf tissue	Retention time of sample (min)	Compound	Retention time of standard (min)	Alkaloid content in leaf (µg/mg FW)
C21H24N2O2	337.191054	○	6.83, 7.83, 8.40, 10.92, 21.85	Catharanthine	10.93	5.199±0.260
C21H24N2O2	337.191054	○	6.83, 7.83, 8.40, 10.92, 21.85	Tabersonine	21.83	0.286±0.024
C21H20N2O3	349.154668	○	6.97	Serpentine	6.96	0.037±0.006
C21H22N2O3	351.170318	○	5.96, 6.45, 7.10, 7.81, 8.21, 9.84			
C21H24N2O3	353.185968	○	7.35, 8.08, 8.84, 9.97, 14.17	Ajmalicine	9.99	0.169±0.007
C21H26N2O3	355.201618	○	6.72, 7.16, 7.56, 10.54, 13.52			
C22H26N2O3	367.201618	○	9.05, 20.50			
C22H28N2O4	385.212183	○	8.56, 9.62			
C23H30N2O4	399.227833	○	10.73			
C23H30N2O5	415.222748	○	7.86	Deacetylvindoline	7.84	
C24H30N2O5	427.222748	○	9.03			
C25H32N2O6	457.233312	○	8.43	Vindoline	8.42	1.6470±0.071
C27H34N2O9	531.233706	○	5.61	Strictosidine	5.62	

○ : Chemical compound exists in the leaf tissues (n=3). Retention time : Mass specific peaks in the leaf tissue.

Table 8. LC-MS/MS analysis of whole leaf data

Compound	[M+H]+	MS/MS fragments of leaf tissue (%)	MS/MS fragments of standard (%)
Catharanthine	337.191054	93.07(17), 133.07(2), 144.08(100), 165.09(18), 173.11(10), 337.19(13)	93.07(18), 133.07(2), 144.08(100), 165.09(17), 173.11(9), 337.19(12)
Tabersonine	337.191054	122.10(6), 136.11(14), 168.08(3), 170.10(3), 216.10(5), 228.10(29), 230.12(4), 249.14(3), 277.17(4), 305.17(68), 337.19(100)	122.10(7), 136.11(17), 168.08(4), 170.10(4), 216.10(6), 228.10(33), 230.12(4), 249.14(3), 277.17(5), 305.17(81), 337.19(100)
Serpentine	349.154668	263.08(7), 295.11(2), 317.13(22), 349.16(100)	263.08(9), 295.11(2), 317.13(28), 349.16(100)
Ajmalicine	353.185968	144.08(100), 178.09(4), 210.11(15), 222.11(3), 321.16(5), 353.19(47)	144.08(100), 178.09(4), 210.11(14), 222.11(3), 321.16(5), 353.19(43)
Deacetylvindoline	415.222748	73.05(26), 91.06(38), 122.10(6), 188.11(74), 344.98(58), 355.20(95), 365.19(26), 397.21(7), 415.22(100)	122.10(6), 188.11(74), 355.20(100), 365.19(25), 397.21(8), 415.22(97)
Demethoxyvindoline	427.222748	158.10(100), 307.18(6), 325.19(2), 335.17(3), 349.19(3), 367.20(50), 409.21(3), 427.22(17)	*143, 158, 367, 409, 427
Vindoline	457.233312	162.09(3), 188.11(100), 222.11(4), 337.19(4), 397.21(30), 457.23(10)	162.09(2), 188.11(100), 222.11(3), 337.19(4), 397.21(24), 457.23(8)
Strictosidine	531.233706	144.08(100), 165.05(43), 170.10(18), 250.09(21), 251.09(40), 274.12(19), 282.11(46), 283.12(32), 302.12(30), 308.13(19), 320.13(35), 334.14(77), 352.15(92), 514.21(40)	144.08(100), 165.06(45), 170.10(19), 250.09(19), 251.09(37), 274.12(21), 282.11(48), 283.12(33), 302.12(32), 308.13(22), 320.13(34), 334.14(82), 352.15(97), 514.21(55)

* : MS/MS fragments of demethoxyvindoline was cited by Zhou et al. (2005).

Chapter 3

Molecular analyses of idioblast cells and laticifer cells in *Catharanthus roseus*

Chapter 3 :

Molecular analyses of idioblast cells and laticifer cells in *Catharanthus roseus*

Summary

The cell-specific localizations of TIA in *C. roseus* stem and leaf tissues have been studied in the former chapters and I revealed that most TIAs localized in idioblast cell and laticifer cell. These results are different from the past findings. The results of TIA localization also suggest that idioblast cell and laticifer cell play an important and a similar role in TIA metabolism in *C. roseus* plant. However, the molecular mechanisms of biosynthesis and accumulation of TIA intermediates in idioblast cell and laticifer cell have not been studied at all. In this chapter, I have conducted cell-specific RNA-seq analyses in order to discover the genes expressed in these cells.

At first, I observed the differentiation of idioblast cells and laticifer cells in stem and leaf tissues. I found that idioblast cells and laticifer cells are not differentiated in upper part of stem compared to other tissues. Moreover, I have conducted metabolome analysis to confirm what kinds of TIAs are contained among upper part of stem, lower part of stem and leaf. These metabolome data showed the differences of TIA accumulation between stem and leaf tissues. The content of serpentine, which shows autofluorescence excited by UV, increased in lower part of the stem. This result coincides that lower part of stem have many idioblast cells. Furthermore, I tried to obtain those idioblast cell-specific RNA-seq data by collecting idioblast cells from lower part of stem in order to investigate the differentiation in idioblast cell in the stem

tissue. The cell-specific RNA-seq analysis in stem tissues revealed that major latex like protein and the candidates of specialized metabolites transporters and enzymes are highly expressed in the fraction of idioblast cell.

For further analysis of the idioblast cells, I have isolated idioblast cells from leaf tissues with Fluorescence activated cell sorting (FACS). By the measurement of gene expression in isolated idioblast cells, higher expressions of genes of TIA enzymes localized in idioblast cells were detected. These results help us to consider the role of idioblast cell and laticifer cell for specialized metabolism in *C. roseus* plants.

Introduction

The secretory cells are classified as cells differentiated from ground parenchyma cells and contain a variety of substances secreted : balsams, resins, oils, tannins, mucilages, gums, crystals, etc. They have been classified as secretory idioblasts conspicuously differed from neighboring cells (Esau, 1965).

One of famous secretory cells is the laticifer cell. Laticifer cells are consist of a single cell or a series of fused cells containing so-called fluid latex. These kinds of cells are localized in various tissues of the plant body. Latex containing plants are estimated to amount about 12,500 species (over 20 plant families) (Hagel et al., 2008). Although it has been considered that laticifer cells have various roles, such as regulator related to water balance or protection against herbivores, their conclusive roles in the plant life is still lacking (Esau, 1965; Pramoolkit et al., 2014). The most accepted interpretation of the role of the laticifer cells is that they form an excretory system, same as other secretory cells. Laticifer cells accumulate many substances that are commonly recognized as excretory, and such substances are more abundant than nutrition (Esau, 1965). For example, latex contains specialized metabolites such as many kinds of terpenoids, cardiac glycosides, alkaloids, cannabinoids and tannins. Since most of those specialized metabolites are cytotoxic, it is also considered that laticifer must have a role as sequestering cells and defensive cells (Facchini et al., 2005; Hagel et al., 2008; Huber et al., 2016). In opium poppy, most alkaloids, such as morphine and codeine, are accumulated in the latex of articulated cells called laticifers (Facchini et al., 2008).

In Chapter 1 and 2, I introduced that *Catharanthus roseus* (L.) G. Don plants have produced those TIAs via various cells including IPAP cells, epidermal cells, etc. Finally, they are accumulated in idioblast cells and laticifer cells classified as nonarticulated, unbranched laticifers (Thamm et al., 2016; Yamamoto et al., 2016). However, Imaging MS analysis and Single-cell MS analysis revealed that the different localizations of TIAs. Especially, strictosidine were existing at the site which is different from producing site based on the localization of TIA enzymes (Yamamoto et al., 2016). Considering these results, I suppose that idioblast cells and laticifer cells are also related to not only an excretory system of toxic TIA compounds but also the TIA intermediates biosynthesis closely. I am also considering the possibility that the transporters of strictosidine and/or other TIAs intermediates might be functioning to localize them in those cells.

These days, RNA-seq data of *C. roseus* revealed TIA biosynthesis related genes, including transporters, transcription factors and enzymes. For instances, master regulators (BIS1, BIS2) that activates the biosynthesises of the iridoids were discovered by transcriptome analysis and fuctional screening (Van Moerkercke et al., 2015). Furthermore, triterpenoids enzymes and catharanthine transporter (CrTPT2 : a member of the pleiotropic drug resistance (PDR) family of ABC transporters) were discovered from the EST and RNA-seq database from epidermal cells (Murata et al., 2008; Yu et al., 2013).

In this chapter, I used transcriptome analyses and tissue-specific metabolome analyses in order to find the candidates of TIA transporters and idioblast specifically

expressed genes. Further, in order to investigate mechanism of TIA synthesis in the idioblast cells in leaf tissue, I attempted to isolate idioblast cells by using FACS.

Result

Localization of idioblast cells and laticifer cells in *C. roseus* aerial part.

Idioblast cells and laticifer cells of *C. roseus* exist in every tissues and organs, such as stem, leaf, flower and root. In leaf tissue, laticifer cells also localized in leaf primordium. On the other hand, it was difficult to observe both idioblast cells and laticifer cells in the youngest internode and second internode of the stem tissue, when I observed under UV (Fig. 21).

LC-MS analysis in *C. roseus* stem tissue.

In order to investigate TIA content in the first leaf (Yamamoto et al., 2016), the upper part of stem and the lower part of stem, I measured them by using LC-MS. Serpentine was accumulated in the lower part of stem compared to the upper part of stem. The catharanthine, tabersonine, ajmalicine and vindoline contents of leaf tissues were higher than that of stem tissues (Yamamoto et al., 2016). According to the present study, I succeeded in detecting the differences of these TIAs contents between upper and lower part of stem tissues. The upper part of stem (about 0.643 μg mg^{-1} FW) accumulated more catharanthine than the lower part of stem (about 0.282 μg mg^{-1} FW). The content of tabersonine is similar amounts in both stem parts. The upper part of stem was accumulated less ajmalicine and serpentine than the lower part of stem (Fig. 22).

RT-PCR in tissue-specific fraction.

Metabolome analyses revealed that the tissue-specific alkaloid accumulation. In order to investigate how such a difference occurs, I conducted RT-PCR of TIA biosynthesis-related genes in *C. roseus* stem and leaf tissues (Fig. 22). Tabersonine 16-hydroxylase 2 (T16H2) produces 16-hydroxytabersonine which is the initial substance in a vindoline pathway. Since it is suggested that T16H2 coordinate vindoline and vindorosine pathways, I investigated the gene expression of this enzyme. The gene expression of T16H2 was upregulated in leaf tissue compared to the stem tissues. Furthermore, the gene expression of T16H2 is activated in the upper part of stem tissue compared to the lower part of stem (Fig. 22).

RNA-seq analyses with cell-specific samples.

In cell-specific RNA-seq analysis, I used a method, which is newly-developed by Hitachi research group for very small tissues (see Material and Methods and Kajiyama et al., 2015). By using a special equipment, I collected idioblast cell and parenchyma cell fractions from under third internode where these cells have already accumulated enough TIAs. On the other hand, because serpentine has not been produced well in the youngest and second internodes compared to other internodes, I could not discover an immature idioblast cell under UV excitation (Fig. 21). The results of cell-specific RNA-seq showed that some of the enzyme genes related to lipid and specialized metabolite synthesis were upregulated in the fraction of idioblast cells (Fig. 23 and Table 9).

Isolation of idioblast cells from *C. roseus* leaf tissue.

In order to obtain the candidate genes expressed in the idioblast cells and to conduct cell biological experiments, I tried to isolate idioblast cells from leaf tissue. Idioblast cells have the features of higher intensity of blue autofluorescence (Figs. 24-26) excited by UV. I used this feature for separating idioblast protoplasts from parenchyma fraction by using FACS. I succeeded in obtaining the fraction of enriched idioblast cells.

I also tried to investigate the gene expression of idioblast cell enrichment fraction. The result of gene expression analysis in the idioblast cell fraction showed that the genes related to vinblastine production are upregulated (Figs. 24-26).

Discussion

Accumulation of serpentine and other TIAs in lower part of stem in *C. roseus*.

Since serpentine was more accumulated in the lower part of stem compared to the upper part of stem (Fig. 22), it is suggested that serpentine biosynthesis is progressing as the stem grows. I also measured ajmalicine contents in each tissue. Interestingly, ajmalicine content of lower part of tissue was higher than that of upper part of stem tissue, too. It is the high possibility that serpentine is produced in lower part of stem. Since it has been considered that peroxidases (Enzyme commission numbers (EC) 1.11.1.7) are involved to serpentine conversion from ajmalicine (Blom et al., 1991), I need to investigate certain peroxidases related to stem growing or senescence in order to detect serpentine biosynthesis enzyme.

Tabersonine 16-Hydroxylase 2 (T16H2) might regulate the biosynthesis of vindoline and vindorosine among stem and leaf tissues in *C. roseus*.

Tissue-specific TIA accumulation among stem and leaf tissues in *C. roseus* was detected by using LC-MS and Single-cell MS analyses (Yamamoto et al., 2016 and Fig. 22). These results show that vindoline, vindorosine and serpentine biosynthesis regulated dependent on the tissues. Vindoline and vindorosine pathways in *C. roseus* have been revealed these days (Qu et al., 2015). It is considered that Tabersonine 16-Hydroxylase 2 (T16H2) is involving to the differentiation of TIA metabolism. In order to reveal whether the differences of vindoline contents are resulted from the expression of T16H2 or not, the gene expression analysis of T16H2 in each tissue was

conducted. As a result, RT-PCR analysis showed that the expression of this gene was upregulated in expanded leaf tissue and almost no expression in the stem tissues (Fig. 22). These results clearly suggest that T16H2 control vindoline accumulation in leaf tissues.

RNA-seq data of other groups showed the same results (Van Moerkercke et al., 2013; Van Moerkercke et al., 2015). This is a reason why vindorosine accumulated in idioblast cells and laticifer cells in the stem, instead of vindoline. It has been still unknown which transcriptional regulation is involved to the gene expression of T16H2.

Pathogenesis-related (PR) protein in *C. roseus* tissue.

PR proteins were induced under pathological or stress situation. I detected many genes of fungal resistance and bet v I family protein, including major latex protein (MLP), in RNA-seq analysis of idioblast cell fraction (Fig. 23). It is reported that MLP accumulated in latex of opium poppy (Nessler et al., 1985). These results also suggested that MLP protein localized in the idioblast cell and this cell has similar features with laticifer cell. Moreover, I detected the enzymes related to specialized metabolites synthesis, such as spermine synthase, in these RNA-seq data (Fig. 23). It is possible that other specialized metabolisms also occur in idioblast cells in *C. roseus*.

What kinds of transporter are involved to TIAs transport.

Little is known about TIA transport system in *C. roseus*, compared to metabolic pathway. These days, the ABCG transporter (i.e. catharanthine transporter) has been identified (Yu et al., 2013). Furthermore, it has been also reported TIA transport system among organelles. Early researchers proposed that ion-trap mechanism for alkaloid accumulation in the vacuoles (Deus-Neumann et al., 1986). However, recent researchers suggest that TIAs are transported to the vacuoles of mesophyll cells in *C. roseus* thorough the H^+/TIA antiport mechanism (Carqueijeiro et al., 2013).

Even though it is the possibility that the plasmodesmata is involved to TIA transport among cells, I am considering that many kinds of transporters, such as ABCG transporter and antiporter, are involved to TIAs transport. Since the method for isolating idioblast cells with FACS was established (Fig. 24), I would like to investigate TIA transporters localized in these cells in the near future.

Material and method

Observation of idioblast cells and laticifer cells with microscope.

Extraction of TIAs from *C. roseus* tissues.

LC-MS Analysis.

Those methods are described in Chapter 1.

Plant material and sampling for metabolome analysis.

C. roseus (L.) G Don (cv. Equator White Eye) was grown at 25 °C under 14 light/10 dark h white fluorescent light photoperiod in a growth chamber (NKsystem). Seeds were purchased from Sakata Seed Corporation.

Upper part of stem, lower part of stem and first pair leaf of *C. roseus* were harvested from about 3-month-old plants (Fig. 22).

Counting the number of idioblast cells and laticifer cells.

The central longitudinal section in *C. roseus* stem tissue was used for counting the number of cells. After I took photos of longitudinal sections under microscope, those photos were integrated on single picture by using e-Tiling (Mitani corporation). The number of idioblast cells and laticifer cells were counted with Image-J.

Sampling from the longitudinal section of *C. roseus* stem tissue.

The longitudinal section of *C. roseus* stem tissue was mounted on a 4% agarose gel containing Tris-HCl pH 8.0 and 1 mM EDTA. The fraction of idioblast cells or

parenchyma cells were sampled by using the homemade sampling device under stereomicroscope. The fractions of these cells were placed into 0.5 μL of PLC buffer (RNeasy, Qiagen) in PCR tubes (Axygen), then these samples were frozen in liquid nitrogen in a moment.

cDNA preparation for RNA-seq.

I followed the protocol (Kajiyama et al., 2015). After these samples were ground with pestle, the ground fractions were collected with centrifuge. I added buffer solution (2.6 μL PBS (pH 7.4), 0.36 μL 10×DNase Ⅰ Buffer and 0.5 μL DNase Ⅰ (Life Technologies)) to the sample solution for degrading genomic DNA. This mixture solution was kept at room temperature for 5 min, then DNase Ⅰ was inactivated by adding 1.2 μL of EDTA (2.5 mM, pH 8.0) at 70℃ for 5 min. I used UP1VN-oligo immobilized beads (Dynabeads® MyOne™ Streptavidin C1, diameter; 1 μm, Dynal) suspension (10^7 of UP1VN-oligo immobilized beads, 1 μL 10 mM dNTP mixture and 16.6 μL T&T Buffer) for cDNA producing. The mixture was heated at 70℃ for 5 min, then cooled down to 4℃ so as to hybridized oligo probes on beads to mRNA. I added 9.0 μL RT solution (6 μL 5×RT Buffer, 1 μL DTT, 1 μL RNase OUT and 1 μL Super Script Ⅲ (Life Technologies)) for reverse transcription reaction. This mixture was shaken with 750 rpm at 50℃ for 30 min in incubator, then kept at 70℃ for 10 min and it was cooled down to 4℃. After the supernatant removed from this mixture, cDNA-immobilized beads washed 50 μL T&T buffer and I added finally 6 μL T&T buffer for the dispersion of these beads.

I added 6.0 μL of tailing solution (0.6 μL 10×PCR Buffer II (Life Technologies), 0.36 μL 25 mM $MgCl_2$, 0.18 μL 100 mM dATP, 0.3 μL RNase H (Life Technologies), 0.3 μL TdT (Life Technologies) and 4.26 μL water) to solution of including cDNA library beads. This mixture was shaken with 750 rpm at 37℃ for 15 min in incubator, then kept at 70℃ for 10 min and it was cooled down to 4℃. I added 50 μL T&T buffer to this mixture for washing. After I removed supernatant, I added finally 12 μL T&T buffer for the dispersion of these beads.

PCR amplification of cDNA.

Amprified PCR were produced with anchored oligo2 primer (UP2VN-oligo; 5'-ATA TCT CGA GGG CGC GCC GGA TCC T (24)VN-3', Integrated DNA Technologies), which hybridize on the poly(A) sequence of the first cDNA strands. After I added the solution (0.114 μL 100 μM UP2VN-oligo, 2.2 μL 10×Ex Taq Buffer, 2.2 μL 2.5 mM dNTP Mix, 0.19 μL of Ex Taq Hot start version (Takara bio) and 5.296 μL water) to the sample, it was heated at 95℃ for 3 min, 44℃ for 5 min, 72℃ for 6 min and finally cooled down to 4℃.

Furthermore I added 19.0 μL of amplification solution (0.418 μL of 100 μM oligo3 primer (UP1-oligo; 5'- ATA TGG ATC CGG CGC GCC GTC GAC T(24) -3', SIGMA-ALDRICH), 1.9 μL of 10×Ex Taq Buffer, 1.9 μL of 2.5 mM dNTP Mix, 0.19 μL of Ex Taq Hot start version and 14.592 μL of water) to the mixture, I conducted PCR (95℃ for 30 sec, 18 thermal cycles of 95℃ for 30 sec, 67℃ for 1 min and 72 ℃ for 6 min).

I prepared cDNA in this way. I used those cDNA for cell-specific RNA-seq analysis.

RNA-seq analysis of idioblast cell.

I analyzed cell-specific RNA-seq data measured with Illumina GAIIx. I used fragments per kilobase of transcript per million mapped reads (FPKM) normalized with RPS9 in order to obtain idioblast cell-specific gene expression data from RNA-seq data (Fig. 23 and Table 9). Table 9 shows genes whose expression level in the idioblast cell is over 10 times higher than that in the parenchyma cell.

FACS analysis.

I used *C. roseus* leaves (about 3 months-6 months) so as to isolate idioblast cells with FACS. *C. roseus* leaves were incubated for 2.5 hours by protoplast making solution (Cellulase Y-C (1%), Macerozyme R-10 (0.5%) solved with protoplast solution (600 mM sorbitol, 10 mM MES, 1 mM $CaCl_2$, pH 6.0 with Tris). After making protoplast, I conducted density gradient centrifugation to remove epidermal cell. Then, I collected parenchyma cell fraction. I used parenchyma cell fraction filtered with 50 μm (BD-falcon) to separate idioblast cells by using FACS. In FACS analysis, idioblast cells were sorted by using parameter of FSC, SSC, APC-cy7 and AmCyan with sheath pressure 10psi, nozzle 130 μm, and flow rate from 1.0 to 3.0 (Fig. 24).

RNA extraction and cDNA synthesis of tissue-specific samples and FACS samples.

RNA was extracted from tissue samples or/and protoplast samples by using RNeasy Plant Mini Kit (QIAGEN, Germany). I also used RNase-Free water DNase set (QIAGEN, Germany) in order to remove DNA contamination.

I followed the protocol of RNeasy Plant Mini Kit to make cDNA of each sample. Oligo dT primer and AMV Transcriptase were used for obtaining first strand cDNA. I used 50 ng RNA of FACS samples or 100 ng RNA of tissue samples to make first strand cDNA.

RT-PCR for tissue and cell-specific samples.

I conducted tissue and cell-specific RT-PCR analysis (Figs. 22 and 26). The sequences of primers were used in Tables 10 and 11. I conducted PCR (94℃ for 1 min, 45 thermal cycles of 94℃ for 15 sec, 65℃ for 20 sec and 72 ℃ for 30 sec, 72℃ 3 min) with thermal cycler.

Figure and Table

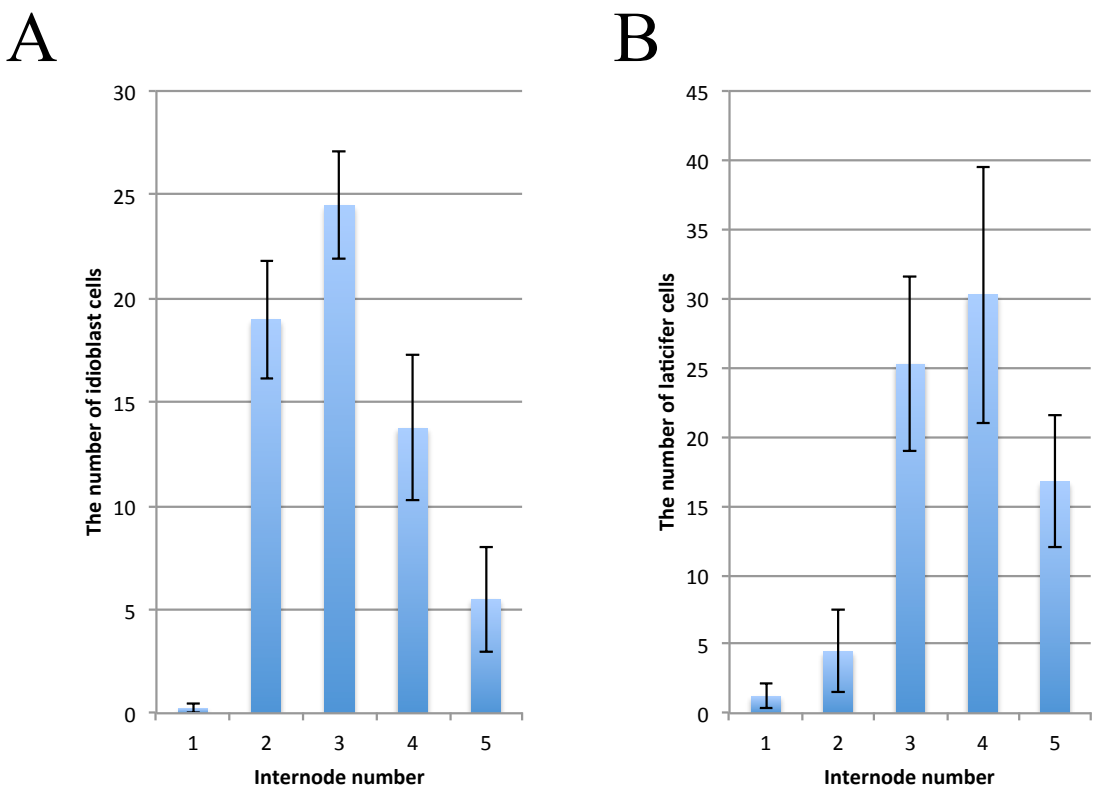

Fig. 21. Idioblast cell distribution in *C. roseus* stem tissue. The number of idioblast cells and laticifer cells increases in the lower part of stem. (A) The number of idioblast cells. (B) The number of laticifer cells. Values are the mean of four measurements (± SEM).

A

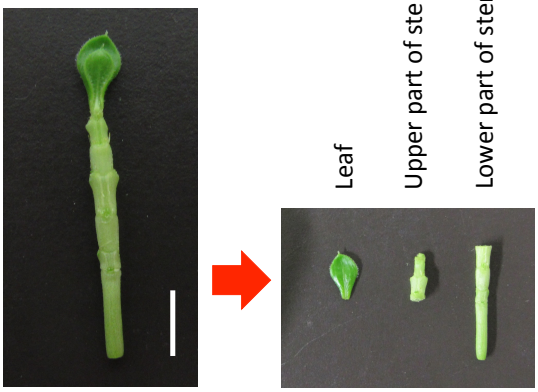

B

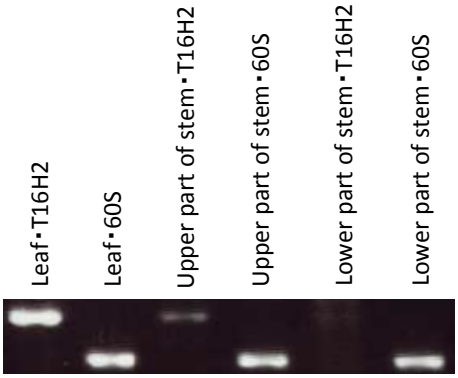

C

	Alkaloid content in leaf μg/mg FW	Alkaloid content in upper part of stem μg/mg FW	Alkaloid content in lower part of stem μg/mg FW
Catharanthine	5.199±0.260	0.643±0.053	0.282±0.059
Tabersonine	0.286±0.024	0.0050±0.0015	0.0032±0.0016
Serpentine	0.037±0.006	0.068±0.011	0.432±0.023
Ajmalicine	0.169±0.007	0.0055±0.0011	0.0476±0.0085
Vindoline	1.6470±0.071	0.0073±0.0015	0.00024±0.00001

Fig. 22. Vindoline synthesis in *C. roseus* stem and leaf tissues. (A) Sampling from *C. roseus* plant (Bar = 5 mm). (B) RT-PCR of T16H2 in stem and leaf tissues. 60S denotes ribosomal protein. (C) TIA content in each tissue. Values are the mean of three measurements (± SEM).

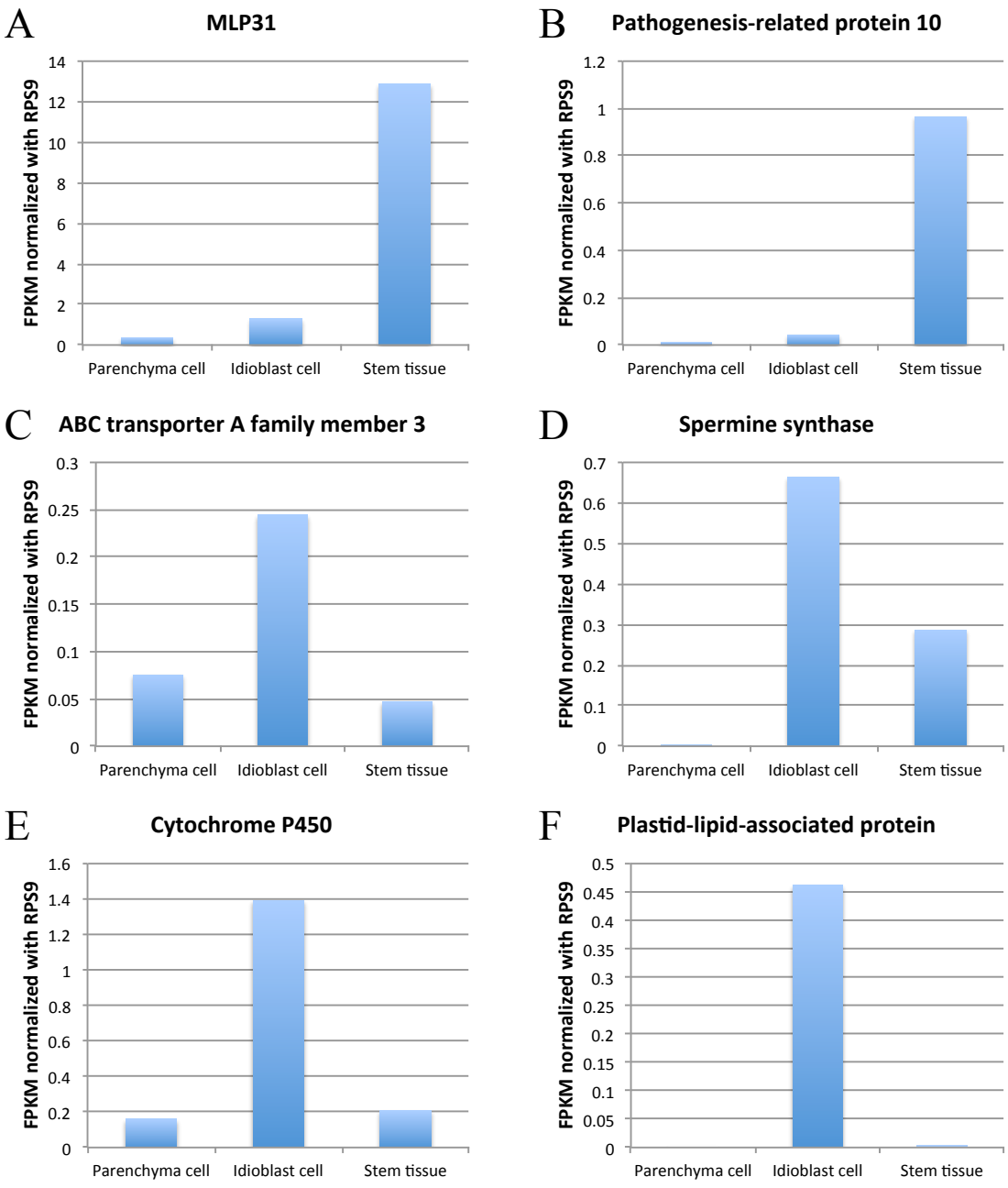

Fig. 23. Cell-specific RNA-seq analysis in *C. roseus* stem tissue. (A) MLP31 (Caros022694.1). (B) Pathogenesis-related protein 10 (Caros014578.1). (C) ABC transporter A family member 3 (Caros000259.1). (D) Spermine synthase (Caros004793.1). (E) Cytochrome P450 (Caros001784.1). (F) Plastid-lipid-associated protein (Caros020215.1). Values are the mean of two measurements.

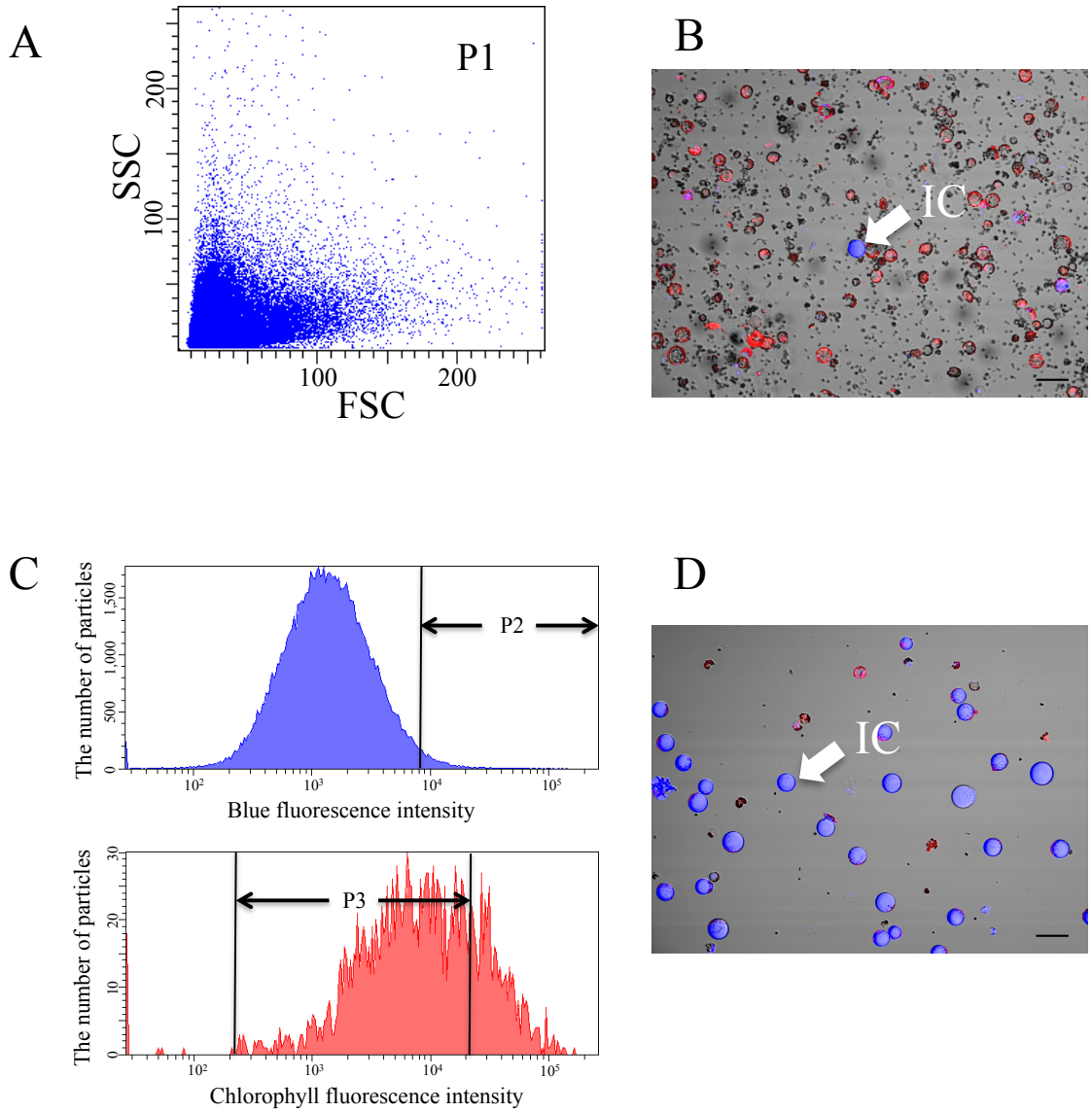

Fig. 24. Isolation of idioblast cell from leaf tissue with FACS. (A) Figure shows all particles derived from cells, organelles and the fractions of cell wall, in measuring by flow cytometer. (B) The fraction of P1 (Before cell sorting). (C) I collected cells that show the high value of blue autofluorescence and have low chlorophyll autofluorescence. (D) The fraction of P3 (After cell sorting).

Abbreviation, FSC : Forward scatter, SSC : Side scatter, IC : Idioblast cell.

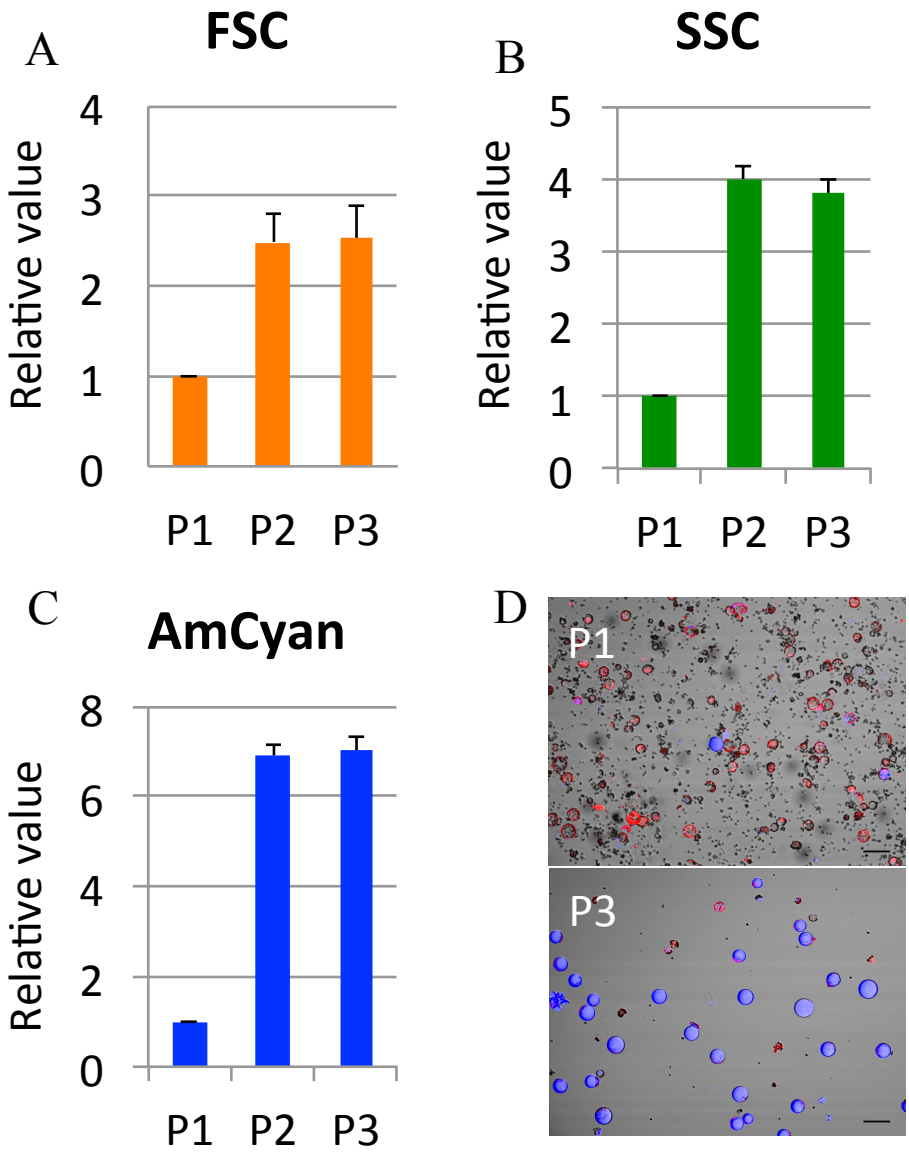

Fig. 25. FACS analysis. I obtained each fraction, such as P1, P2 and P3, derived from the measurement of Fig. 24. (A) FSC value shows the size of cell. (B) SSC value shows the complexity inside cell. (C) AmCyan value shows the blue autofluorescence. (D) Images of P1 and P3 fraction. Values are the mean of three measurements (± SEM).

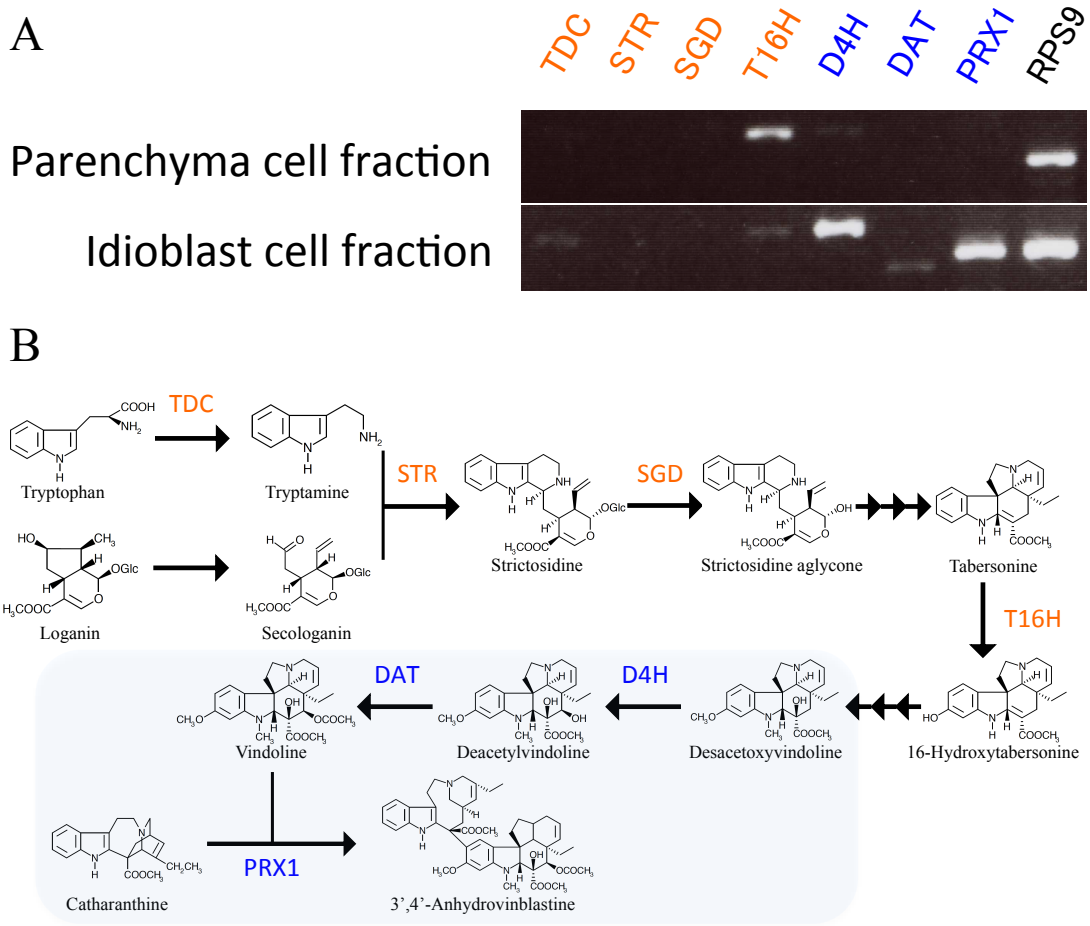

Fig. 26. RT-PCR of FACS samples. (A) RT-PCR results of TIA synthesis enzymes in the fraction of idioblast cells (P3 fraction) and that of parenchyma cells (P1 fraction). (B) TIA biosynthetic pathway in *C. roseus*. Orange font represents TIA enzymes localized in epidermal cells. Blue represents TIA enzymes localized in idioblast cells and laticifer cells.

Table 9. RNA-seq analysis of idioblast cell (Top 200)

Gene ID	Detection (Gene ID: ORCAE database)	Parenchyma cell (FPKM normalized with RPS9)	Idioblast cell (FPKM normalized with RPS9)	Stem tissue (FPKM normalized with RPS9)
c14479_g1	Caros004346.1__(chrom01)__(mRNA)_(n/a)__(No_hits_found)	1.924312264	25.23536528	4.41327817
c13977_g1	Caros007833.2__(chrom02)__(mRNA)_(n/a)__(hypothetical_protein_Kpol_1058p4)	0.306694111	6.085190422	1.060073578
c25719_g1	Caros009944.1__(chrom02)__(mRNA)_(n/a)__(hypothetical_protein)	0.305778554	5.608179696	0.629841179
c1560_g1	Caros007833.2__(chrom02)__(mRNA)_(n/a)__(hypothetical_protein_Kpol_1058p4)	0.24783969	5.048294068	0.371340333
c1624_g1	Caros007833.2__(chrom02)__(mRNA)_(n/a)__(hypothetical_protein_Kpol_1058p4)	0.284914848	4.930685248	0.815595005
c7111_g1	Caros024555.1__(chrom05)__(mRNA)_()__(hypothetical_protein_OsI_32184)	0.298561899	4.625883782	0.082892621
c14463_g1	Caros006241.2__(chrom02)__(mRNA)_(n/a)__(No_hits_found)	0	4.32791645	0.362169115
c11556_g1	Caros016298.1__(chrom04)__(mRNA)_()__(SAUR_family_protein)	0.108209404	3.697678983	0
c761_g1	Caros024532.1__(chrom05)__(mRNA)_(n/a)__(RING-H2_finger_protein_ATL80-like)	0.076105772	3.316878852	1.445362195
c12849_g1	Caros001321.1__(chrom01)__(mRNA)_()__(armadillo_repeat-containing_protein_8)	0.034302609	2.821021602	0.062071651
c2646_g1	Caros004341.1__(chrom01)__(mRNA)_(n/a)__(putative_constans-like_protein)	0.151897139	2.722290617	1.21034239
c13654_g1	Caros000256.1__(chrom01)__(mRNA)_()__(hypothetical_protein_SORBIDRAFT_06g025790)	0.145496539	2.549644931	0.109952799
c13330_g1	Caros006097.1__(chrom02)__(mRNA)_()__(yellow_stripe-like_transporter_12)	0.153358645	2.50879175	0.125170335
c10362_g1	Caros009669.1__(chrom02)__(mRNA)_()__(putative_cytidine_deaminase)	0.185392169	2.468407249	0.365000164
c12323_g1	Caros005941.1__(chrom02)__(mRNA)_(n/a)__(unknown)	0.004715573	2.428333088	0.031334554
c8860_g1	Caros006799.2__(chrom02)__(mRNA)_(n/a)__(No_hits_found)	0.15749418	2.361338088	0.929529281
c9084_g1	Caros009123.1__(chrom02)__(mRNA)_()__(pyruvate_decarboxylase_;_Pyruvate_decarboxylase_[EC:4.1.1.1])	0.024898526	2.323593626	0.349606986
c8561_g1	Caros009632.2__(chrom02)__(mRNA)_(n/a)__(No_hits_found)	0.1591506	2.31364369	0.351833248
c11361_g1	Caros004740.2__(chrom01)__(mRNA)_(n/a)__(hypothetical_protein_SELMODRAFT_43579)	0.140212227	2.277779402	0.809087488
c13221_g1	Caros006863.3__(chrom02)__(mRNA)_(n/a)__(EIN3-binding_F-box_protein_1-like)	0.052378421	2.250644035	0.306040474
c9502_g1	Caros005081.1__(chrom02)__(mRNA)_(n/a)__(LITAF-domain-containing_protein)	0.15823752	2.244008556	0.686558315
c10297_g1	Caros005596.1__(chrom02)__(mRNA)_(n/a)__(hypothetical_protein)	0.01795947	2.090197222	0.199297959

c8673_g1	Caros005189.1__(chrom02)__(mRNA)_(n/a)__(uncharacterized_protein)	0.13913235	2.004647733	0.322966054
c7077_g1	Caros004336.1__(chrom01)__(mRNA)_(n/a)__(myb-related_protein_Myb4-like)	0.190345902	1.926124279	0.190471239
c4408_g1	Caros017505.1__(chrom04)__(mRNA)_(n/a)__(No_hits_found)	0.067763983	1.889661785	0.816963946
c13393_g1	Caros000026.1__(chrom01)__(mRNA)_()__(genomic_reference:SL2.40ch01_gene_region:79309371-79310664_transcript_region:SL2.40ch01:79309371..79310664+_go_terms:GO:0004842_functional_description:U-box_domain-containing_protein_4)	0.014900316	1.867766434	0.070900356
c30360_g1	Caros000584.1__(chrom01)__(mRNA)_(n/a)__(14_kDa_proline-rich_protein_DC2.15-like)	0.059989256	1.81920161	0.319165447
c12295_g1	Caros004893.2__(chrom01)__(mRNA)_(n/a)__(predicted_protein)	0.066995463	1.743297094	0.3088423
c13092_g1	Caros002314.2__(chrom01)__(mRNA)_()__(heat_shock_protein_70)	0.133931236	1.618686014	0.190847655
c30609_g1	Caros011881.2__(chrom03)__(mRNA)_()__(S-adenosylmethionine_decarboxylase_uORF)	0.040694204	1.521559647	1.146343171
c5759_g1	Caros001786.1__(chrom01)__(mRNA)_(n/a)__(probable_E3_ubiquitin-protein_ligase_HERC1-like)	0	1.507968069	0.101812459
c11222_g1	Caros016027.1__(chrom04)__(mRNA)_(n/a)__(No_hits_found)	0.124380708	1.495138779	0.031338686
c11330_g1	Caros008054.1__(chrom02)__(mRNA)_(n/a)__(No_hits_found)	0.142340178	1.469772682	0.850588516
c10628_g1	Caros003238.1__(chrom01)__(mRNA)_(n/a)__(No_hits_found)	0.091847359	1.467904165	0.360521597
c14667_g1	Caros010604.1__(chrom03)__(mRNA)_()__(monodehydroascorbate_reductase;_ATMDAR4/MDAR4;_ATMDAR4/MDAR4_(MONODEHYDROASCORBATE_REDUCTASE_4);_monodehydroascorbate_reductase_(NADH)_;_K08232_monodehydroascorbate_reductase_(NADH)_[EC:1.6.5.4])	0.019742733	1.455613169	1.078107133
c13471_g1	Caros010939.1__(chrom03)__(mRNA)_()__(hypothetical_protein-1)	0.128310752	1.419828325	0.056627348
c14704_g1	Caros005784.1__(chrom02)__(mRNA)_(n/a)__(hypothetical_protein_OsJ_20291)	0.060014147	1.408572364	1.846845422
c29618_g1	Caros025729.1__(chrom06)__(mRNA)_()__(conserved_hypothetical_protein)	0.137959804	1.388213935	1.65360342
c11655_g1	Caros000342.2__(chrom01)__(mRNA)_(n/a)__(No_hits_found)	0.112211246	1.378809164	0.460383876
c26153_g1	Caros001021.1__(chrom01)__(mRNA)_()__(quinone_reductase)	0.130170716	1.368466203	0.915269961
c13860_g1	Caros000628.2__(chrom01)__(mRNA)_(n/a)__(No_hits_found)	0.093314285	1.365594234	0.206370204
c13184_g1	Caros003214.1__(chrom01)__(mRNA)_()__(DDB1-_and_CUL4-associated_factor)	0.030442309	1.337827376	0.455851146
c12918_g1	Caros015430.1__(chrom04)__(mRNA)_()__(F-box/kelch-repeat_protein_At3g06240-like)	0.066361249	1.324212787	0.006444847
c34193_g1	Caros002908.1__(chrom01)__(mRNA)_(n/a)__(predicted_protein)	0.014139259	1.315570612	0.213540213
c10472_g1	Caros001330.1__(chrom01)__(mRNA)_(n/a)__(predicted_protein)	0.001783263	1.314501395	0.134991557
c8677_g1	Caros002919.1__(chrom01)__(mRNA)_()__(DNA-directed_RNA_polymerase_II_subunit_RPB7)	0.018153465	1.264676223	0.266787945

c4272_g1	Caros009354.1__(chrom02)__(mRNA)_(n/a)__(No_hits_found)	0.093684713	1.245924804	0.057992227
c14056_g1	Caros001932.1__(chrom01)__(mRNA)_()__(hypersensitive-induced_response_protein_4-like)	0.097608042	1.226335934	0.189288023
c12281_g1	Caros010539.1__(chrom03)__(mRNA)_(n/a)__(No_hits_found)	0.08979735	1.225647205	0.189442799
c15057_g1	Caros004632.1__(chrom01)__(mRNA)_(n/a)__(No_hits_found)	0.097378082	1.202019032	0.999626076
c11238_g1	Caros004099.1__(chrom01)__(mRNA)_()__(transmembrane_9_superfamily_member_3)	0.061332299	1.192949153	0.324373532
c13594_g1	Caros010539.2__(chrom03)__(mRNA)_(n/a)__(predicted_protein)	0.00165642	1.161398754	0.300999531
c9781_g1	Caros020759.1__(chrom05)__(mRNA)_()__(hypothetical_protein_ARALYDRAFT_495837)	0.017924538	1.156068017	0.80322967
c13557_g1	Caros008877.1__(chrom02)__(mRNA)_()__(Chorismate_mutase_;_Chorismate_mutase_[EC:5.4.99.5])	0.027267637	1.134172543	0.3672907
c12129_g1	Caros005894.1__(chrom02)__(mRNA)_()__(conserved_hypothetical_protein)	0.004267892	1.116314154	0.097291847
c12193_g1	Caros003310.1__(chrom01)__(mRNA)_(n/a)__(No_hits_found)	0.092602817	1.110833656	0.267761723
c9750_g1	Caros011334.1__(chrom03)__(mRNA)_(n/a)__(No_hits_found)	0.029106727	1.109241626	0.308144059
c13555_g1	Caros001257.1__(chrom01)__(mRNA)_(n/a)__(No_hits_found)	0.105719871	1.102449356	0.654751774
c16514_g1	Caros001165.1__(chrom01)__(mRNA)_(n/a)__(No_hits_found)	0.071076822	1.100406361	2.316188731
c10465_g1	Caros026678.2__(chrom06)__(mRNA)_()__(genomic_reference:SL2.40ch08_gene_region:331751-332734_transcript_region:SL2.40ch08:331751..332734+_go_terms:GO:0008270_functional_description:CAX-interacting_protein_4)	0	1.094694112	0.077434348
c10655_g1	Caros017604.1__(chrom04)__(mRNA)_(n/a)__(No_hits_found)	0.000887901	1.091433993	0.03556071
c14167_g1	Caros013771.1__(chrom03)__(mRNA)_(n/a)__(cellulose_synthase)	0.056781203	1.077482833	0.080346654
c9152_g1	Caros007952.1__(chrom02)__(mRNA)_(n/a)__(No_hits_found)	0.060436937	1.073317319	1.332488652
c7539_g1	Caros014766.1__(chrom03)__(mRNA)_(n/a)__(No_hits_found)	0.008535785	1.072925817	0.157588729
c11797_g2	Caros005695.3__(chrom02)__(mRNA)_()__(hypothetical_protein_MTR_1g110370_(Higher_score_ortholog_with_unknown_function:_MT6G008660_))	0.007386737	1.063954725	0.210396085
c8798_g1	Caros013674.1__(chrom03)__(mRNA)_(n/a)__(unknown)	0.038978093	1.061662762	0.405921833
c8295_g1	Caros000965.1__(chrom01)__(mRNA)_()__(putative_germin-like_protein_2-1)	0.035470123	1.052014328	0.014859363
c14044_g1	Caros003776.1__(chrom01)__(mRNA)_()__(ATPase)	0.004327583	1.044785457	0.25644646
c6679_g1	Caros007820.2__(chrom02)__(mRNA)_(n/a)__(unknown)	0.002357787	1.043645346	0.162614806
c13170_g1	Caros008216.1__(chrom02)__(mRNA)_()__(U4/U6.U5_tri-snRNP-associated_protein)	0.044454725	1.040800236	0.327487282

c11300_g1	Caros000467.1__(chrom01)__(mRNA)_(n/a)__(No_hits_found)	0.07769504	1.038174192	0.537088317
c13959_g1	Caros012255.4__(chrom03)__(mRNA)_(n/a)__(No_hits_found)	0.03576086	1.031290459	0.375378397
c12699_g1	Caros005003.3__(chrom02)__(mRNA)_()__(mate_efflux_family_protein)	0.08062735	1.02933984	0.18949029
c10424_g1	Caros018680.1__(chrom04)__(mRNA)_(n/a)__(predicted_protein)	0.021324131	1.023300129	0.007976749
c12854_g1	Caros004358.2__(chrom01)__(mRNA)_(n/a)__(No_hits_found)	0.095272632	1.021333861	0.211554387
c7424_g1	Caros008943.1__(chrom02)__(mRNA)_(n/a)__(No_hits_found)	0.007692555	1.020821306	0.34923845
c9630_g2	Caros002413.3__(chrom01)__(mRNA)_()__(Ubiquitin_domain-containing_protein)	0.004969259	1.018396513	0.194188179
c12477_g1	Caros004389.1__(chrom01)__(mRNA)_(n/a)__(No_hits_found)	0.03248569	1.003052294	0.574321589
c13547_g1	Caros010310.2__(chrom03)__(mRNA)_(n/a)__(No_hits_found)	0	0.999894861	0.196220852
c26017_g1	Caros001989.1__(chrom01)__(mRNA)_(n/a)__(predicted_protein)	0	0.997775488	0.02750682
c12589_g1	Caros009360.1__(chrom02)__(mRNA)_()__(plant_synaptotagmin)	0.075420709	0.988730181	0.462955066
c9527_g1	Caros001880.1__(chrom01)__(mRNA)_()__(Os02g0475300)	0	0.979963034	0.018605209
c8962_g1	Caros013806.1__(chrom03)__(mRNA)_()__(STM1_protein)	0	0.978119605	0.505820328
c12927_g1	Caros005431.1__(chrom02)__(mRNA)_(n/a)__(No_hits_found)	0.008230462	0.974721615	0.0869478
c13152_g1	Caros008217.2__(chrom02)__(mRNA)_(n/a)__(No_hits_found)	0.080754193	0.967117743	0.079165252
c10495_g1	Caros008162.1__(chrom02)__(mRNA)_(n/a)__(predicted_protein)	0.028057982	0.965798126	0
c14208_g1	Caros003079.2__(chrom01)__(mRNA)_(n/a)__(No_hits_found)	0.060436937	0.963664765	1.275726044
c12676_g1	Caros001929.1__(chrom01)__(mRNA)_()__(receptor_kinase)	0	0.959757467	0.032444248
c13538_g1	Caros006679.1__(chrom02)__(mRNA)_()__(GYF_domain-containing_protein)	0.029418472	0.959219632	0.522169856
c8884_g1	Caros007589.1__(chrom02)__(mRNA)_()__(protein_SCAI_isoform_2)	0.044075214	0.951075431	0.098958617
c13190_g1	Caros010480.1__(chrom03)__(mRNA)_(n/a)__(predicted_protein)	0.018720528	0.943610252	0.235046936
c12813_g1	Caros007176.1__(chrom02)__(mRNA)_(n/a)__(probable_methyltransferase_PMT8)	0.079418612	0.941493618	0.298012065
c5413_g1	Caros004088.1__(chrom01)__(mRNA)_(n/a)__(cysteine/histidine-rich_C1_domain-containing_protein)	0	0.941451167	0.021248675
c6492_g1	Caros001837.1__(chrom01)__(mRNA)_(n/a)__(EID1-like_F-box_protein_2-like)	0.008595475	0.937329403	0.1556292

c28290_g1	Caros024245.1__(chrom05)__(mRNA)_(n/a)__(No_hits_found)	0	0.9371571	0.137734654
c12440_g1	Caros006374.1__(chrom02)__(mRNA)_(n/a)__(high_mobility_group_family)	0.023689787	0.93336296	0.249058508
c8017_g1	Caros001595.1__(chrom01)__(mRNA)_()__(polygalacturonase-like_protein-like)	0.09190145	0.927917373	0.262533643
c13039_g1	Caros005021.1__(chrom02)__(mRNA)_(n/a)__(No_hits_found)	0.087633558	0.927504619	0.270219033
c26328_g1	Caros015689.1__(chrom04)__(mRNA)_()__(Ferric-chelate_reductase)	0.046678207	0.922258503	0.092186263
c8761_g1	Caros015803.1__(chrom04)__(mRNA)_(n/a)__(tonoplast_intrinsic_protein)	0.003820211	0.921720284	2.628857195
c33438_g1	Caros007008.1__(chrom02)__(mRNA)_()__(hypothetical_protein_SORBIDRAFT_03g003810)	0.007640423	0.921281436	1.005870456
c11589_g1	Caros001471.1__(chrom01)__(mRNA)_()__(isochorismate_synthase_;_Isochorismate_synthase_[EC:5.4.4.2])	0.054960306	0.91913244	0.339999317
c11062_g1	Caros014200.1__(chrom03)__(mRNA)_()__(genomic_reference:SL2.40ch03_gene_region:9745193-9745957_transcript_region:SL2.40ch03:9745193..9745957-_functional_description:Genomic_DNA_chromosome_5_TAC_clone_K1F13)	0	0.915149582	0.030136785
c13309_g1	Caros004593.1__(chrom01)__(mRNA)_(n/a)__(serine/threonine-protein_kinase_OXI1-like)	0.006849865	0.903419228	0.257031757
c8136_g1	Caros007236.1__(chrom02)__(mRNA)_()__(probable_protein_phosphatase_2C_43)	0.049887553	0.902122703	0.720449901
c4097_g1	Caros003408.1__(chrom01)__(mRNA)_()__(putative_pterin-4-alpha-carbinolamine_dehydratase_isoform_1)	0.060377246	0.901500303	0.44560628
c11762_g1	Caros010619.2__(chrom03)__(mRNA)_(n/a)__(No_hits_found)	0.051266937	0.900537777	0.277512482
c6085_g1	Caros006269.1__(chrom02)__(mRNA)_(n/a)__(unknown)	0	0.88531634	0.064086581
c22113_g1	Caros005053.1__(chrom02)__(mRNA)_()__(acyl-protein_thioesterase_2-like)	0.008916313	0.885301478	0.919163559
c11419_g1	Caros019513.1__(chrom04)__(mRNA)_()__(zinc_finger_CCCH_domain-containing_protein_3-like)	0	0.882513028	1.090977551
c12467_g1	Caros000311.1__(chrom01)__(mRNA)_()__(Os08g0230500)	0.087059034	0.88230462	0.125653432
c12741_g1	Caros014040.1__(chrom03)__(mRNA)_(n/a)__(unknown)	0.076232615	0.881709857	0.140002707
c8176_g1	Caros002361.1__(chrom01)__(mRNA)_(n/a)__(No_hits_found)	0.035284725	0.881632805	0.142022328
c8688_g1	Caros011046.1__(chrom03)__(mRNA)_(n/a)__(uncharacterized_protein_LOC100853355)	0.014967469	0.878904446	0.806049592
c10581_g1	Caros028224.1__(chrom06)__(mRNA)_(n/a)__(multiple_C2_and_transmembrane_domain-containing_protein_2-like)	0.036172626	0.8775558	0.003968354
c499_g1	Caros010232.1__(chrom03)__(mRNA)_()__(hypothetical_protein_RCOM_1407360)	0.005349788	0.872762434	0.152148622
c8623_g1	Caros000079.1__(chrom01)__(mRNA)_(n/a)__(choline/ethanolamine_kinase)	0.05559452	0.869683242	0.155633377
c13516_g1	Caros008677.1__(chrom02)__(mRNA)_()__(AP2_domain-containing_transcription_factor)	0.044768101	0.864464215	0.100295483

c12576_g1	Caros005783.1__(chrom02)__(mRNA)_()__(probable_LRR_receptor-like_serine/threonine-protein_kinase_At1g56140-like)	0.002865158	0.864432108	0.181667398
c7574_g1	Caros003109.1__(chrom01)__(mRNA)_(n/a)__(putative_peptidyl-tRNA_hydrolase_PTRHD1-like)	0	0.854669844	0.307350435
c11517_g1	Caros009724.2__(chrom02)__(mRNA)_()__(hypothetical_protein_VITISV_022650)	0.047125888	0.853938251	0.281158825
c727_g1	Caros009711.2__(chrom02)__(mRNA)_(n/a)__(unknown)	0.045832344	0.852887777	0.233207696
c10218_g1	Caros015460.1__(chrom04)__(mRNA)_(n/a)__(probable_serine/threonine-protein_kinase_At1g18390-like)	0.027256312	0.846018496	0.143383073
c6861_g1	Caros012336.1__(chrom03)__(mRNA)_(n/a)__(No_hits_found)	0.006950185	0.845852037	0.045612048
c7249_g1	Caros007549.2__(chrom02)__(mRNA)_(n/a)__(homeobox-leucine_zipper_protein_HAT5-like)	0.043848246	0.845437238	0.289166002
c3522_g1	Caros013049.1__(chrom03)__(mRNA)_()__(Os05g0304100)	0	0.844980201	0.092958947
c10749_g1	Caros012346.1__(chrom03)__(mRNA)_(n/a)__(nitrate_transporter_1.2-like)	0	0.837749644	0.284810251
c11804_g1	Caros018130.1__(chrom04)__(mRNA)_(n/a)__(No_hits_found)	0.003059154	0.837123556	0.340696299
c6732_g1	Caros008620.2__(chrom02)__(mRNA)_(n/a)__(RabGAP/TBC_domain-containing_protein)	0.062338978	0.834128029	0.219799734
c15602_g1	Caros003964.1__(chrom01)__(mRNA)_(n/a)__(predicted_protein)	0.037769355	0.833701359	0.148059155
c18244_g1	Caros001786.1__(chrom01)__(mRNA)_(n/a)__(probable_E3_ubiquitin-protein_ligase_HERC1-like)	0	0.833333333	0.005760107
c9206_g1	Caros009444.1__(chrom02)__(mRNA)_()__(hypothetical_protein_MTR_3g091280)	0.007133051	0.832170835	0.843257289
c11854_g1	Caros007882.1__(chrom02)__(mRNA)_(n/a)__(unknown)	0	0.826141203	0.348320442
c33518_g1	Caros007781.2__(chrom02)__(mRNA)_(n/a)__(No_hits_found)	0.001335582	0.817366223	0.300213913
c8921_g1	Caros010730.1__(chrom03)__(mRNA)_()__(hypothetical_protein_VITISV_019343)	0	0.80354777	0.049510138
c9155_g1	Caros005969.1__(chrom02)__(mRNA)_(n/a)__(No_hits_found)	0	0.802831262	0.100477384
c11700_g2	Caros001660.1__(chrom01)__(mRNA)_()__(Serine_carboxypeptidase-like_protein)	0.03133021	0.802733658	0.236094219
c10993_g1	Caros008946.1__(chrom02)__(mRNA)_(n/a)__(No_hits_found)	0.022784729	0.801985704	0.108036063
c11336_g1	Caros007006.1__(chrom02)__(mRNA)_()__(hypothetical_protein_OsJ_30844)	0.03757536	0.787866474	0.07839724
c12413_g1	Caros007901.2__(chrom02)__(mRNA)_()__(elongation_factor_P)	0.011400943	0.785005719	0.150759525
c14210_g2	Caros010806.1__(chrom03)__(mRNA)_(n/a)__(mitochondrial_inner_membrane_protease_subunit_2-like)	0.001716111	0.783307685	0.363259126
c12782_g1	Caros009002.1__(chrom02)__(mRNA)_(n/a)__(protein_NSP-INTERACTING_KINASE_1-like)	0.00082821	0.781196767	0.30548429

c10748_g1	Caros001693.2__(chrom01)__(mRNA)_(n/a)__(No_hits_found)	0.061839671	0.779101235	0.749362342
c13169_g1	Caros015552.1__(chrom04)__(mRNA)_(n/a)__(No_hits_found)	0.070338821	0.775927661	0.078499506
c14394_g1	Caros009494.1__(chrom02)__(mRNA)_(n/a)__(zinc_finger_CCCH_domain-containing_protein_48-like)	0.013184206	0.775636509	0.32861074
c10516_g1	Caros006690.1__(chrom02)__(mRNA)_(n/a)__(No_hits_found)	0.042477467	0.773220301	0.151815879
c232_g1	Caros001650.1__(chrom01)__(mRNA)_(n/a)__(unknown)	0.054960306	0.773159928	0.329934117
c14277_g1	Caros012933.1__(chrom03)__(mRNA)_()__(armadillo_repeat-containing_kinesin-like_protein_2-like)	0.068225132	0.772278964	0.450400507
c35291_g1	Caros012032.2__(chrom03)__(mRNA)_(n/a)__(hypothetical_protein_ARALYDRAFT_313968)	0.002357787	0.77170162	0.055825549
c27838_g1	Caros007410.1__(chrom02)__(mRNA)_(n/a)__(No_hits_found)	0.026174417	0.76972291	0.578616402
c4463_g1	Caros003901.1__(chrom01)__(mRNA)_(n/a)__(No_hits_found)	0	0.769280468	0
c2509_g1	Caros007841.1__(chrom02)__(mRNA)_()__(beta-galactosidase_(EC:3.2.1.23))	0	0.768676128	0.002492051
c29552_g1	Caros020596.1__(chrom05)__(mRNA)_()__(formate_dehydrogenase_;_formate_dehydrogenase_[EC:1.2.1.2])	0.067569987	0.768194344	1.111928093
c10001_g1	Caros000082.2__(chrom01)__(mRNA)_(n/a)__(No_hits_found)	0.042029786	0.767520067	0.350260424
c10301_g1	Caros013133.1__(chrom03)__(mRNA)_(n/a)__(putative_disease_resistance_protein)	0.008884554	0.766998708	0.203850919
c12805_g1	Caros012416.1__(chrom03)__(mRNA)_(n/a)__(ribosomal_RNA-processing_protein_8)	0.065025667	0.766425273	0.58883713
c15715_g1	Caros021189.1__(chrom05)__(mRNA)_(n/a)__(poly(rC)-binding_protein_3-like)	0	0.76321213	0.426880219
c6741_g1	Caros029171.1__(chrom06)__(mRNA)_(n/a)__(CST_complex_subunit_CTC1)	0.035284725	0.76289075	0.00630268
c246_g1	Caros026425.1__(chrom06)__(mRNA)_(n/a)__(No_hits_found)	0	0.76198203	0.041186135
c11054_g1	Caros001700.1__(chrom01)__(mRNA)_()__(WD_repeat_domain-containing_protein_83-like_(Higher_score_ortholog_with_unknown_function:_MT8G092620_))	0.064811582	0.757690237	0.114389651
c12766_g2	Caros011579.1__(chrom03)__(mRNA)_()__(Ammonium_transporter)	0.003439682	0.75429128	0.441310074
c3460_g1	Caros025302.1__(chrom06)__(mRNA)_(n/a)__(No_hits_found)	0.042544619	0.753336601	0
c11377_g1	Caros004205.1__(chrom01)__(mRNA)_(n/a)__(No_hits_found)	0.054258939	0.75238399	0.035994403
c13238_g1	Caros005206.2__(chrom02)__(mRNA)_(n/a)__(No_hits_found)	0.064512863	0.750681064	0.201014628
c5918_g1	Caros014147.1__(chrom03)__(mRNA)_(n/a)__(pentatricopeptide_repeat-containing_protein)	0	0.744728672	0.010662191
c33368_g1	Caros012439.2__(chrom03)__(mRNA)_()__(genomic_reference:SL2.40ch07_gene_region:59672873-59673307_transcript_region:SL2.40ch07:59672873..59673307-_functional_description:Genomic_DNA_chromosome_3_TAC_clone_K7L4)	0	0.744188709	0.02109244

c3538_g1	Caros008485.1__(chrom02)__(mRNA)_(n/a)__(zinc_finger_CCCH_domain-containing_protein_44-like)	0	0.741723988	0.019929409
c12948_g1	Caros006349.1__(chrom02)__(mRNA)_(n/a)__(hypothetical_protein_VITISV_030961)	0.003118844	0.741071587	0.112915219
c11441_g1	Caros015383.2__(chrom04)__(mRNA)_(n/a)__(No_hits_found)	0.004327583	0.740518895	0.187079439
c34600_g1	Caros005252.1__(chrom02)__(mRNA)_(n/a)__(GTP-binding_protein_At2g22870-like)	0.003887363	0.740201386	0.125683237
c9579_g1	Caros000553.3__(chrom01)__(mRNA)_()__(Zinc_finger_protein_CONSTANS-like_protein)	0.054579777	0.73798126	1.788345993
c11814_g1	Caros006287.2__(chrom02)__(mRNA)_(n/a)__(No_hits_found)	0.028591894	0.735803821	0.2151149
c13366_g1	Caros001507.1__(chrom01)__(mRNA)_(n/a)__(hypothetical_protein_SELMODRAFT_438020)	0.024197159	0.735394668	1.045640221
c9645_g1	Caros013079.1__(chrom03)__(mRNA)_()__(hypothetical_protein_VITISV_038181)	0.057377783	0.729825517	0.121276866
c10975_g1	Caros000570.1__(chrom01)__(mRNA)_()__(UDP-glycosyltransferase_92A1-like)	0.049437805	0.727513839	0.033342133
c406_g1	Caros011726.1__(chrom03)__(mRNA)_()__(GAGA-binding_transcriptional_activator)	0.007327046	0.723282499	0.315372482
c6235_g1	Caros003792.1__(chrom01)__(mRNA)_(n/a)__(DOG1_alpha_splice_variant)	0.038657255	0.722857169	0
c11036_g1	Caros005849.1__(chrom02)__(mRNA)_()__(conserved_hypothetical_protein)	0.001977258	0.722716418	0.224707447
c14160_g1	Caros006953.1__(chrom02)__(mRNA)_(n/a)__(No_hits_found)	0.037361275	0.717513398	0.189093746
c3939_g1	Caros005214.1__(chrom02)__(mRNA)_(n/a)__(No_hits_found)	0.056683878	0.716856258	0.576344154
c8128_g1	Caros016753.2__(chrom04)__(mRNA)_(n/a)__(ATP-dependent_RNA_helicase_dbp9)	0.012182718	0.712289577	0.146803354
c10501_g1	Caros007945.1__(chrom02)__(mRNA)_()__(CONSTANS_interacting_protein_4)	0.009550528	0.712179563	0.249002914
c8038_g1	Caros004444.1__(chrom01)__(mRNA)_()__(DEAD-box_ATP-dependent_RNA_helicase_30-like)	0.062205702	0.710828439	0.178352429
c11192_g1	Caros012943.1__(chrom03)__(mRNA)_()__(conserved_hypothetical_protein)	0.005924312	0.710260447	0.190376113
c1428_g1	Caros001042.1__(chrom01)__(mRNA)_(n/a)__(No_hits_found)	0	0.709889265	0.033423284
c13505_g1	Caros010032.1__(chrom03)__(mRNA)_()__(glutamate-rich_WD_repeat-containing_protein_1-like)	0.05633189	0.706887809	0.385415863
c10656_g1	Caros010180.3__(chrom03)__(mRNA)_()__(DBP1;_Dbp1p_;_K11594_ATP-dependent_RNA_helicase_bel_[EC:3.6.1.-])	0.034963887	0.706626102	0.230804488
c15416_g1	Caros006203.1__(chrom02)__(mRNA)_()__(La_protein_1)	0.058332836	0.706456275	0.469703893
c12543_g1	Caros009879.1__(chrom02)__(mRNA)_()__(TATA-binding_protein-associated_factor_172-like)	0.016737953	0.701494155	0.311856682
c14266_g3	Caros008913.1__(chrom02)__(mRNA)_()__(hypothetical_protein_OsJ_07117)	0.03426252	0.695147571	0.265300638

c24443_g1	Caros016115.1__(chrom04)__(mRNA)_(n/a)__(No_hits_found)	0.01737145	0.694744832	0
c13158_g1	Caros008469.1__(chrom02)__(mRNA)_(n/a)__(trypsin-like_protein)	0.049864203	0.694657109	0.187612218
c11562_g1	Caros002509.1__(chrom01)__(mRNA)_()__(MUT9-related_serine/threonine_protein_kinase)	0.009296842	0.693435581	0.214418337
c13350_g3	Caros020439.1__(chrom05)__(mRNA)_(n/a)__(No_hits_found)	0.066682087	0.690969304	0.111344969
c2999_g1	Caros004376.1__(chrom01)__(mRNA)_(n/a)__(late_embryogenesis_abundant_protein)	0.053418774	0.689990781	0.722675154
c13008_g1	Caros005672.2__(chrom02)__(mRNA)_(n/a)__(No_hits_found)	0.031464514	0.684262104	0.79132274
c14154_g1	Caros000857.1__(chrom01)__(mRNA)_()__(genomic_reference:SL2.40ch02_gene_region:13906095-13908491_transcript_region:SL2.40ch02:13906095..13908491-_go_terms:GO:0005515_functional_description:Heterogeneous_nuclear_ribonucleoprotein_A3-like_p)	0.02923357	0.683760079	0.736830216
c8513_g1	Caros014888.1__(chrom03)__(mRNA)_(n/a)__(predicted_protein)	0.003118844	0.683325973	0.157282404
c24029_g1	Caros010379.1__(chrom03)__(mRNA)_(n/a)__(F16A14.21)	0.04260431	0.679852268	0.126556682
c9209_g1	Caros016149.1__(chrom04)__(mRNA)_(n/a)__(No_hits_found)	0.033687996	0.671805808	0.293051271

Table 10. RT-PCR primers for investigation of tissue-specific gene expression

Primer name	Primer sequence
T16H2-F	GATCAACTCACAGTGGCAGTC
T16H2-R	GACTTGAGGACTTGTGATTGGC
PCR-60S-F	TCTTAGTTGGAATGTTCAGCACCTG
PCR-60S-R	CAAGGTTGGAGCCCCTGCTCGTGTT

Table 11. RT-PCR primers for investigation of gene expression in FACS samples

Primer name	Primer sequence
TDC-RT01	CGCCTGTATATGTCCCGAGT
TDC-RT02	GTTGCGATTTGCCAATTTTT
STR-RT01	ACCATTGTGTGGGAGGACAT
STR-RT02	CCATTTGAATGGCACTCCTT
SGD-RT01	ATTTGCACCAGGAAGAGGTG
SGD-RT02	TATGAACCATCCGAGCATGA
T16H-RT01	GCTTCATCCACCAGTTCCAT
T16H-RT02	CCGGACATATCCTTCTTCCA
D4H-RT01	TTGACATTTGGGACAAGCAA
D4H-RT02	CCAAAAGCAACAGCAACAGA
DAT-RT01	CTTCTTCTCATCACGTACCAACTC
DAT-RT02	ATACCAAACTCAACGGCCTTAG
PRX1-RT01	TAGCTCAAACAACTCGGCCACC
PRX1-RT02	GCAGCACTGATGAATCGCACC
RPS9-RT01	AGCGCCGCCTTCAAACCCTT
RPS9-RT02	GCCAGGACGACCACCACCGA

General discussion and concluding remarks

TIA biosynthesis mechanism in *Catharanthus roseus* plant

General discussion and concluding remarks :

TIA biosynthesis mechanism in *Catharanthus roseus* plant

TIA localization in *C. roseus* stem and leaf tissues.

In the present study, metabolome analyses using Imaging MS and Single-cell MS revealed that most TIAs and strictosidine localized in idioblast cells and laticifer cells in *C. roseus* (Yamamoto et al., 2016). Strictosidine is well known as a central precursor of all TIAs. Thus far, it has been supposed that strictosidine is produced in the vacuole of epidermal cells and subsequent biosynthesis from strictosidine also occurs in the nucleus of the epidermal cells (Thamm et al., 2016). Present results showed that strictosidine also localized in both idioblast cells and laticifer cells. My results suggested that both idioblast cell and laticifer cell play important roles not only for accumulation of TIAs end products but also for temporary accumulation of TIAs intermediates or/and strictosidine biosynthesis (Fig. 12). Furthermore, according to TIA intermediates localized in *C. roseus* idioblast cell and laticifer cell, it might be possible that TIA biosynthesis related genes are expressed in these types of cells, such as homologous genes of strictosidine synthase, strictosidine β-glucosidase or subsequent TIA biosynthesis enzymes. If these TIAs intermediates are produced in only the epidermal cells as suggested before, these intermediates must be needed to be transported from idioblast cells and laticifer cells to epidermal cells when these substances are used for subsequent TIA biosynthesis. It is the high possibility that idioblast cell and laticifer cell also have transporters of TIA intermediates, such as

strictosidine transporters. Recent investigation revealed that ABC transporter of *C. roseus* (CrTPT2) transports catharanthine from the epidermal cell to wax layer (Yu et al., 2013). This is the only detected *C. roseus* TIA transporter so far. Recent investigation also suggested that further ABC transporter and H^+ antiport system are related to TIA metabolism in *C. roseus*. (Carqueijeiro et al., 2013). Since catharanthine and other TIA intermediates were accumulated both in the idioblast cell and laticifer cell, it is the possibility that other catharanthine and TIA transporters might localize in idioblast cell and laticifer cell.

Vindoline is mainly produced in *C. roseus* leaf tissues.

When I investigate the metabolite distribution in stem idioblast cell and laticifer cell by using Single-cell MS, I could not detect any vindoline and vindoline intermediates in these cells. However, when I investigated metabolites in leaf idioblast cell and laticifer cell by the same method, both vindoline and vindoline intermediates were localized in those cells. Furthermore, I investigated vindoline content in laticifer cells of each tissue, i.e. leaf tissue, leaf primordium and stem tissue. This result showed that vindoline accumulated in leaf tissues and vindoline content in laticifer cells increased as leaf expanded (Fig. 27). It is important that vindoline biosynthesis pathway is supported by the development of cells surrounding laticifer cells. Especially, it is suggested that epidermal cells are deeply involved in this vindoline biosynthesis because Tabersonine 16-hydroxylase 2 (T16H2) are expressed in the epidermal cells of leaf tissues (Besseau et al., 2013). T16H2 enzyme is known as a key enzyme to coordinate between vindoline

and vindorosine pathways (Besseau et al., 2013). Down-regulation of T16H2 led to decrease 16-hydroxytabersonine, deacetylvindoline and vindoline contents. On the other hand, this down-regulation increased deacetylvindorosine and vindorosine contents (Besseau et al., 2013). I also obtained similar expression data of T16H2 in *C. roseus* stem and leaf tissues (Fig. 22). From these results and reports, it is suggested that T16H2 act as a coordinator of vindoline and vindorosine pathway in those tissues. Investigaton on the regulatory factor of T16H2 will lead to reveal how and when vindoline pathway is activated.

Transcriptional regulation of metabolism and differentiation in idioblast cell and laticifer cell.

TIA metabolism is also regulated by plant hormones, such as jasmonate and salicylic acid, in *C. roseus*. These days, it has been revealed the complicated transcriptional regulation involved in iridoid and TIA biosynthesis in *C. roseus* (Pan et al., 2016). ORCA2 and ORCA3, that is AP2/ERF family transcription factors, regulate the expression of TIA enzymes such as strictosidine synthase (STR) and desacetoxyvindoline 4-hydroxylase (D4H) (Van Der Fits et al., 2000). BIS1 and BIS2, those are the bHLH transcription factors, control the iridoid biosynthetic pathway (Van Moerkercke et al., 2015; Van Moerkercke et al., 2016). Zinc finger–binding protein genes (ZCTs) and *Cr*MYC also regulate TIA biosynthesis complicatedly (Pan et al., 2016).

Although it has been that several transcription factors affect the expression of

TIA biosynthetic enzymes localized in idioblast cells and laticifer cells, it has been still unknown how the lipid biosynthesis and serpentine biosynthesis were regulated. Lipid and serpentine biosynthesis are important characteristics of idioblast cells and laticifer cells. If I can reveal the transcriptional regulation of lipid biosynthesis and additional TIA biosynthesis, these results would lead us to understand how idioblast cells and laticifer cells are differentiated (Fig. 28).

Iridoids have the role for protection against insects.

Iridoid is one of monoterpenoid produced from IPP and these compounds are glycosylated usually. It is believed that over 50 plants families produce iridoid glycosides (Lampert et al., 2010). Iridoids are well known as defense compounds that were used not only plants but also insects. Some butterflies utilize plant iridoid to protect against vertebrate (gray jay) and invertebrate predators (ants and spiders) (Nishida, 2002). Our results showed that iridoids including loganin and secologanin localized in epidermal cell in stem and leaf tissues (Yamamoto et al., 2016). It is a suitable distribution of iridoids to protect themselves from predators. I consider that these iridoids localized in epidermal cells will have the biological activities for protection against predators (Figs. 3 and 17), but that mechanism has still been unknown.

The role of idioblast cells and laticifer cells.

Idioblast cell and laticifer cell differed in their form, size, contents, and cell structure, compared with common cell types such as parenchyma cell or epidermal cell (Foster, 1956) (Figs. 3L, 4 and 15). In *C. roseus*, idioblast cells and laticifer cells were classified as plant idioblasts using the broad definition of this cell type. PCA also showed that idioblast cell and laticifer cell have many similar features (Fig. 10), which imply that these cell types play a similar role in plant (Hagel et al., 2008). The physiological differences between idioblast cells and laticifer cells remain unclear.

In this study, I revealed the localization of iridoids and TIAs in *C. roseus* stem and leaf tissues. Although iridoids, including loganin and secologanin, localized and accumulated in epidermal cells, most of TIAs localized in idioblast cells and laticifer cells. These data help us to investigate which metabolic systems are progressed in the idioblast cells and laticifer cells in this plant. The number of latex containing plants is estimated to be about 12,500 and latex synthesis might be related to specialized metabolism. Although some reports latex metabolites benefits plant under herbivore attack (Huber et al., 2016), it is poorly understood why those special secretory idioblasts are needed in plant life. In the near future, I would like to know the relationship between specialized metabolism and secretory idioblasts in plants.

Figure

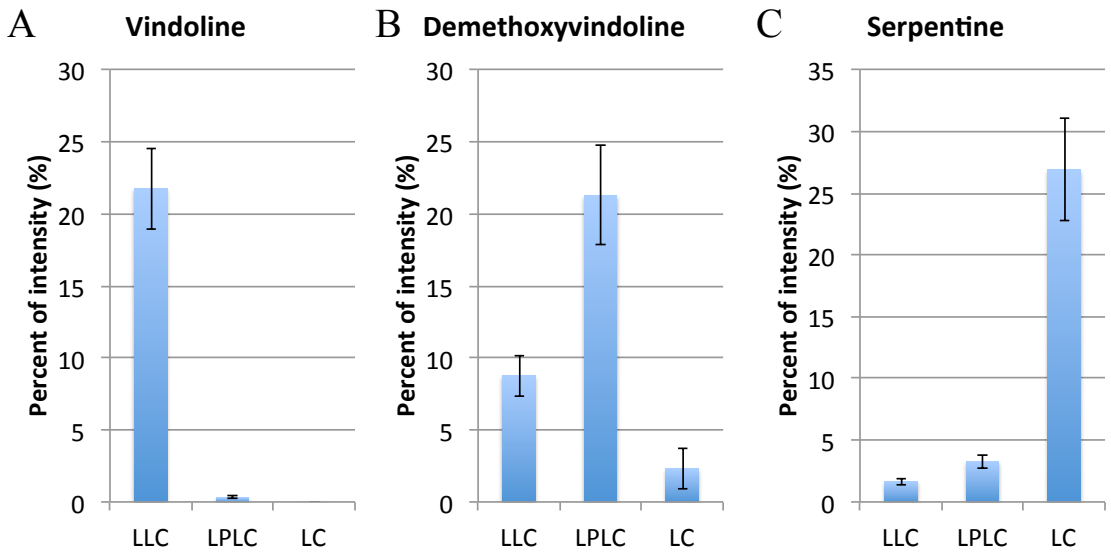

Fig. 27. TIA localization in laticifer cells in each tissue. (A) Vindoline. (B) Demethoxyvindoline. (C) Serpentine. Vindoline is accumulated in leaf laticifer cell as leaf expands. Values are the mean of three measurements (± SEM).

Abbreviation, LLC : Leaf laticifer cell, LPLC : Leaf primordium laticifer cell, LC : Stem laticifer cell.

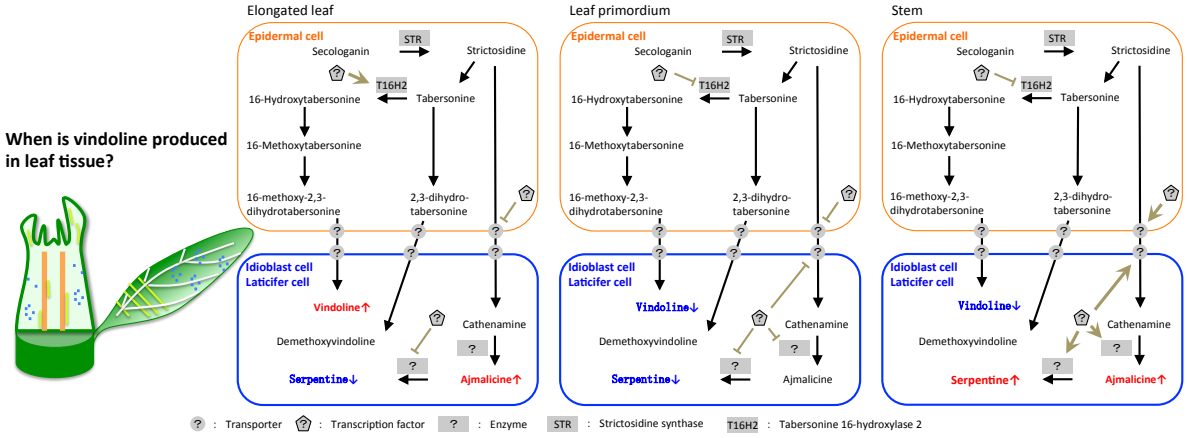

Fig. 28. TIA metabolism in *C. roseus* stem and leaf tissues. TIA biosynthesis is regulated complicatedly.

References

1. Balsevich J, Hogge LR, Berry AJ, Games DE, Mylchreest IC (1988). Analysis of indole alkaloids from leaves of Catharanthus roseus by means of supercritical fluid chromatography/mass spectrometry. J Nat Prod 51(6):1173-1177.
2. Beaudoin GA, Facchini PJ (2014). Benzylisoquinoline alkaloid biosynthesis in opium poppy. Planta 240(1):19-32.
3. Besseau S, et al. (2013) A pair of tabersonine 16-hydroxylases initiates the synthesis of vindoline in an organ-dependent manner in Catharanthus roseus. Plant Physiol 163(4):1792-1803.
4. Bird DA, Franceschi VR, Facchini PJ (2003) A tale of three cell types: Alkaloid biosynthesis is localized to sieve elements in opium poppy. Plant Cell 15(11):2626-2635.
5. Blom TJM, et al. (1991) Uptake and accumulation of ajmalicine into isolated vacuoles of cultured cells of Catharanthus roseus (L.) G. Don. and its conversion into serpentine. Planta 183(2):170-177.
6. Brown S, Clastre M, Courdavault V, O'Connor SE (2015) De novo production of the plant-derived alkaloid strictosidine in yeast. Proc Natl Acad Sci USA 112(11):3205-3210.
7. Burlat V, Oudin A, Courtois M, Rideau M, St-Pierre B (2004) Co-expression of three MEP pathway genes and geraniol 10-hydroxylase in internal phloem parenchyma of Catharanthus roseus implicates multicellular translocation of intermediates during the biosynthesis of monoterpene indole alkaloids and

isoprenoid-derived primary metabolites. Plant J 38(1):131-141.

8. Carqueijeiro I, et al. (2016). Isolation of Cells Specialized in Anticancer Alkaloid Metabolism by Fluorescence-Activated Cell Sorting. Plant Physiol 171(4):2371-2378.
9. Carqueijeiro I, Noronha H, Duarte P, Geros H, Sottomayor M (2013) Vacuolar transport of the medicinal alkaloids from Catharanthus roseus is mediated by a proton-driven antiport. Plant Physiol 162(3):1486-1496.
10. De Luca V (2011) Monoterpenoid indole alkaloid biosynthesis. Plant Metabolism and Biotechnology, eds Ashihara H, Grozier A, Komamine A (Wiley, New York), pp263-291.
11. Deus-Neumann B, Zenk MH (1986) Accumulation of alkaloids in plant vacuoles does not involve an ion-trap mechanism. Planta 167(1):44-53.
12. Dugé de Bernonville T, et al. (2015) Phytochemical genomics of the Madagascar periwinkle: Unravelling the last twists of the alkaloid engine. Phytochem 113:9-23.
13. Esau K (1965) Plant anatomy second edition (Wiley, New York), pp317-337.
14. Facchini PJ, De Luca V (2008). Opium poppy and Madagascar periwinkle: model non-model systems to investigate alkaloid biosynthesis in plants. Plant J 54(4):763-784.
15. Facchini PJ, St-Pierre B (2005) Synthesis and trafficking of alkaloid biosynthetic enzymes. Curr Opin Plant Biol 8(6):657-666.
16. Foster AS (1956) Plant idioblasts: Remarkable examples of cell specialization. Protoplasma 46(1):184-193.

17. Gigant B, et al. (2005) Structural basis for the regulation of tubulin by vinblastine. Nature 435(7041):519-522.

18. Góngora-Castillo E, et al. (2012) Development of transcriptomic resources for interrogating the biosynthesis of monoterpene indole alkaloids in medicinal plant species. PLoS One 7(12):e52506.

19. Guirimand G, et al. (2011) The subcellular organization of strictosidine biosynthesis in Catharanthus roseus epidermis highlights several trans-tonoplast translocations of intermediate metabolites. FEBS J 278(5):749-763.

20. Hagel JM, Yeung EC, Facchini PJ (2008) Got milk? The secret life of laticifers. Trends Plant Sci 13(12):631-639.

21. Hemalatha RG, Pradeep T (2013) Understanding the molecular signatures in leaves and flowers by desorption electrospray ionization mass spectrometry (DESI MS) imaging. J Agric Food Chem 61(31):7477-7487.

22. Hisiger S, Jolicoeur M (2005) Plant cell culture monitoring using an in situ multiwavelength fluorescence probe. Biotechnol Prog 21(2):580-589.

23. Huber M, et al. (2016) A latex metabolite benefits plant fitness under root herbivore attack. PLoS Biol 14(1):e1002332.

24. Kajiyama T, et al. (2015) Position-specific gene expression analysis using a microgram dissection method combined with on-bead cDNA library construction. Plant and Cell Physiol 56(7):1320-1328.

25. Kavallaris M (2010) Microtubules and resistance to tubulin-binding agents. Nat Rev Cancer 10(3):194-204.

26. Kutchan TM (2005) A role for intra- and intercellular translocation in natural product biosynthesis. Curr Opin Plant Biol 8(3):292-300.

27. Lampert EC, Bowers MD (2010) Host plant influences on iridoid glycoside sequestration of generalist and specialist caterpillars. J Chem Ecol 36(10):1101-1104.

28. Lee EJ, Hagel JM, Facchini PJ (2013) Role of the phloem in the biochemistry and ecophysiology of benzylisoquinoline alkaloid metabolism. Front Plant Sci 4(182):182.

29. Li B, Bhandari DR, Janfelt C, Römpp A, Spengler B (2014) Natural products in Glycyrrhiza glabra (licorice) rhizome imaged at the cellular level by atmospheric pressure matrix-assisted laser desorption/ionization tandem mass spectrometry imaging. Plant J 80(1):161-171.

30. Lorenzo Tejedor M, Mizuno H, Tsuyama N, Harada T, Masujima T (2012) In situ molecular analysis of plant tissues by live single-cell mass spectrometry. Anal Chem 84(12):5221-5228.

31. Mahroug S, Courdavault V, Thiersault M, St-Pierre B, Burlat V (2006) Epidermis is a pivotal site of at least four secondary metabolic pathways in Catharanthus roseus aerial organs. Planta 223(6):1191-1200.

32. Mersey BG, Cutler AJ (1986) Differential distribution of specific indole alkaloids in leaves of Catharanthus roseus. Can J Bot 64(5):1039-1045.

33. Mizuno H, Tsuyama N, Harada T, Masujima T (2008) Live single-cell video-mass spectrometry for cellular and subcellular molecular detection and cell classification.

J Mass Spectrom 43(12):1692-1700.

34. Murata J, De Luca V (2005) Localization of tabersonine 16-hydroxylase and 16-OH tabersonine-16-O-methyltransferase to leaf epidermal cells defines them as a major site of precursor biosynthesis in the vindoline pathway in Catharanthus roseus. Plant J 44(4):581-594.
35. Murata J, Roepke J, Gordon H, De Luca V (2008) The leaf epidermome of Catharanthus roseus reveals its biochemical specialization. Plant Cell 20(3): 524-542.
36. Nessler CL, Allen RD, Galewsky S (1985) Identification and characterization of latex-specific proteins in opium poppy. Plant Physiol 79(2):499-504.
37. Nishida R (2002) Sequestration of defensive substances from plants by Lepidoptera. Annu Rev Entomol 47(1):57-92.
38. O'Keefe BR, Mahady GB, Gills JJ, Beecher CWW, Schilling AB (1997) Stable vindoline production in transformed cell cultures of Catharanthus roseus. J Nat Prod 60(3):261-264.
39. Onoyovwe A, et al. (2013) Morphine biosynthesis in opium poppy involves two cell types: Sieve elements and laticifers. Plant Cell 25(10):4110-4122.
40. Pan Q, et al. (2016) Monoterpenoid indole alkaloids biosynthesis and its regulation in Catharanthus roseus: A literature review from genes to metabolites. Phytochem Rev 15(2):221-250.
41. Pramoolkit P, et al. (2014) Involvement of ethylene-responsive microRNAs and their targets in increased latex yield in the rubber tree in response to ethylene

treatment. Plant Physiol Biochem 84:203-212.

42. Qu Y, et al. (2015). Completion of the seven-step pathway from tabersonine to the anticancer drug precursor vindoline and its assembly in yeast. Proc Natl Acad Sci U S A. 112(19):6224-6229.

43. Roepke J, et al. (2010) Vinca drug components accumulate exclusively in leaf exudates of Madagascar periwinkle. Proc Natl Acad Sci USA 107(34):15287-15292.

44. Singh D, et al. (2008) Predominance of the serpentine route in monoterpenoid indole alkaloid pathway of Catharanthus roseus. Proc Indian Natl Sci Acad 74(3):97-109.

45. St-Pierre B, Vazquez-Flota FA, De Luca V (1999) Multicellular compartmentation of Catharanthus roseus alkaloid biosynthesis predicts intercellular translocation of a pathway intermediate. Plant Cell 11(5):887-900.

46. Stoeckli M, Chaurand P, Hallahan DE, Caprioli RM (2001) Imaging mass spectrometry: A new technology for the analysis of protein expression in mammalian tissues. Nat Med 7(4):493-496.

47. Takahashi K, Kozuka T, Anegawa A, Nagatani A, Mimura T (2015) Development and application of a high-resolution imaging mass spectrometer for the study of plant tissues. Plant Cell Physiol 56(7):1329-1338.

48. Thamm AM, Qu Y, De Luca V (2016) Discovery and metabolic engineering of iridoid/secoiridoid and monoterpenoid indole alkaloid biosynthesis. Phytochem Rev 15(3):339-361.

49. Thunig J, Hansen SH, Janfelt C (2011) Analysis of secondary plant metabolites by indirect desorption electrospray ionization imaging mass spectrometry. Anal Chem 83(9):3256-3259.

50. Van Der Fits L, Memelink J (2000) ORCA3, a jasmonate-responsive transcriptional regulator of plant primary and secondary metabolism. Science 289(5477):295-297.

51. Van Der Heijden R, Jacobs DI, Snoeijer W, Hallard D, Verpoorte R (2004) The Catharanthus alkaloids: Pharmacognosy and biotechnology. Curr Med Chem 11(5):607-628

52. Van Moerkercke A, et al. (2013). CathaCyc, a metabolic pathway database built from Catharanthus roseus RNA-Seq data. Plant Cell Physiol 54(5):673-685.

53. Van Moerkercke A, et al. (2015). The bHLH transcription factor BIS1 controls the iridoid branch of the monoterpenoid indole alkaloid pathway in Catharanthus roseus. Proc Natl Acad Sci USA 112(26):8130-8135.

54. Van Moerkercke A, et al. (2016). The basic helix-loop-helix transcription factor BIS2 is essential for monoterpenoid indole alkaloid production in the medicinal plant Catharanthus roseus. Plant J 88(1):3-12.

55. Verma P, Mathur AK, Srivastava A, Mathur A (2012) Emerging trends in research on spatial and temporal organization of terpenoid indole alkaloid pathway in Catharanthus roseus: a literature update. Protoplasma 249(2):255-268.

56. Yamamoto K, et al. (2016). Cell-specific localization of alkaloids in Catharanthus roseus stem tissue measured with Imaging MS and Single-cell MS. Proc Natl Acad

Sci U S A. 113(14):3891-3896.

57. Yoder LR, Mahlberg PG (1976) Reactions of alkaloid and histochemical indicators in laticifers and specialized parenchyma cells of Catharanthus roseus (Apocynaceae). Am J Bot 63(9):1167-1173.

58. Yu F, De Luca V (2013) ATP-binding cassette transporter controls leaf surface secretion of anticancer drug components in Catharanthus roseus. Proc Natl Acad Sci USA 110(39):15830-15835.

59. Zhou H, Tai Y, Sun C, Pan Y (2005) Rapid identification of vinca alkaloids by directinjection electrospray ionisation tandem mass spectrometry and confirmation by high-performance liquid chromatography-mass spectrometry. Phytochem Anal 16(5):328-333.

Acknowledgments

At First, I would like to show my greatest appreciation to my supervisor Dr. Tetsuro Mimura for the continuous kind supports of my Ph.D study and allowing me to study specialized metabolism. I was really happy to keep the research related to specialized metabolism in Kobe University and learned many things from you.

Furthermore, I would like to thank the rest of my Ph.D thesis committee : Dr. Hidehiro Fukaki, Dr. Seiji Yamato and Dr. Yuji Kageyama for their comments and encouragement for my Ph.D thesis work.

I am deeply grateful to Dr. Kimitsune Ishizaki, Dr. Miwa Ohnishi, Dr. Aya Anegawa, Dr. Chizuko Shichijo, Dr. Tatsuaki Goh, Dr. Koichi Toyokura, Dr. Akio Murakami and Dr. Tetsushi Iwasaki for kind supports and discussions of my research.

I would like to express my gratitude to Dr. Katsutoshi Takahashi for measurement of Imaging MS and many advices for MS analysis. I would like to thank Dr. Tomoharu Kajiyama and Dr. Tetsuya Kurata for supports of cell-specific RNA-seq analysis developed by Hitachi research group. I would like to express my gratitude to Dr. Tsutomu Masujima and Dr. Hajime Mizuno for measurement of Single-cell MS and many kind supports. I would like to thank Dr. Sarah O'Connor for dividing of strictosidine standard. I am deeply grateful to Dr. Mami Yamazaki and Dr. Jun Murata for many advices of research related to alkaloids biosynthesis.

Especially, I am deeply grateful to all lab members, i.e. Mimura group, Fukaki group, Ishizaki group, Shichijo group, Masujima group, Sharma group and

Martinoia group. All of you have been there to support me when I recruited patients and collected data for my Ph.D thesis.

Finally, I would like to thank my friends and families who supported my research and everything.